Recent developments in magnetocaloric materials

K A Gschneidner Jr[1,2,3], **V K Pecharsky**[1,2] **and A O Tsokol**[1]

[1] Materials and Engineering Physics Program, Ames Laboratory, Iowa State University, Ames, IA 50011-3020, USA
[2] Department of Materials Science and Engineering, Iowa State University, Ames, IA 50011-2300, USA

E-mail: cagey@ameslab.gov

Abstract

The recent literature concerning the magnetocaloric effect (MCE) has been reviewed. The MCE properties have been compiled and correlations have been made comparing the behaviours of the different families of magnetic materials which exhibit large or unusual MCE values. These families include: the lanthanide (R) Laves phases (RM_2, where M = Al, Co and Ni), $Gd_5(Si_{1-x}Ge_x)_4$, $Mn(As_{1-x}Sb_x)$, $MnFe(P_{1-x}As_x)$, $La(Fe_{13-x}Si_x)$ and their hydrides and the manganites ($R_{1-x}M_xMnO_3$, where R = lanthanide and M = Ca, Sr and Ba). The potential for use of these materials in magnetic refrigeration is discussed, including a comparison with Gd as a near room temperature active magnetic regenerator material.

(Some figures in this article are in colour only in the electronic version)

[3] Author to whom any correspondence should be addressed.

Contents

1. Introduction

Many events related to the coupling of magnetic sublattices with an external magnetic field can be triggered by varying the latter around a solid. This includes the magneto-thermodynamic phenomenon known as the magnetocaloric effect (MCE), which in a way resembles processes that occur in a gas in response to the changing pressure. In a gaseous system, positional disorder and, therefore, the corresponding component of the entropy are suppressed during isothermal compression. Similarly, isothermal magnetizing of a paramagnetic solid near absolute zero or a ferromagnetic material near its spontaneous magnetic ordering temperature—the Curie temperature, T_C—greatly reduces the disorder of a spin system, thus substantially lowering the magnetic part of the total entropy. In the reverse process, which is similar to the expansion of a gas at constant temperature, isothermal demagnetizing restores the zero field magnetic entropy of a system. These transformations of a solid can be quantified by means of an extensive parameter representing the MCE—the isothermal magnetic entropy change, ΔS_M. When a gas is compressed adiabatically, its total entropy remains constant, whereas the velocities of the constituent molecules and, therefore, the temperature of the gas both increase. Likewise, the sum of the lattice and electronic entropies of a solid must change by the opposite of ΔS_M as a result of adiabatically magnetizing (or demagnetizing) the material, thus resulting in an increase (decrease) of the lattice vibrations and the adiabatic temperature change, ΔT_{ad}, which is an intensive thermodynamic quantity also used to measure and express the MCE.

Although the MCE was discovered in 1881 [1], the first major advance occurred in the late 1920s when cooling via adiabatic demagnetization was independently proposed by Debye [2] and Giauque [3]. The process was demonstrated for the first time in the history of physics a few years later when Giauque and MacDougall in 1933 [4] reached 0.25 K. Between 1933 and 1997, a number of advances in utilization of the MCE for cooling occurred (these have been described in recent reviews [5–8]). However, two major developments occurred in 1997. The first was the February 20, 1997 unveiling of a proof-of-principle magnetic refrigerator demonstrating that magnetic refrigeration is a viable and competitive cooling technology in the near room temperature region [9] with potential energy savings of up to 30%. In addition, magnetic refrigeration is an environmentally friendly technology since it eliminates ozone depleting gases, reduces the need for global warming greenhouse effect gases, and other hazardous gaseous refrigerants. The second breakthrough was the announcement of the discovery of the giant MCE (GMCE) in $Gd_5(Si_2Ge_2)$ on June 9, 1997 [10]. The details of these two breakthroughs and the resultant flurry of research activities[4] that occurred up to 2000 have been summarized in a number of reviews [5–8] and [11–13] and will not be repeated here. This review will be primarily concerned with the developments that have taken place since 1 January 2000 and 1 September 2004.

Most authors report the MCE as ΔS_M using the units of $J\,kg^{-1}K^{-1}$, but other units are also used ($J\,mol^{-1}\,K^{-1}$ and $mJ\,cm^{-3}\,K^{-1}$). Usually the same authors note their materials would be useful magnetic refrigerants and compare them with selected prototype materials; unfortunately most of the comparisons are meaningless since the wrong units are used. For a magnetic refrigerator, the engineer or designer needs to know the cooling per unit volume, and

---

[4] According to the two commonly known databases—*ISI Web of Knowledge*, http://isi4.isiknowledge.com/portal.cgi and *Chemical Abstracts*, http://www.cas.org/—the number of research articles containing the word 'magnetocaloric' in the title, the abstract or in the list of keywords more than doubled over each of the two five-year periods from 1995 to 1999 and from 2000 to 2004 when compared with the average over all of the five-year periods from 1970 to 1994, i.e. 22 per five years before 1995, to 79 and 311, respectively, according to *ISI Web of Knowledge*. Even though the figures extracted from the *Chemical Abstracts* are different, which is related to the differences in both the database content and in the search-and-match algorithms, the trend is practically the same: from 54 on average per five-year period between 1970 and 1995 to 135 and 438 over each of the last two five-year periods.
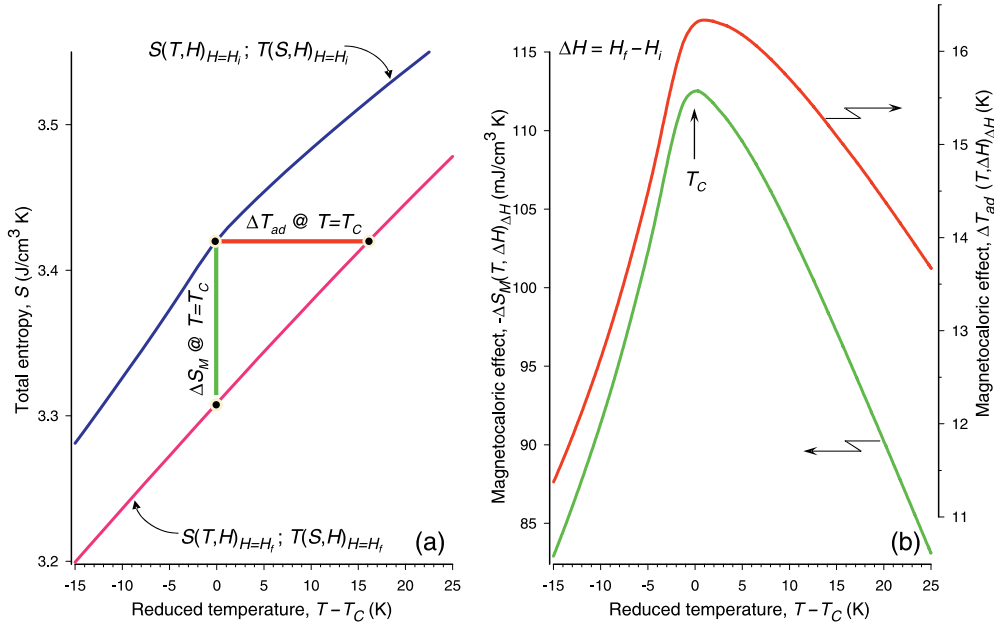
Figure 1. The total entropies in the initial (H_i) zero and final H_f) magnetic fields (*a*), and the MCE (*b*) in the vicinity of the Curie temperature of gadolinium, a ferromagnet with zero coercivity and remanence plotted as functions of reduced temperature.

thus the only units which are meaningful for such comparisons are mJ cm^{-3} K^{-1}, and for this reason we have converted the reported ΔS_M to volumetric entropy units in this review. Since the J kg^{-1}K^{-1} units are easily converted to the mJ cm^{-3} K^{-1} values if the density is known and since the density is not readily available (although it is easy to calculate if the crystal structure and lattice parameters are known), we have included the densities in the tables along with the ΔS_M values, and after the compound if ΔS_M is given in the text. This will enable the reader to quickly change the values given in this review to the J kg^{-1} K^{-1} of J mol^{-1} K^{-1} scales.

Furthermore, since in the vast majority of cases the magnetic entropy change is negative when the magnetic field increases but materials where the sign of the MCE is reversed are also known, the sign of ΔS_M will be properly reflected in all the tables and in the figures. In the text and in all the discussions when we compare the MCEs of several materials, we will compare the magnitudes only. Hence, a 50% reduction of the ΔS_M, for example, means that its absolute value (and therefore the magnetothermal response) is reduced by 50%.

2. Theory

For a given material at a constant pressure, the two quantitative characteristics of the MCE are functions of the absolute temperature (T) and the magnetic field change ($\Delta H = H_f - H_i$), where H_f and H_i are the final and initial magnetic fields, respectively, experienced by the material. The MCE can be easily computed [14] provided the behaviour of the total entropy (S) of a compound is known as a function of temperature in constant magnetic fields H_f and H_i, e.g. see figure 1(*a*) which depicts the total entropies and figure 1(*b*) which illustrates both ΔS_M and ΔT_{ad} of a ferromagnetic material in the vicinity of its Curie temperature:

$$\Delta S_M(T, \Delta H)_{\Delta H} = S(T, H)_{T,H=H_f} - S(T, H)_{T,H=H_i}, \tag{1}$$

$$\Delta T_{ad}(T, \Delta H)_{\Delta H} = T(S, H)_{S,H=H_f} - T(S, H)_{S,H=H_i}. \tag{2}$$

Direct isothermal measurements of the heat transfer and, therefore, direct measurements of ΔS_{M} using equation (1) are inconvenient and they are rarely, if ever, performed in practice. However, equation (2), in which the dependent variable (entropy) and the independent variable (temperature) are switched when compared with equation (1), can be and are often straightforwardly employed in direct measurements of ΔT_{ad} [15–17]. Thus, the temperature of a sample is measured in both H_{i} and H_{f}, i.e. before and after the magnetic field has been changed. The difference between the two temperatures yields the intensive MCE value. Both ΔS_{M} and ΔT_{ad} are usually reported as functions of temperature when $H_{\mathrm{i}} = 0$ and $H_{\mathrm{f}} > H_{\mathrm{i}}$.

At equilibrium, the MCE is correlated with the magnetization (M), magnetic field strength (H), heat capacity at constant pressure (C) and absolute temperature by one of the following fundamental Maxwell equations (where μ_0 is the permeability of vacuum):

$$\Delta S_{\mathrm{M}}(T, \Delta H)_{\Delta H} = \mu_0 \int_{H_{\mathrm{i}}}^{H_{\mathrm{f}}} \left(\frac{\partial M(T, H)}{\partial T} \right)_H \mathrm{d}H, \tag{3}$$

$$\Delta T_{\mathrm{ad}}(T, \Delta H)_{\Delta H} = -\mu_0 \int_{H_{\mathrm{i}}}^{H_{\mathrm{f}}} \left(\frac{T}{C(T, H)} \times \frac{\partial M(T, H)}{\partial T} \right)_H \mathrm{d}H. \tag{4}$$

As immediately follows from equations (1)–(4), materials whose total entropy is strongly influenced by a magnetic field and whose magnetization varies rapidly with temperature are expected to exhibit an enhanced MCE. The latter peaks when $|(\partial M(T, H)/\partial T)_H|$ is the greatest, i.e. around the T_{C} in a conventional ferromagnet or near the absolute zero temperature in a paramagnet. The MCE of a simple ferromagnet is usually gradually lowered both below and above the T_{C}, as is clearly seen in figure 1(*b*).

Equations (3) and (4) are easily derived from general thermodynamics (e.g. see [13]), yet both fail to describe the MCE in the vicinity of a truly discontinuous first-order phase transition when either $[\partial M(T, H)/\partial T]_H$ or $[T/C(T, H)]_H$ or both do not exist. This occurs because, by definition, the partial first derivatives of the Gibbs free energy with respect to intensive thermodynamic variables, e.g. T, P or H, vary discontinuously at the first-order phase transition. As a result, the bulk magnetization is expected to undergo a discontinuous change at constant temperature; and the heat capacity is expected to be infinite during a first-order phase transformation. Thus, in theory, $[\partial M(T, H)/\partial T]_H$ and $[T/C(T, H)]_H$ do not exist at the temperature of the first-order transition. In reality, these changes occur over a few Kelvin wide temperature range, and both functions can be measured experimentally. Other factors, for example time-, rate of temperature or magnetic field change-, temperature- and magnetic history-dependence of the magnetization, may severely affect the accuracy of numerical integration using equations (3) and (4), and therefore, they must be applied with caution. Equations (1) and (2), on the other hand, fully define the MCE regardless of the thermodynamic nature of the phase transformation that occurs, if any, in a material.

Equation (3) is commonly employed to evaluate the isothermal magnetic entropy change (e.g. see [18] and [19]) because bulk magnetization data as a function of temperature and magnetic field are relatively easy to obtain. Equation (4), however, is seldom used for practical computations since it is difficult to measure the magnetic field and temperature dependent heat capacity with the resolution and accuracy required for a reliable numerical integration.

For a first-order phase transition, it is also possible to employ an approximation which is based on the Clausius–Clapeyron equation:

$$-\left(\frac{\mathrm{d}H}{\mathrm{d}T} \right)_{\mathrm{eq}} = \left(\frac{\Delta S}{\Delta M} \right)_{\mathrm{T}}. \tag{5}$$

In equation (5), the left-hand side derivative is taken under equilibrium conditions, i.e. when the Gibbs free energies of the two phases are identical to one another. For the right-hand

side, $\Delta S = S_f - S_i$ and $\Delta M = M_f - M_i$, where the subscripts i and f correspond to phases in the initial magnetic field and in the final magnetic field states, respectively. Obviously, equation (5) is only applicable when H_f is strong enough to complete the transformation from a state i to a state f and when the quantity dH/dT at equilibrium is known. In other words, the H–T phase diagram for the system must be well established. Furthermore, by using the Clausius–Clapeyron equation, an estimate of only the extensive MCE, $\Delta S_M = \Delta S$, is possible. In order to find more about the thermodynamics of the MCE, we refer the interested reader to several recent reviews [6, 7, 20], and a monograph by Tishin and Spichkin [13]. A few updates in the understanding of the MCE that occurred after these reviews were published are briefly mentioned in the following paragraphs.

Gschneidner et al [21] described successful use of the alloy theory, based on which they were able to design novel materials exhibiting enhanced MCEs below 100 K. The major issues taken into account by this work were the availability of the magnetic entropy (i.e. the theoretical entropy change when a spin system switches from a complete disorder to a perfect magnetic order), the systematic variation of the magnetic properties of lanthanides as the number of 4f-electrons changes and the ability to adjust the Curie temperature of a material by alloying with other lanthanides, as well as with the non-magnetic elements. Typical improvements over the existing prototypes reported in [21] were of the order of 30%.

Pecharsky et al [14] give a detailed examination of the behaviour of the total entropy in the vicinities of both first- and second-order phase transitions. They conclude that in second-order magnetic phase transition (SOMT) systems, the largest MCE is expected when the heat capacity of a material is strongly influenced by the magnetic field. In the case of first-order magnetic phase (FOMT) transformations, the maximum magnetic entropy change is principally defined by the difference in the entropies of the low- and high-magnetic field phases—the larger the entropy difference, the larger the corresponding ΔS_M. The largest ΔT_{ad} are predicted to occur in first-order materials whose Curie temperature is strongly affected by the magnetic field, in other words the greater dT_C/dH corresponds to the greater ΔT_{ad}.

By using Ginzburg–Landau theory to analyse available experimental data for $Co(S,Se)_2$, $Lu(Co,Al)_2$, $Lu(Co,Ga)_2$, $U(Co,Fe)Al$, $MnFe(P,As)$ and $La(Fe,Si)_{13}$ compounds, Yamada and Goto [22, 23] show that in the case of itinerant electron metamagnetic (IEM) systems exhibiting the GMCE, the temperature dependence of the critical magnetic field of the metamagnetic transition plays an important role in maximizing the isothermal magnetic entropy change. Furthermore, the GMCE in other IEM systems is expected to occur when the M^4 pre-factor in the Landau energy expansion with respect to magnetization is negative and large. The latter coincides with conclusions arrived at by Amaral and Amaral [24] who applied Landau theory to ferromagnetic systems with magnetoelastic and magnetoelectronic couplings. Similar results were also reported by von Ranke et al [25], who modelled the effects of both externally (magnetic field and pressure) and internally (deformation of the unit cell) controlled parameters on the MCE in systems with localized magnetic moments.

Lima et al [26] derived the anisotropic MCE in single crystals of some RAl_2 and RNi_2 compounds, where R = lanthanides, considering a Hamiltonian which takes into account crystalline electric field (CEF) and quadrupolar effects in addition to magnetoelastic coupling and nearest neighbour interactions. In some cases, both the MCE and cooling capacity may be considerably increased if during the magnetizing–demagnetizing of a magnetocaloric material the orientation of the magnetic field vector is synchronized with the variable easy magnetization direction of such a crystal. An interesting claim has been made recently by Zhitomirsky [27], who finds that the MCE in strongly frustrated Heisenberg antiferromagnetic systems, such as those containing triangular networks of atoms (e.g. kagome nets), is intrinsically higher than in non-frustrated systems. The enhancement originates from a number of soft modes present

in frustrated systems below the saturation field. By using a Hamiltonian that takes into account the dipolar and quadrupolar interactions in addition to CEFs, de Oliveira *et al* [28] theoretically examined the nature of a nearly flat, 'table-like' MCE of the doublet–triplet Γ_3–Γ_5 reduced magnetic system. While it has been found experimentally (e.g. see [29]) that the table-like MCE is the result of successive magnetic phase transformations, de Oliveira and co-workers established a suitable energy gap between Γ_3–Γ_5 that permits successive magnetic orderings at different temperatures. It is worth noting that their theoretical predictions of the table-like MCE in TmZn and TmCd await an experimental verification.

3. Elements and their solid solutions

Little research has been carried out on the pure magnetic elements and their solid solution alloys in the past four years. The status of the MCE in these materials will be found in [7, 12, 13].

Chernyshov *et al* [30] have studied the MCE of a single crystal of a high purity Dy metal when the magnetic field was applied in the easy magnetization direction (the *a*-axis) in fields up to 14 kOe. In general, their results were in good agreement with the prior results on lower purity polycrystalline Dy. However, the authors discovered two new high-magnetic field phases in the 105 to 127 K and 179 to 182 K temperature regions, and a new magnetic phase diagram was proposed. A fairly substantial positive MCE (i.e. $\Delta T_{ad} > 0$) is observed at $\sim$90 K at the first-order antiferromagnetic to ferromagnetic transition (on cooling) which rises much more steeply and is about 10–30% larger than previously observed. Between 160 and 180 K there is a small negative ΔT_{ad} which is about the same as previously observed. However, between 180 and 210 K there is again a positive MCE which is about a factor of 2 larger than previously observed in the lower-purity polycrystalline Dy.

The effect of doping a 50 : 50 Gd : Dy alloy with Nd (up to 30%) was studied by Dai *et al* [31], who found that the Curie temperature is lowered from 235 K for the parent alloy to 165 K for $Gd_{0.35}Dy_{0.35}Nd_{0.30}$. The ΔS_M was reduced by 15% at the respective ordering temperature by the substitution of Nd for Gd : Dy. Upon storage in air for two years, the magnetization of the Nd containing alloys decreased by about 20%, while those with no Nd did not change. This will have a notable effect on the MCE properties of the Nd substituted alloys.

The doping of $Gd_{1-x}Tb_x$ alloys with Nd up to 15% was studied by Zhang *et al* [32]. They found that both Tb and Nd additions to Gd lower the Curie temperature of Gd and that small additions of Nd ($\sim$5%) have only a slight influence on the MCE of the $Gd_{1-x}Tb_x$ alloy.

Wang *et al* [33] found that B additions to Gd (2, 5 and 7 at%) expanded the unit cell volume, raised T_C by 4 to 298 K, increased the refrigeration capacity, q, by 12% and had no effect on ΔS_M. The variation of the lattice parameters and T_C with the B content suggested that the maximum solid solubility of B in Gd is 2 at% or less. However, the second phase GdB_2 seems to increase q by increasing the breadth of the caret-like shape of the ΔS_M versus T peak.

The temperature dependence of the MCE of Er is quite complex, as one might expect, since it has a first-order magnetic transition at 18.7 K, two second-order transitions at 52.7 and 86.4 K and a spin–slip transition at 26.2 K. The addition of Pr to Er ($Er_{1-x}Pr_x$ for $0 \leqslant x \leqslant 0.30$) has been studied by Wu *et al* [34]. They found that the 86.4 K ordering temperature is lowered and that of the first-order peak at 18.7 K is raised by Pr additions. As a result, the ΔT_{ad} at 18.7 K in pure Er is reduced by about one-third for $x \geqslant 0.1$ for a magnetic field change of 0 to 20 kOe, while the MCE of the upper transition (86.4 K) increases by a factor of 2. This results in a nearly constant MCE between 35 and 50 K for $0.1 \leqslant x \leqslant 0.3$. For a 0 to 50 kOe field change, the MCE associated with the 18.7 K transformation is also decreased for $0.1 \leqslant x \leqslant 0.2$, but for
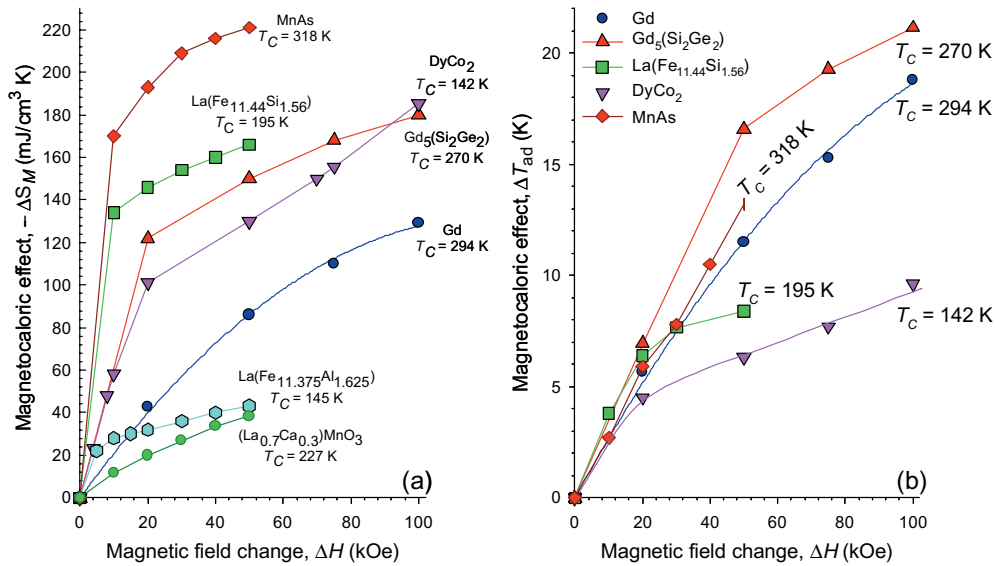
Figure 2. The isothermal entropy change as a function of the magnetic field change for DyCo$_2$ [48–50], Gd$_5$(Si$_2$Ge$_2$) [51], La(Fe$_{11.44}$Si$_{1.56}$) [52], La(Fe$_{11.375}$Al$_{1.625}$) [53], Gd [54], (La$_{0.7}$Ca$_{0.3}$)MnO$_3$ [55] and MnAs [56]. The data points for DyCo$_2$ at 4, 8 and 10 kOe were taken from [48], the data points at 20, 50, 75 and 100 kOe from [49] and that at 70 kOe from [50]. The highest values of $-\Delta S_M$ for Gd$_5$(Si$_2$Ge$_2$) and the two highest values for Gd are unpublished results of the authors (*a*). The adiabatic temperature rise as a function of the magnetic field change for DyCo$_2$ [49], Gd$_5$(Si$_2$Ge$_2$) [51], La(Fe$_{11.44}$Si$_{1.56}$) [52], Gd [7] and MnAs [56]. The highest value of ΔT_{ad} for Gd$_5$(Si$_2$Ge$_2$) is an unpublished result of the authors (*b*).

$x = 0.2$ the upper ordering temperature has been lowered to ~50 K and its MCE is increased by ~20% compared with the ΔT_{ad} value for the 18.7 K peak of pure Er.

4. Binary and ternary intermetallic compounds

4.1. Laves phases

4.1.1. RCo$_2$-based systems. The RCo$_2$ phases have been extensively studied because three of them exhibit a first-order paramagnetic–ferromagnetic transition (R = Dy, Ho and Er) while the other RCo$_2$ phases become ferromagnetic via a second-order transition. The work carried out before 2000 is summarized in [7, 12]. Most of the recent studies involve the substitution of a rare-earth metal for one of the magnetic lanthanides [35–39] or the substitution of a non-rare-earth metal for Co [36, 40–47]. But as a result of these studies most investigators also measured ΔS_M for the pure binary RCo$_2$ phase and confirmed the earlier reported results. One exception was the study by Wang *et al* [48], who measured the variation of ΔS_M at low fields (4, 8 and 10 kOe); in all the earlier studies the lowest applied magnetic field was 10 kOe or higher. The variation of ΔS_M versus the applied magnetic field for DyCo$_2$ is shown in figure 2(*a*) and ΔT_{ad} is shown in figure 2(*b*) along with several other materials which are discussed in later sections. It is seen that the ΔS_M values for DyCo$_2$ are fairly large and are grouped with other materials which have FOMT [Gd$_5$(Si$_2$Ge$_2$), MnAs and La(Fe$_{11.44}$Si$_{1.56}$)], but ΔT_{ad} is quite small and is close to that of La(Fe$_{11.44}$Si$_{1.56}$), but is significantly smaller than those for MnAs and the 4f-based materials [Gd and Gd$_5$(Si$_2$Ge$_2$)]. It is noted that ΔS_M values reported by [36] for $\Delta H = 20$ kOe and 50 kOe for DyCo$_2$ are ~30% and ~15% smaller, respectively, than

Table 1. The magnetocaloric properties of selected RM$_2$ Laves phases.

Compound	T_C (K)	$-\Delta S_M$ (mJ cm^{-3} K^{-1})		ΔT_{ad} (K)		Density (g cm^{-3})	Ref.
		0–20 kOe	0–50 kOe	0–20 kOe	0–50 kOe		
TbCo$_2$	236	26	48	1.9	3.6	9.087	[49]
DyCo$_2$	142	101	128	4.5	6.3	10.013	[49]
HoCo$_2$	83	112	203	4.0	8.8	10.172	[49]
ErCo$_2$	37	300	331	3.0	7.4	10.343	[49]

the results given in figure 2(*a*). However, the values reported by the same authors for TbCo$_2$ and HoCo$_2$ are in much better agreement with the results reported by other investigators. The MCE properties of some of the RCo$_2$ phases for magnetic field changes of 0 to 20 kOe and 0 to 50 kOe are shown in table 1. As expected, the RCo$_2$ phases undergoing an FOMT exhibit hysteresis, which is fairly small (2 kOe) for DyCo$_2$ but increases with decreasing T_C (5 kOe) for ErCo$_2$. For more details and further discussion, see section 11.3.1 and table 8.

The effect of substituting one magnetic lanthanide, R$'$, for the original lanthanide, R, raises or lowers T_C as one might expect from the respective de Gennes values of R and R$'$. The MCE of DyCo$_2$ is rapidly lowered by Gd substitution [35] and that of TbCo$_2$ is raised by Er substitutions [37]. de Oliveira *et al* [39] calculated the variation of T_C, ΔS_M and ΔT_{ad} for $(Er_{1-x}Dy_x)Co_2$ alloys for $0.2 \leqslant x \leqslant 1.0$ based on the measured values of ErCo$_2$. Duc *et al* [36, 38] noted that when 35% of Y and Lu were substituted for Gd in GdCo$_2$ there was little effect on ΔS_M, and similarly for a $(Gd_{0.4}Tb_{0.6})Co_2$ alloy.

The influence of M substitutions (M = Al, Si, Ga, Ge) for Co in the DyCo$_2$ compound has been extensively studied, especially for M = Si [41, 43–45], while only [42] and [44] studied M = Al, and [44] examined Ga and Ge substitutions. The behaviours of the four M elements are similar: (1) T_C is increased and Al is more effective than Ga, which is followed by Si and then Ge; (2) ΔS_M drops off rapidly for $x > 0.02$ because the FOMT is destroyed by M substitutions and is changed to an SOMT; and (3) ΔS_M reaches a value 70% of the ΔS_M value of pure DyCo$_2$ (see table 1) when $x = 0.1$ for M = Al, Ga and Ge (the maximum solubility of Si in DyCo$_2$ is 7%, i.e. $x = 0.07$).

Troper *et al* [46] calculate the effect of Rh substitution for Co on the magnetic behaviour of HoCo$_2$. The T_C of HoCo$_2$ (83 K) is rapidly lowered by initial Rh addition to $\sim$55 K at 5 at% Rh, and then more slowly to HoRh$_2$ ($T_C = 20$ K). The FOMT of HoCo$_2$ changes to an SOMT between 5 and 15 at% Rh. The ΔS_M of HoCo$_2$ for a field change of 50 kOe increases by $\sim$12% for Ho(Co$_{0.95}$Rh$_{0.05}$)$_2$ and drops by $\sim$40% at 15 at% Rh. The ΔT_{ad} for the same ΔH is predicted to drop slightly for a 5 at% Rh substitution ($\sim$7%) and then drop more rapidly for a 15 at% Rh substitution ($\sim$35%).

When Si is substituted for Co in ErCo$_2$ ($0 \leqslant x \leqslant 0.15$), T_C raised from $\sim$35 to $\sim$60 K while ΔS_M is lowered 37% for $x = 0.05$ and 85% for $x = 0.15$ [36]. The rapid drop in ΔS_M is due to the change of the FOMT in ErCo$_2$ to SOMT when some of the Co is replaced by Si, i.e. when $x > 0.02$. Similar results were reported by Singh *et al* [47]. When Ni is substituted for Co in ErCo$_2$, T_C is lowered to $\sim$12 K at $x = 0.10$, while ΔS_M and ΔT_{ad} remain about the same for $x = 0.05$, but then decrease by $\sim$20% and $\sim$30%, respectively, for $x = 0.10$.

Duc *et al* [36] noted that ΔS_M decreases with increasing temperature for the R(Co$_{1-x}$Si$_x$)$_2$ compounds, where R = Er and Ho, and the $(Dy_{1-x}Y_x)Co_2$ phases which exhibit FOMT, and that it lies well above the ΔS_M values for the RAl$_2$-based compounds and Er(Co$_{1-x}$Si$_x$)$_2$ for $x = 0.10$ and 0.15 phases which exhibit SOMT. A modified version of this plot is shown in
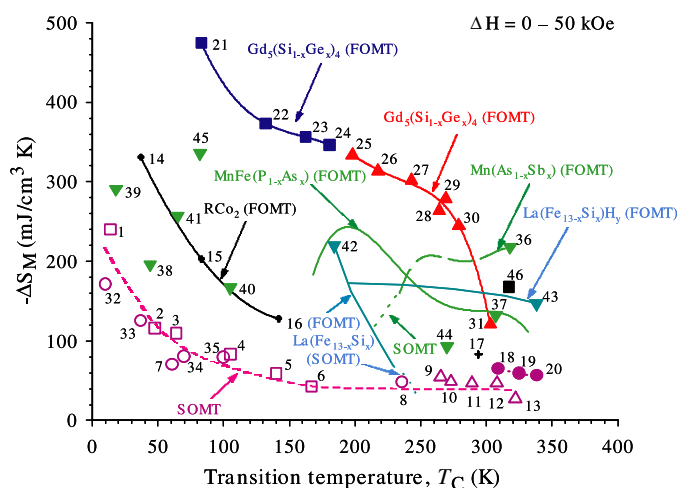
Figure 3. The magnetic entropy change for $\Delta H = 50$ kOe for the RCo_2, RAl_2, $Gd_5(Si_{1-x}Ge_x)_4$, $Mn(As_{1-x}Sb_x)$, $MnFe(P_{1-x}As_x)$ and $La(Fe_{13-x}Si_x)$ families plus a number of individual compounds versus the Curie temperature. The original plots for the RCo_2 and RAl_2 families given in [36] had many more data points, but only selected values were used here, primarily because density or lattice parameters were not available for most of the ternary compounds and thus the entropy units used in [36] could not be converted to the volumetric units used in this figure. The solid lines tie together those members of a family which exhibit a FOMT, while the dashed line and dotted line tie together those compounds of a family which have a SOMT. For the $Gd_5(Si_{1-x}Gd_x)_4$ family the solid squares are for those compounds which exhibit FMOT O(I)–O(II) transition, the solid triangles represent those for the FOMT O(I)–M transition, while the solid dots are for the SOMT O(I) ferromagnetic-paramagnetic transition (see section 5 for more details). The value for Gd was taken from [54]. The values in square brackets after the compounds in the legend identifying the compounds are the densities in g cm^{-3} units.

Compound legend

1—ErAl$_2$ [6.204]	16—DyCo$_2$ [10.013]	31—Gd$_5$Si$_{2.1}$Ge$_{1.9}$ [7.493]
2—(Dy$_{0.7}$Er$_{0.3}$)Al$_2$ [6.048]	17—Gd [7.901]	32—HoCoAl [7.961]
3—DyAl$_2$ [5.981]	18—Gd$_5$Si$_{2.3}$Ge$_{1.7}$ [7.472]	33—DyCoAl [7.619]
4—TbAl$_2$ [5.817]	19—Gd$_5$Si$_3$Ge [7.279]	34—TbCoAl [7.649]
5—(Tb$_{0.4}$Gd$_{0.6}$)Al$_2$ [5.719]	20—Gd$_5$Si$_4$ [6.987]	35—GdCoAl [7.575]
6—GdAl$_2$ [5.690]	21—Gd$_5$Si$_{0.5}$Ge$_{3.5}$ [7.909]	36—MnAs [6.799]
7—Er(Co$_{0.85}$Si$_{0.15}$)$_2$ [9.937]	22—Gd$_5$SiGe$_3$ [7.777]	37—MnFeP$_{0.45}$As$_{0.55}$ [7.256]
8—TbCo$_2$ [9.087]	23—Gd$_5$Si$_{1.2}$Ge$_{2.8}$ [7.722]	38—TbN [9.567]
9—Gd$_4$Bi$_3$ [10.073]	24—Gd$_5$Si$_{1.3}$Ge$_{2.7}$ [7.700]	39—HoN [10.26]
10—Gd$_4$(Bi$_{2.25}$Sb$_{0.75}$) [9.679]	25—Gd$_5$Si$_{1.5}$Ge$_{2.5}$ [7.663]	40—Tb$_5$Si$_2$Ge$_2$ [7.670]
11—Gd$_4$(Bi$_{1.5}$Sb$_{1.5}$) [9.679]	26—Gd$_5$Si$_{1.6}$Ge$_{2.4}$ [7.647]	41—Dy$_5$Si$_3$Ge [7.739]
12—Gd$_4$(Bi$_{0.75}$Sb$_{2.25}$) [8.834]	27—Gd$_5$Si$_{1.8}$Ge$_{2.2}$ [7.575]	42—La(Fe$_{11.7}$Si$_{1.3}$) [7.300]
13—Gd$_4$Sb$_3$ [8.414]	28—Gd$_5$Si$_{1.95}$Ge$_{2.05}$ [7.530]	43—La(Fe$_{11.5}$Si$_{1.5}$)H$_{1.8}$ [7.003]
14—ErCo$_2$ [10.343]	29—Gd$_5$Si$_{1.98}$Ge$_{2.02}$ [7.525]	44—La$_{1.4}$Ca$_{1.6}$Mn$_2$O$_7$ [5.536]
15—HoCo$_2$ [10.172]	30—Gd$_5$Si$_{2.02}$Ge$_{1.98}$ [7.517]	45—Gd$_5$Sn$_4$ [8.727]
		46—Ni$_{55.2}$Mn$_{18.6}$Ga$_{26.2}$ [8.247]

figure 3, where the ΔS_M values for the FOMT RCo_2-based phases (points 14–16) lie above those for the SOMT RCo_2-based and RAl_2-phase compounds. Also shown are the ΔS_M values for several families of compounds, some of which have both FOMT and SOMT. The ΔS_M values for the FOMT $R_5(Si_{1-x}Ge_x)_4$ compounds lie well above those for the FOMT RCo_2 materials. However, the ΔS_M values for the SOMT phases of these families are comparable with those of the SOMT RCo_2 intermetallics (points 7 and 8 in figure 3). The similarities in the

behaviours (i.e. the large difference in FOMT and SOMT ΔS_M values) of the $Gd_5(Si_{1-x}Ge_x)_4$ intermetallics and the RCo_2-based compounds is evident.

Theoretical modelling of the MCE in $(Er_{1-x}Y_x)Co_2$ for $x = 0$ and 0.2 [57] and for $Er(Co_{1-x}Ni_x)_2$ [58] has been carried out using a mean-field approach and treating the disorder in the coherent-potential approach, also see section 2. The calculated ΔS_M and ΔT_{ad} values are in good agreement with earlier published experimental data.

4.1.2. RAl_2-based systems.   Only seven papers have been published on the RAl_2 phases since 1999, four experimental and three theoretical. The MCE of $GdAl_2$ [58, 59], $TbAl_2$ [60], $(Gd_{0.6}Tb_{0.4})Al_2$ [60] and a series of $(Tb_{1-x}Y_x)Al_2$ alloys [61] have been measured, while theoretical calculations of the MCE of RAl_2 (R = Pr, Nd, Tb, Dy, Ho, Er and Tm) [62], $DyAl_2$ [63] and the $(Dy_{1-x}Er_x)Al_2$ pseudo-binary system [64] were reported.

The experimental data reported for $GdAl_2$, $TbAl_2$ and $(Gd_{0.6}Tb_{0.6})Al_2$ are consistent with the other RAl_2 values, see figure 3, points 1–6. For $(Tb_{1-x}Y_x)Al_2$ (density for $x = 0.5$ is $4.866\,g\,cm^{-3}$), Bohigas *et al* [61] found spin glass behaviour for $0.50 \leqslant x \leqslant 0.85$, with the ordering temperatures falling from 30 K at $x = 0.50$ to 10 K at $x = 0.85$, and the MCE also decreased rapidly with increasing x, by 85% over the same concentration range. The authors reported $\Delta S_M = -37\,mJ\,cm^{-3}\,K^{-1}$ for a 0 to 20 kOe magnetic field change for $x = 0.50$ ($T_C = 30\,K$). We estimate ΔS_M to be about $-90\,mJ\,cm^{-3}\,K^{-1}$ for $\Delta H = 50\,kOe$, which is significantly smaller than the expected value for $T_C = 30\,K$ for the RAl_2 phases (see figure 3). But this value is not unreasonable since the concentration of the magnetic metal (Tb), which accounts for the MCE, is 50% of that found in undiluted RAl_2 phases which established the SOMT curve shown in figure 3.

The Brazilian group [62–64] have carried out theoretical calculations for many of the RAl_2 compounds using a Hamiltonian which included the CEF and exchange interactions. von Ranke *et al* calculated ΔS_M for the RAl_2 phases where R = Pr, Nd, Tb, Dy, Ho, Er and Tm. The theoretical values for $ErAl_2$ were in fair agreement with experimental results and in good agreement for $DyAl_2$. The experimental MCE values for the other RAl_2 were not known at that time, but they predicted that the maximum ΔS_M value would be for $ErAl_2$ and decrease in the order Ho to Dy to Tb for the heavy lanthanides with atomic numbers (Z) less than that of Er. The ΔS_M value for $TmAl_2$ (where Z is one larger than that of Er) is less than that of the $ErAl_2$ value but larger than that of $HoAl_2$. For the light lanthanides $PrAl_2$ and $NdAl_2$, the MCE values are less than that of the heavy lanthanide with the same T_C values.

In an earlier paper these authors [63] predicted a negative MCE when the magnetic field was applied along the $\langle 111 \rangle$ direction in $DyAl_2$ because there is an FOMT in the magnetization in this direction at a critical field of 58 kOe. They also predicted that the MCE would be normal in the $\langle 100 \rangle$ and $\langle 110 \rangle$ directions. They [64] were also able to explain the anomalous peak observed in the MCE at $\sim 10\,K$ for the $(Dy_{1-x}Er_x)Al_2$ alloys for $x = 0.3$ and 0.5. In addition, the calculated ΔT_{ad} values were in good agreement with experiment for all the measured compositions between $DyAl_2$ and $ErAl_2$.

4.1.3. RNi_2-based systems.   Two theoretical studies on the RNi_2 phases have been carried out on the RNi_2 phases with R = Pr, Nd, Gd, Tb, Dy, Ho and Er. von Ranke *et al* [65], using a model Hamiltonian that included anisotropic CEF and exchange interactions, predicted the MCE properties of the RNi_2 phases for R = Pr, Nd, Gd, Tb, Ho and Er. For the $ErNi_2$ phase, the theoretical values for ΔS_M were in excellent agreement with experiment and in fair agreement for ΔT_{ad}. The other RNi_2 phases have not been studied experimentally. The maximum ΔS_M is predicted to occur for $HoNi_2$, followed by Tb, Er, Gd, Nd and Pr. These MCE

values are comparable with those calculated by the same authors [62] for the corresponding RAl_2 compounds. The ΔT_{ad} values are also a maximum at $HoNi_2$, but the order is somewhat different from that for the ΔS_M values, i.e. the ΔT_{ad} value is second highest for $ErNi_2$, followed by Dy, Tb, Nd, Gd and Pr [65]. The authors also predicted a second peak in the MCE values at ~ 1.5 K for $HoNi_2$ which they thought was due to a high density of states at low temperatures.

In a more recent paper, von Ranke $et\ al$ [66] examined the MCE in RNi_2 for R = Nd, Gd, Tb, Dy, Ho and Er as potential magnetic refrigerants for an Ericsson cycle. They proposed a composite material consisting of $ErNi_2$–$DyNi_2$–$TbNi_2$ as a refrigerant for the 7 K to 22 K temperature range.

4.2. Miscellaneous intermetallic compounds

A number of other intermetallic compounds have been studied for their MCE properties, both binary and ternary, and the reported results are divided into these two categories. In general the compounds are listed in order of increasing atomic number of the non-rare-earth metal (or element). There are, however, several important families of intermetallic compounds which are being treated separately—the $R_5(Si,Ge)_4$ phases, the Mn-based materials and the $La(Fe,M)_{13}$ compounds—sections 5, 6 and 7, respectively.

4.2.1. Binary compounds. Nakagawa $et\ al$ [67] measured ΔS_M and T_C for seven compositions in the $(Gd_{1-x}Dy_x)N$ system. T_C was lowered in a nearly linear fashion from 61 K for GdN to 21 K for DyN. The MCE for a 0 to 10 kOe field change, however, was a maximum at DyN and decreased in a nearly linear fashion by $\sim 40\%$ for $(Gd_{0.9}Dy_{0.1})N$, but it jumped to a significantly higher value at GdN (only $\sim 10\%$ smaller than that of DyN). They also reported that $\Delta S_M = -167$ mJ cm^{-3} K^{-1} for $\Delta H = 50$ kOe for DyN (density is 9.933 g cm^{-3}). This value is comparable with those of the RAl_2 phases at the corresponding T_C, see figure 3.

The MCE properties of TbN and HoN were measured by Yamamoto $et\ al$ [68]. They reported that $\Delta S_M = -196$ mJ cm^{-3} K^{-1} for a 0 to 50 kOe field change for TbN, $T_C = 44$ K; and $\Delta S_M = -291$ mJ cm^{-3} K^{-1} for the same ΔH for HoN, $T_C = 18$ K. Both these values lie well above the SOMT line established by the RAl_2 phases (figure 3), points 38 and 39, respectively, but below the RCo_2 FOMT line.

The Gd-rich alloys in the $(Gd_{1-x}Tb_x)_3Al_2$ system $x = 0, 0.1, 0.2$ and 0.3 were studied by Long $et\ al$ [69]. They found that Tb additions lower T_C from 280 K for Gd_3Al_2 to 255 K for $x = 0.3$ and increase the ΔS_M values for $\Delta H = 10$ kOe from -14.9 mJ cm^{-3} K^{-1} for $x = 0$ to -18.0 mJ cm^{-3} K^{-1} at $x = 0.1$, and with further Tb addition ΔS_M falls slightly to -17.4 mJ cm^{-3} K^{-1} at $x = 0.3$. The ΔS_M values are about 75% of that of Gd metal, which suggests that for $\Delta H = 50$ kOe these alloys would be close to the SOMT line of figure 3.

The antiferromagnetically ordered Nd compounds NdP ($T_N = 11$ K) and NdAs ($T_N = 12$ K) were studied both theoretically and experimentally by Plaza $et\ al$ [70]. The theoretical ΔS_M value was calculated using a Hamiltonian that included CEF interactions and molecular and quadrupolar fields. The agreement with experiment was quite good on the high temperature side of the caret-like shape of the MCE peak, but ~ 10 K above T_N, the theoretical values became significantly higher than the observed ΔS_M curve. The experimental ΔS_M values at T_C were -52.6 mJ cm^{-3} K^{-1} for $\Delta H = 50$ kOe for NdP (density is 6.149 g cm^{-3}) and -70.2 mJ cm^{-3} K^{-1} for $\Delta H = 70$ kOe for NdAs (density is 7.840 g cm^{-3}). As expected for antiferromagnets, the ΔS_M values are significantly smaller than those of ferromagnetic substances.

The MCE properties of Nd_2Fe_{17} ($T_C = 325$ K) were determined by Dan'kov $et\ al$ [59], see table 2: the ΔS_M was slightly smaller than those of the Si-rich $Gd_5(Si_{1-x}Ge_x)_4$ alloys (figure 3) and ΔT_{ad} was significantly smaller (see figure 4).
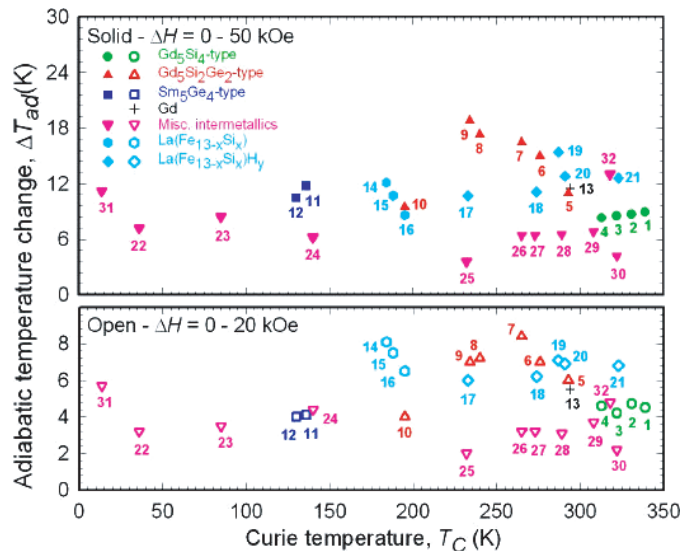
Figure 4. The adiabatic temperature change for the $Gd_5(Si_{1-x}Ge_x)_4$ and $La(Fe_{13-x}Si_x)H_y$ families, and other selected compounds. The values for $ErAl_2$ (point number 31) are unpublished results obtained by the authors.

Compound legend

1—$Gd_{5.00}Si_{4.00}$	12—$Gd_5Si_{0.90}Ge_{3.10}$	23—$HoCo_2$
2—$Gd_5Si_{3.50}Ge_{0.50}$	13—Gd	24—$DyCo_2$
3—$Gd_5Si_{3.00}Ge_{1.00}$	14—$La(Fe_{11.70}Si_{1.30})$	25—$TbCo_2$
4—$Gd_5Si_{2.50}Ge_{1.50}$	15—$La(Fe_{11.57}Si_{1.43})$	26—Gd_4Bi_3
5—$Gd_5Si_{2.09}Ge_{1.91}$	16—$La(Fe_{11.44}Si_{1.56})$	27—$Gd_4(Bi_{2.25}Sb_{0.75})$
6—$Gd_5Si_{2.00}Ge_{2.00}$	17—$La(Fe_{11.44}Si_{1.56})H_{0.5}$	28—$Gd_4(Bi_{1.5}Sb_{1.5})$
7—$Gd_5Si_{1.98}Ge_{2.02}$	18—$La(Fe_{11.44}Si_{1.56})H_{1.0}$	29—$Gd_4(Bi_{0.75}Sb_{2.25})$
8—$Gd_5Si_{1.80}Ge_{2.20}$	19—$La(Fe_{11.70}Si_{1.30})H_{1.1}$	30—Gd_4Sb_3
9—$Gd_5Si_{1.72}Ge_{2.28}$	20—$La(Fe_{11.57}Si_{1.43})H_{1.3}$	31—$ErAl_2$
10—$Gd_5Si_{1.50}Ge_{2.50}$	21—$La(Fe_{11.44}Si_{1.56})H_{1.5}$	32—MnAs
11—$Gd_5Si_{1.00}Ge_{3.00}$	22—$ErCo_2$	

The ΔT_{ad} value of 5 K for Gd_3Co at $T_C = 135$ K for $\Delta H = 40$ kOe [71] is rather modest compared with other materials which have comparable T_Cs, see figure 4.

The MCE in TmCu and TmAg, which have the simple CsCl-type structure, was studied extensively by Rawat and Das [72]. Tm has both a large magnetic moment and a 4f-electronic-quadrupole in these two compounds and this leads to interesting magnetic behaviours at low temperatures. TmCu orders antiferromagnetically with an incommensurate antiferromagnetic structure at 7.7 K, which transforms to a commensurate structure at 6.7 K. Both transformations are first order. In TmAg, there is only one second-order paramagnetic to antiferromagnetic transition at 9.5 K. The antiferromagnetic nature of the ground states of TmCu and TmAg leads to a negative MCE at low temperatures less than 8 K and 10 K, respectively, and a normal MCE above these two temperatures, see table 2. The corresponding absolute MCE peak values are much larger for TmCu than for TmAg, but even the normal MCE values for TmCu are significantly smaller than that observed in other materials which order magnetically below 10 K, such as ErNiAl and $ErNi_2$ [12].

Aoki *et al* [73] studied the low temperature magnetothermal properties of single crystalline $HoGa_2$, which has the hexagonal AlB_2-type structure, and initially orders antiferromagnetically

Table 2. The magnetocaloric properties of selected binary intermetallic compounds.

Compound	T_C (K)	$-\Delta S_M$ (mJ cm^{-3} K^{-1})		ΔT_{ad} (K)		Density (g cm^{-3})	Ref.
		0–20 kOe	0–50 kOe	0–20 kOe	0–50 kOe		
Nd$_2$Fe$_{17}$	325	25	46	1.9	4.0	7.797	[59]
Gd$_7$Pd$_3$	323	22	57	3.0	8.5	8.707	[75]
Gd$_4$Bi$_3$	332	15	27	2.2	4.2	10.073	[77]
Gd$_4$(Bi$_{2.25}$Sb$_{0.75}$)	308	27	47	3.7	6.8	9.679	[77]
Gd$_4$(Bi$_{1.5}$Sb$_{1.5}$)	289	24	47	3.1	6.5	9.259	[77]
Gd$_4$(Bi$_{0.75}$Sb$_{2.25}$)	273	26	49	3.2	6.4	8.834	[77]
Gd$_4$Sb$_3$	265	29	55	3.2	6.4	8.414	[77]
Gd$_2$In	194	18.5	37	2.0	4.4	8.316	[76]
Gd$_2$In	~50[a]	−12	−4	−0.7	−0.2	8.316	[76]
TmAg	~12[b]	11	74[c]	0.8	4.2[c]	10.169	[72]
TmAg	~7[a]	−26	−55[c]	−0.4	−0.9[c]	10.169	[72]
TmCu	~10[b]	25	118[c]	0.6	3.6[c]	9.692	[72]
TmCu	6.7[d]	−68	−131[c]	−0.4	−1.8[c]	9.692	[72]

[a] Temperature at which ΔS_M has the largest positive value and ΔT_{ad} has the largest negative MCE value.

[b] Maximum in MCE (no magnetic ordering observed at this temperature).

[c] Interpolated.

[d] Néel temperature.

below 8.5 K. HoGa$_2$ has a complicated magnetic phase diagram and thus exhibits unusual MCEs as a function of temperature and applied magnetic field. Both positive and negative ΔT_{ad} values have been observed, while ΔS_M tends to be primarily positive. Both ΔT_{ad} and ΔS_M are fairly small.

The MCE in YbAs has been studied theoretically by von Ranke *et al* [74] because it is a heavy fermion compound in which there is a competition between magnetic interaction and Kondo hybridization. The authors calculated that YbAs, which orders antiferromagnetically at 0.49 K and $H = 0$, will exhibit a negative MCE between 33 and 84 K when ΔH is less than 23.5 kOe, and for field changes greater than this critical field the MCE is predicted to be normal.

Gd$_7$Pd$_3$, which orders at 323 K, has MCE values (see table 2) [75] comparable with those of Gd$_5$Si$_3$Ge (see figures 3 and 4), which has a similar Curie temperature.

Ilyn *et al* [76] studied the magnetothermal properties of Gd$_2$In which orders ferromagnetically at 194 K and antiferromagnetically at 91 K. At 194 K, normal MCE values were measured (see table 2), with ΔS_M values being slightly smaller than those of the RAl$_2$ Laves phases (figure 3) and ΔT_{ad} values about half of those of the RAl$_2$ compounds. But below ~100 K negative MCE values are observed for small ΔH, i.e. <50 kOe. The maximum anomalous MCE values of ΔS_M and ΔT_{ad} occur at ~50 K for $\Delta H = 20$ kOe and the absolute values are small, see table 2.

A series of alloys of the Gd$_4$(Bi$_x$Sb$_{1-x}$)$_3$ system, which have the cubic anti-Th$_3$P$_4$ type structure, were examined by Niu *et al* [77] and Niu [78]. All alloys order ferromagnetically from 332 K for Gd$_4$Bi$_3$ to 265 K for Gd$_4$Sb$_3$. The MCE values for Gd$_4$Bi$_3$ (table 2) are significantly smaller than those of Gd$_5$(Si$_3$Ge) phase which orders at about the same temperature. But the MCE values for Gd$_4$(Bi$_x$Sb$_{1-x}$)$_3$ for $0 \leqslant x \leqslant 0.75$ (table 2) are significantly larger than for the pure Gd$_4$Bi$_3$ phase and are in line with the trends established in figures 3 (points 9–13) and 4 (points 26–30).

The magnetic phase diagram of PrPb$_3$, like HoGa$_2$ (see above), is also complicated [79]. PrPb$_3$ exhibits an antiferroquadrupolar transition at 0.39 K and $H = 0$, which increases to

0.66 K at 60 kOe. It also forms a new magnetic phase at $H > 15$ kOe. As a result, ΔT_{ad} has all positive values at 0.23 K for all field changes up to 60 kOe, and both positive and negative values at 0.5 K as a function of the applied field.

4.2.2. Ternary and quaternary compounds. The ternary intermetallic compounds reviewed in this section are discussed in the sequence aluminides, silicides, germanides and stannides, and within each group by the simplest to the more complex chemical formula. The ternary $R_5(Si_{1-x}Ge_x)_4$ compounds, however, are discussed in section 5, along with the $R_5(M, Sn)_4$ stannides, while ternary silicides and germanides containing Mn are reviewed in section 6 and the $La(Fe_{13-x}M_x)$ phases in section 7. The one quaternary compound, $HoNi_2B_2C$, is the last compound to be discussed in this subsection.

Si *et al* [80] measured the MCE properties (ΔS_M) of amorphous NdFeAl (the density was assumed to be the same as for the crystalline form, i.e. 6.56 g cm^{-3}), which has a Curie temperature of 110 K. The maximum ΔS_M of -37 mJ cm^{-3} K^{-1} for $\Delta H = 50$ kOe is quite low compared with most crystalline compounds (see figure 3) and is about typical for amorphous materials [7].

The crystalline RCoAl compounds, where R = Gd, Tb, Dy and Er, were studied by Zhang *et al* [81] and have MCE values which are similar to those of alloys which exhibit a second-order magnetic transition (i.e. the SOMT line in figure 3). The T_C and ΔS_M values are listed in table 3 and shown in figure 3 (points 32–35). The complex $Nd_7Co_6Al_7$ (density is 6.487 g cm^{-3}) alloy has small MCE values ($\Delta S_M = -30$ mJ cm^{-3} K^{-1} and $\Delta T_{ad} = 2.7$ K for a 0–50 kOe field change) at $T_C = 15.5$ K [82].

Most of the rare-earth ternary silicides have low MCE values [83–87] with the exception of $GdPd_2Si$ and possibly GdFeSi. The only reported MCE values for GdFeSi ($T_C = 118$ K) were for a 0–90 kOe field change [83]. Prorating the MCE values for a 0–50 kOe field change suggests that the ΔS_M value would lie above the dashed curve in figure 3, but ΔT_{ad} would be significantly lower than the values shown in figure 4 near 120 K. $GdPd_2Si$, which has two ordering temperatures, 13 and 17 K, undergoes a metamagnetic transition at 10 kOe [84]. The maximum ΔS_M values (table 3) lie well below the SOMT line curve of figure 3, but the ΔT_{ad} (table 3) is quite large, comparable with the materials shown in figure 4. Das and Rawat [85] reported ΔT_{ad} values for $PrCo_2Si_2$ and $(Pr_{0.8}La_{0.2})Co_2Si_2$. Both compounds exhibit complex behaviours of the MCE. The former orders at 10, 17 and 31 K, and ΔT_{ad} is negative at all temperatures between 4 and 40 K with peaks (less negative ΔT_{ad} values) at the ordering temperatures for both $\Delta H = 20$ kOe and $\Delta H = 80$ kOe, the peaks being more pronounced for $\Delta H = 80$ kOe, while $(Pr_{0.8}La_{0.2})Co_2Si_2$ orders at 9 and 26 K and ΔT_{ad} is positive below 9 K and just barely negative from 9 to 80 K for $\Delta H = 20$ kOe, and for $\Delta H = 80$ kOe ΔT_{ad} is positive below 11 K and above 26 K and negative between 11 and 26 K [85]. The MCE of polycrystalline Gd_2PdSi_3 [86] and single crystal Tb_2PdSi_3 [87] have been reported. As with many of the ternary compounds, the MCE (both ΔS_M and ΔT_{ad}) behaviour for the two compounds is quite complex—exhibiting both positive and negative values. Gd_2PdSi_3 is an antiferromagnet ($T_N = 21$ K) in low-magnetic fields, but becomes ferro- (or ferri-) magnetic for $H > 5$ kOe. Tb_2PdSi_3 ($T_N = 23$ K) orders ferromagnetically along the [10$\bar{1}$0] direction. The crystal structures of these two compounds are unknown, and so it is not possible to calculate the ΔS_M values in mJ cm^{-3} K^{-1} units; however, a reasonable estimate of the density (~ 8 g cm^{-3}) suggests that the ΔS_M values lie well below the SOMT line drawn in figure 3. The ΔT_{ad} values for Gd_2PdSi_3 also seem to be somewhat low compared with the materials shown in figure 4.

The MCE (ΔS_M) has been measured for three RTiGe phases, R = Dy, Ho and Tm [88]. The three compounds order antiferromagnetically at 180 K, 92 K and 15 K, respectively. For the 0–20 kOe and 0–50 kOe field changes, the Dy and Ho compounds exhibit a negative MCE

Table 3. The magnetocaloric properties of selected ternary intermetallic compounds.

Compound	$T_C{}^a$ (K)	$-\Delta S_M$ (mJ cm^{-3} K^{-1})		ΔT_{ad} (K)		Density (g cm^{-3})	Ref.
		0–20 kOe	0–50 kOe	0–20 kOe	0–50 kOe		
GdCoAl	100	37	79	—	—	7.575	[81]
TbCoAl	70	41	80	—	—	7.649	[81]
DyCoAl	37	70	125	—	—	7.619	[81]
GdRu$_2$Ge$_2$	34	23	56^b	1.5	4.0^c	9.459	[91]
GdPd$_2$Si	17	42	142	3.2	8.6	9.358	[84]
HoCoAl	10	100	171	—	—	7.961	[81]

^{a} Curie temperature, or temperature at the maximum (or minimum) MCE value.
^{b} Estimated from values obtained for magnetic field changes of 20 and 40 kOe.
^{c} Interpolated from values obtained for magnetic field changes of 40 and 60 kOe.

below T_N but change to small positive MCE at T_N due to a field induced antiferromagnetic to ferromagnetic transition. The corresponding ΔS_M values for TmTiGe are positive, which means that fields >20 kOe are sufficient to suppress the antiferromagnetic state. For a 0–50 kOe field change the MCE at T_N is $\Delta S_M = -14$ mJ cm^{-3} K^{-1} for DyTiGe (density is 7.571 g cm^{-3}), -49 mJ cm^{-3} K^{-1} for HoTiGe (density is 7.698 g cm^{-3}) and -75 mJ cm^{-3} K^{-1} for TmTiGe (density is 8.024 g cm^{-3}), all of which are significantly smaller than the values which were used to establish the SOMT curve in figure 3. The ΔT_{ad} values have been reported for CeCu$_{0.86}$Ge$_2$ and PrCu$_{0.76}$Ge$_2$ by Rawat and Das [89]. The former orders at 17 K and has $\Delta T_{ad} = 3.2$ K for $\Delta H = 50$ kOe, while the latter orders at $\sim$23 K and its $\Delta T_{ad} = 4.0$ K for $\Delta H = 50$ kOe. The authors did not report $\Delta H = 50$ kOe data, but we have estimated ΔT_{ad} by interpolation using the 0 to 40 and 0 to 80 kOe curves. As seen, these ΔT_{ad} values are quite a bit lower than the values of other materials shown in figure 4 for the corresponding ordering temperature. The MCE (both ΔS_M and ΔT_{ad}) of GdRu$_2$Ge$_2$ was determined by Tegus *et al* [90], see table 3. GdRu$_2$Ge$_2$ undergoes two magnetic transitions at 29 and 32 K, but only one MCE peak is observed at 34 K. The MCE is quite small: the $|\Delta S_M|$ value lies well below the SOMT line shown in figure 3, and the ΔT_{ad} values also lie well below the data points in figure 4.

The MCE (both ΔS_M and ΔT_{ad}) of Er$_6$Ni$_2$Sn (density is 9.613 g cm^{-3}) was measured for magnetic field changes of 0 to 10, 25, 30 and 80 kOe [91]. This compound orders at 7, 17 and 35 K, and the maximum MCE values were observed at 17 K. By interpolation, the estimated ΔS_M values for $\Delta H = 20$ kOe and 50 kOe are -24 mJ cm^{-3} k^{-1} and -91 mJ cm^{-3} K^{-1}, respectively. The latter value falls well below the SOMT curve in figure 3. The corresponding ΔT_{ad} values are 0.8 K and 2.7 K, respectively, which also are quite low compared with the values plotted in figure 4 near $T = 20$ K.

The MCE properties of single crystal HoNi$_2$B$_2$C (density is 8.063 g cm^{-3}), which orders antiferromagnetically at 4.5 K, were measured by El Massalami *et al* [92]. Negative MCE values (for H parallel to a) were observed for field changes up to 10 kOe at $\sim$5 K for ΔS_M and at $\sim$20 K for ΔT_{ad}. For field changes $\geqslant$20 kOe positive MCE values were measured: for a 0–50 kOe field change $\Delta S_M = -128$ mJ cm^{-3} K^{-1} and $\Delta T_{ad} = 12$ K at $\sim$8 K. These values were obtained by interpolation of the reported $\Delta H = 40$ kOe and $\Delta H = 60$ kOe results.

5. Gd$_5$(Si$_{1-x}$Ge$_x$)$_4$ and related 5 : 4 materials

5.1. General comments

Since the discovery of the GMCE in Gd$_5$Si$_2$Ge$_2$ in 1997 [10], about 140 papers have been published by mid-2004 on the R$_5$T$_4$ materials, where R = a rare-earth element and

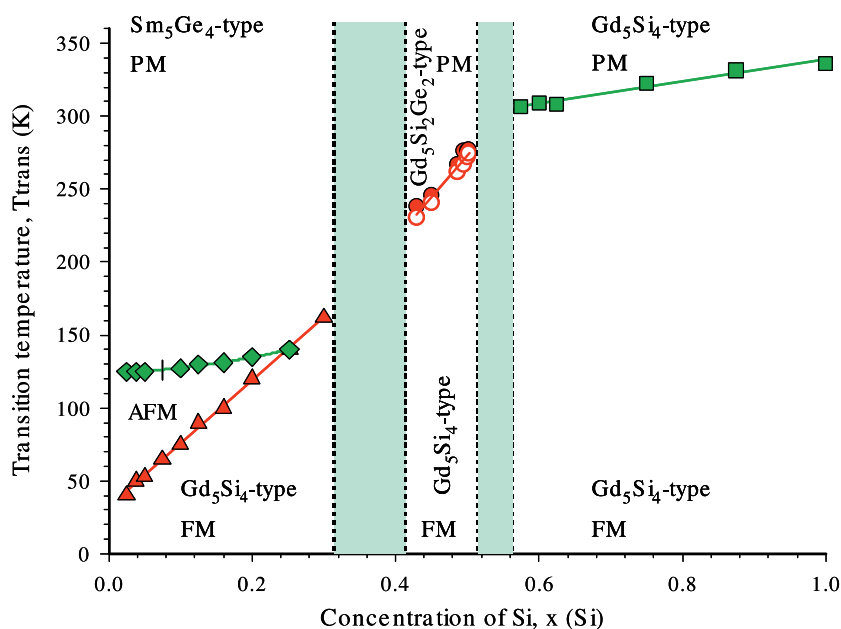**Figure 5.** The magnetic phase diagram of the Gd_5Si_4–Ge_5Ge_4 pseudo-binary system. The thin solid lines indicate magnetic phase boundaries, and the vertical dotted lines delineate the regions where the alloys are single phase materials (the compositions within shaded areas are two-phase alloys). The circles (open [heat treated] and solid [as cast]) refer to magnetic transition temperatures of the monoclinic $Gd_5Si_2Ge_2$-type phase, the solid squares indicate the magnetic transition temperatures of the orthorhombic Gd_5Si_4-based phase, and the solid triangles and diamonds refer to the magnetic transition temperatures of the orthorhombic Gd_5Ge_4-based phase, respectively, [98]. PM—paramagnetic, FM—ferromagnetic and AFM—antiferromagnetic.

T = Si, Ge or Sn. The interest in these phases and the excitement is not only due to the GMCE, but can also be ascribed to a number of other unusual features observed in these compounds, such as a colossal magnetostriction and giant magnetoresistance (see [93] and references cited therein). These extremum behaviours are due to a coupled magnetic–structural first-order transition in which slabs of a well defined arrangement of R and T atoms shift ∼0.5 Å with respect to one another along the *a*-axis when the material transforms under the influence of temperature, magnetic field or pressure [94–96]. This shift gives rise to an ∼1% volume change at the FOMT. The phenomenon, which gives rise to the GMCE and other extremum behaviours, is the transformation on cooling or the application of a magnetic field from either the paramagnetic (P) monoclinic $Gd_5(Si_2Ge_2)$-type structure to the ferromagnetic orthorhombic Gd_5Si_4-type structure, or the antiferromagnetic (AFM) Sm_5Ge_4-type structure to the ferromagnetic (FM) orthorhombic Gd_5Si_4-type structure. The interesting features of these transformations are that T–T bonds between the slabs are absent in the Sm_5Ge_4-type structure, or that they are absent between alternate slabs (i.e. two slabs have paired T–T atoms between them, but there are no T–T atom bonds between the paired slabs and the neighbouring slabs) in the $Gd_5(Si_2Ge_2)$-type structure, but that the T–T atoms are present between all the slabs in the Gd_5Si_4-type structure [93, 95]. Another interesting feature is that the FOMT temperature in the $Gd_5(Si_{1-x}Ge_x)_4$ is strongly dependent on the Si : Ge ratio, especially for $x \geqslant 0.5$ [97], see figure 5.

The MCE values reported by various researchers can vary considerably, but this can be ascribed to the complex structural–metallurgical behaviour of many of these materials

especially for the $Gd_5(Si_{1-x}Ge_x)_4$ phases for $x \cong 0.5$ [51, 98–100]. Also interstitial impurities, especially C, can have a pronounced effect on the MCE behaviour [101–103]. Unfortunately many researchers do not realize that most commercially available rare-earth metals have a large content of interstitial impurities, primarily H, C, N and O. When considered on an atomic basis, the interstitial content varies from 2 to 5 at%, that is, the purity of the starting rare-earth metals is 98–95 at% (see [104] and references cited therein). Thus, unless the interstitial content is taken into account the desired composition of the alloy is incorrect. In addition, the alloy will contain a substantial amount of C, N and O, and generally the H is lost in the preparation process due to its high vapour pressure. It is noted that most vendors claim their rare-earth metals are 99.9% pure; this, however, is in reference to the other rare-earth elements only.

5.2. $Gd_5(Si_{1-x}Ge_x)_4$ alloys

The MCE in $Gd_5(Si_{1-x}Ge_x)_4$ alloys has been reported by a number of investigators [10, 51, 97–101, 103, 105–109]. The original report [10] of the GMCE in $Gd_5(Si_2Ge_2)$ showed a large narrow FOMT heat capacity peak at 276 K and a small lambda-type SOMT heat capacity peak at 299 K. The original interpretation of these data was that there was a PM to AFM transformation at 299 K and a first-order AFM to FM transformation at 276 K. However, later research showed that this sample actually consisted of two polymorphic phases of the $Gd_5(Si_2Ge_2)$ composition, and that by proper heat treatment one could obtain either polymorph free from the other phase [51, 98–100]. By proper heat treatment, the originally reported ΔS_M value for the GMCE [10] was increased by 80% and ΔT_{ad} was increased by 55% [51]. The ΔS_M values reported by the Ames Laboratory group [51, 98–100] using high purity (99.89 at%) Gd for the $Gd_5(Si_{1-x}Ge_x)_4$ alloys for a 0 to 50 kOe field change are plotted in figure 3 (points 18–31) as a function of the magnetic ordering temperature, while the corresponding ΔT_{ad} values for 0–20 and 0–50 kOe field changes are plotted in figure 4 (points 1–12), also as a function of the magnetic ordering temperature. The field dependence of ΔS_M and ΔT_{ad} of $Gd_5(Si_2Ge_2)$ is shown in figures 2(a) and (b), respectively, along with several other potential magnetic refrigerants including Gd metal. It is seen that the field dependence of the GMCE compares quite favourably with the other substances, especially ΔT_{ad}.

The observed MCE behaviours can be correlated with the phase relationships in the Gd_5Si_4–Gd_5Ge_4 pseudo-binary system. As shown in figure 5 there are two terminal solid solutions and one intermediate solid solution region in this system. The Si-rich terminal solid solution has the Gd_5Si_4-type crystal structure from the melting point to 0 K and it undergoes a PM to FM SOMT upon cooling. It is interesting to note all these alloys have T_Cs which are greater than that of pure Gd ($T_C = 293$ K). The MCE for the Si-rich alloys, i.e. $x \geqslant 0.56$ is better than those of materials which order magnetically above 300 K and undergo an SOMT (see figures 3 [ΔS_M] and 4 [ΔT_{ad}]), but are smaller than those which exhibit an FOMT (see figures 3 and 4). In the intermediate solid solution region ($0.42 \leqslant x \leqslant 0.52$), the alloys undergo a coupled structural/magnetic FOMT from the PM monoclinic $Gd_5(Si_2Ge_2)$-type structure to the FM Gd_5Si_4-type orthorhombic structure upon cooling. In the Ge-rich side of this pseudo-binary system ($x \leqslant 0.32$) things are a little more complicated. The room temperature form has the Sm_5Ge_4-type orthorhombic structure which transforms magnetically from a PM state to an AFM state upon cooling as shown in figure 5. Upon further cooling, the AFM state undergoes a coupled structural/magnetic FOMT to the FM modification which has the Gd_5Si_4-type orthorhombic structure. It is quite obvious that the $Gd_5(Si_{1-x}Ge_x)_4$ alloys have significantly higher ΔS_M values (see figure 3, solid squares [points 21–24] and solid triangles [points 25–31]) than any other material which orders below $\sim$300 K. This is due to the unique combination of a coupled first-order magnetic–structural transformation. This

is especially evident when the $Gd_5(Si_{1-x}Ge_x)_4$ values are compared with those of the RCo_2 phases (points 14–16), which exhibit an FOMT, but there is no structure change associated with the magnetic transformation, only a phase volume discontinuity. A similar trend is observed for ΔT_{ad} (figure 4) but it is not quite as distinct as seen in ΔS_M.

Other MCE measurements on the $Gd_5(Si_{1-x}Ge_x)_4$ alloys have been reported by Tegus *et al* [88], Thuy *et al* [105], Thuy [106] and Zhuo *et al* [107]. Tegus *et al* [88] found that ΔS_M (-252 mJ cm^{-3} K^{-1}) for polycrystalline $Gd_5(Si_{1.65}Ge_{2.35})$, which orders at 222 K, was significantly smaller when compared with other reported values for alloys near this composition, and they thought it might be due to the quality of their sample or the presence of impurities. They also studied single crystal $Gd_5(Si_{1.7}Ge_{2.3})$, $T_C = 241$ K and found that there was a measurable anisotropy of the MCE: ΔS_M (all in mJ cm^{-3} K^{-1}) $= -335$ when H was parallel to the a-axis, -350 when parallel to b, and -297 when parallel to c. The average, -327 mJ cm^{-3} K^{-1}, falls close to the solid curve for the $Gd_5(Si_{1-x}Ge_x)_4$ series in figure 3. Thuy *et al* [105] and Thuy [106] reported a ΔS_M value of -150 mJ cm^{-3} K^{-1} for $Gd_5(Si_2Ge_2)$ ($T_C = 276$ K), which falls below the $Gd_5(Si_{1-x}Ge_x)_4$ data shown in figure 3. The low value may be due to co-existence of the monoclinic and orthorhombic polymorphs in their sample (see above). Thuy [106] also measured ΔS_M for higher Ge content alloys: $Gd_5(Si_{1.72}Ge_{2.28})$, $T_C = 247$ K and $\Delta S_M = -251$ mJ cm^{-3} K^{-1}; $Gd_5(SiGe_3)$, $T_C = 147$ K and $\Delta S_M = -463$ mJ cm^{-3} K^{-1}; and $Gd_5(Si_{0.32}Ge_{3.68})$, $T_C = 58$ K and $\Delta S_M = -119$ mJ cm^{-3} K^{-1}. The ΔS_M value for $Gd_5(Si_{1.72}Ge_{2.28})$ falls well below, while that for $Gd_5(SiGe_3)$ lies well above the solid curve drawn through the $Gd_5(Si_{1-x}Ge_x)_4$ data in figure 3. The MCE value for the $Gd_5(Si_{0.32}Ge_{3.68})$ alloy is much smaller than the earlier value reported by Pecharsky and Gschneidner for $Gd_5(Si_{0.33}Ge_{3.67})$, i.e. $\Delta S_M = -287$ mJ cm^{-3} K^{-1} [97]. Zhuo *et al* [107] also measured three Ge-rich $Gd_5(Si_{1-x}Ge_x)_4$ alloys: $Gd_5(Si_{0.75}Ge_{3.25})$, $T_C = 108$ K and $\Delta S_M = -377$ to -408 mJ cm^{-3} K^{-1}; $Gd_5(Si_{0.6}Ge_{3.4})$, $T_C = 92$ K and $\Delta S_M = -315$ to -355 mJ cm^{-3} K^{-1}; and $Gd_5(Si_{0.33}Ge_{3.67})$, $T_C = 67$ K and $\Delta S_M = -318$ to -358 mJ cm^{-3} K^{-1}. The results for the first alloy lie close to the $Gd_5(Si_{1-x}Ge_x)_4$ curve in figure 3, while that for the second alloy falls well below this curve. The ΔS_M for the last alloy is larger than the Pecharsky–Gschneidner value just cited above for an alloy of the same composition.

The adiabatic temperature rise has also been measured directly on $Gd_5(Si_2Ge_2)$ [108, 109]. Giguère *et al* [108] measured ΔT_{ad} by the normal technique of rapidly inserting the sample into a magnetic field and obtained a value of 8.5 K. Gschneidner *et al* [109] measured ΔT_{ad} to be 16.5 K, when the magnetic field was ramped up to a rate of 20 kOe min^{-1}. The latter value agreed quite well with the ΔT_{ad} value calculated from heat capacity measurements made on the same sample, 16.8 K [109]. This difference in values will be discussed in connection with results obtained on the $La(Fe_{1-x}S_x)_{13}$ samples, see section 10.1.

As might be expected, the $Gd_5(Si_{1-x}Ge_x)_4$ alloys which undergo an FOMT exhibit considerable hysteresis. This is discussed in the context of magnetic refrigeration, see section 11.3.1 and table 8.

5.2.1. Substitution of Gd by other R. Spichkin *et al* [110] studied the effect of Pr and Tb substitutions for Gd in $(Gd_{1-y}R_y)_5Si_4$. Both Pr and Tb lower T_C of Gd_5Si_4 (346 K) to 292 K for Pr and $y = 1.0$, and to 280 K for Tb and $y = 2.5$. Pr also lowers the MCE (ΔS_M by $\sim$25% for a field change of 50 kOe), while Tb may enhance ΔS_M slightly. When Dy replaced Gd in Gd_5Si_4, Xie *et al* [111] found that T_C was lowered in a linear fashion from Gd_5Si_4 ($T_C = 338$ K) to Dy_5Si_4 ($T_C = 140$ K) but ΔS_M was only slightly lowered, by $\sim$8% for $(Gd_{2.5}Dy_{2.5})Si_4$.

5.2.2. Theory and correlations. A simple phenomenological model was used by von Ranke *et al* [112] to correlate the influence of external parameters, i.e. magnetic field, pressure

Table 4. The magnetocaloric properties of selected $Tb_5(Si_{1-x}Ge_x)_4$ and $Dy_5(Si_{1-x}Ge_x)_4$ compounds.

Compound	Structure type	T_C (K)	$-\Delta S_M$ (mJ cm^{-3} K^{-1}) 0–50 kOe	ΔT_{ad} (K) 0–50 kOe	Density (g cm^{-3})	Ref.
Tb_5Si_4	Gd_5Si_4	225	71	—	7.206	[118]
Tb_5Si_4	Gd_5Si_4	225	72	6.8	7.206	[119]
$Tb_5(Si_3Ge)$	$Gd_5(Si_2Ge_2)$	215	50	—	7.506	[106, 119]
$Tb_5(Si_3Ge)$	Gd_5Si_4	210	63	5.8	7.506	[119]
$Tb_5(Si_2Ge_2)$	$Gd_5(Si_2Ge_2)$	116	97	—	7.589	[106, 119]
$Tb_5(Si_2Ge_2)$	$Gd_5(Si_2Ge_2)$	110	171	—	7.589	[105]
$Tb_5(Si_2Ge_2)$	$Gd_5(Si_2Ge_2)$	105	167	—	7.670	[118]
$Tb_5(Si_2Ge_2)$	$Gd_5(Si_2Ge_2)$	101	117	7.3	7.773	[119]
Tb_5Ge_4	Sm_5Ge_4	91[a]	31	—	8.303	[118]
Dy_5Si_4	Gd_5Si_4	141	96	—	7.475	[122]
$Dy_5(Si_{3.5}Ge_{0.5})$	Gd_5Si_4	136	91	4.8	7.613	[122]
$Dy_5(Si_3Ge)$	$Gd_5(Si_2Ge_2)$	65	257	—	7.739	[122]
$Dy_5(Si_{2.3}Ge_{1.5})$	Sm_5Ge_4	56	55	—	7.841	[122]
$Dy_5(Si_2Ge_2)$	Sm_5Ge_4	54	56	—	7.995	[122]
$Dy_5(SiGe_3)$	Sm_5Ge_4	50	58	—	8.284	[122]
Dy_5Ge_4	Sm_5Ge_4	46	60	—	8.563	[122]

[a] Néel temperature.

and volume deformation, on the MCE. Using two empirical parameters they determined the temperature dependence of ΔS_M for two $Gd_5(Si_{1-x}Ge_x)$ alloys, $x = 0.5$ and 0.57, and found good agreement with the experimental results. Casanova *et al* [113, 114] proposed that ΔS_M of $Gd_5(Si_{1-x}Ge_x)_4$ can be scaled with the transition temperatures, which is tuned by x and the applied field. The curve of Casanova *et al* [113, 114] above 125 K is similar to that shown in figure 3 for the $Gd_5(Si_{1-x}Ge_x)_4$ alloys.

5.2.3. Other comments. Lewis *et al* found that the MCE of $Gd_5(Si_{1.5}Ge_{2.5})$ particles could be enhanced by ∼11% and ∼20% by coatings of Fe [115] and Al [116], respectively, which is thought to be due to a strain that the coatings impart on the particles. Also see section 11.3.3.

Fujieda *et al* [117] measured the thermal conductivity (κ) and thermal diffusivity (α) of several magnetocaloric regenerator materials, including $Gd_5(Si_2Ge_2)$, from 4 to 350 K. Both α and κ of $Gd_5(Si_2Ge_2)$ fall about halfway between those of Gd (higher) and MnAs (lower), with an average value for κ of ∼5.5 W mK^{-1} between 40 and 325 K.

5.3. Other $R_5(Si_{1-x}Ge_x)_4$ systems

5.3.1. $Nd_5(Si_{1-x}Ge_x)_4$ alloys. Thuy *et al* [105] measured the MCE of $Nd_5(Si_2Ge_2)$. They did not report the crystal structure of their sample, but reported $T_C = 110$ K and $\Delta S_M = -39$ mJ cm^{-3} K^{-1}. The value for ΔS_M falls well below the dashed SOMT line shown in figure 3.

5.3.2. $Tb_5(Si_{1-x}Ge_x)_4$ alloys. After the $Gd_5(Si_{1-x}Ge_x)_4$ system, the $Tb_5(Si_{1-x}Ge_x)_4$ materials have been the second most studied R_5T_4 system. The MCE values reported for the $Tb_5(Si_{1-x}Ge_x)_4$ alloys [105, 106, 118–120] are listed in table 4. The Si-rich alloys have the orthorhombic Gd_5Si_4 structure and exhibit an SOMT. The MCE values are comparable

with those reported for other materials which have SOMT (see figures 3 and 4). There is some doubt that the structure reported for $Tb_5(Si_3Ge)$ by Thuy [106] and Thuy *et al* [120] as being the monoclinic $Gd_5(Si_2Ge_2)$ is correct, especially in view of the result reported by Huang *et al* [119], i.e. it has the orthorhombic Gd_5Si_4-type structure and the fact that MCE effect has the typical caret-like shape which is indicative of an SOMT. If it had the monoclinic structure an FOMT is expected to occur (see below) and the MCE would be two to three times as large and have a skyscraper-like shape. It is possible that interstitial impurities may have stabilized the monoclinic form for the alloy of Thuy *et al* (see section 5.1).

Four different investigators have measured the MCE of $Tb_5(Si_2Ge_2)$, and two of the studies [106, 120] {the same authors} and [119] report a substantially lower ΔS_M ($-97\,\mathrm{mJ\,cm^{-3}\,k^{-1}}$ and $-117\,\mathrm{mJ\,cm^{-3}\,K^{-1}}$, respectively) than the other two [105, 118] ($\Delta S_M = -171\,\mathrm{mJ\,cm^{-3}\,k^{-1}}$ and $-167\,\mathrm{mJ\,cm^{-3}\,K^{-1}}$, respectively). An interesting fact is that the same authors [105, 106, 120] report both the highest and lowest values; presumably that latest value reported by [106, 120] is the correct one (i.e. $\Delta S_M = -97\,\mathrm{mJ\,cm^{-3}\,K^{-1}}$). The low ΔS_M values fall on about the SOMT line of figure 3, while the high ΔS_M values lie close to the RCo_2 (FOMT) line of figure 3, point 40. Tegus *et al* [121] have also measured the MCE of '$Tb_5(Si_2Ge_2)$', but the lattice parameters are much larger than those reported by Morellon *et al* [118] and Huang *et al* [119], and it is quite likely that the sample of Tegus *et al* is richer in Ge than the composition quoted by the authors. Also, the low ordering temperature of 76 K compared with the values reported by others, 101–116 K (see table 4), also supports the proposition it has a higher Ge concentration, i.e. $Tb_5(Si_{2-x}Ge_{2+x})$. Their sample has a fairly large MCE ($\Delta S_M = -148\,\mathrm{mJ\,cm^{-3}}$) and is consistent with an FOMT.

The ΔS_M value for Tb_5Ge_4 (table 4) is quite low, but that is not unexpected since it orders antiferromagnetically.

5.3.3. $Dy_5(Si_{1-x}Ge_x)_4$ alloys. The MCE of seven alloys in the $Dy_5Si_4 - Dy_5Ge_4$ pseudo-binary has been reported by Ivtchenko *et al* [122]. Their results are listed in table 4. The two Si-rich alloys which have the Gd_5Si_4 orthorhombic structure have ΔS_M values which are slightly higher than the SOMT curve drawn in figure 3. The $Dy_5(Si_3Ge)$ alloy has the monoclinic $Gd_5(Si_2Ge_2)$-type structure and undergoes an FOMT. Its ΔS_M value falls close to the RCo_2 (FOMT) line shown in figure 3, point 41.

The four Ge-rich alloys which have the orthorhombic Sm_5Ge_4-type structure order at a fairly low, nearly constant temperature (table 4). Their ΔS_M values fall well below the SOMT line of figure 3.

5.3.4. $Ho_5(Si_2Ge_2)$. The MCE of $Ho_5(Si_2Ge_2)$ (density is $8.239\,\mathrm{g\,cm^{-3}}$), which was measured in very high-magnetic fields, is the only $Ho_5(Si_{1-x}Ge_x)$ alloy studied to date. This compound orders antiferromagnetically at ~25 K and has the Sm_5Ge_4 orthorhombic type structure [123]. The authors report $\Delta S_M = -482\,\mathrm{mJ\,cm^{-3}\,K^{-1}}$ for a 0–380 kOe field change. No lower field MCE values were given, and so it is difficult to compare this value with the ΔS_M values reported for other $R_5(Si_{1-x}Ge_x)_4$ compounds. Presumably the ΔS_M value for a 0–50 kOe field change is greater than $-63\,\mathrm{mJ\,cm^{-3}\,K^{-1}}$—the value obtained assuming ΔS_M varies linearly with field; but as shown in figure 2(*a*), ΔS_M versus H shows considerable curvature for most materials and one would expect the low field ΔS_M to be higher than a value obtained by a linear interpolation.

5.4. Sn containing R_5T_4 compounds

Ryan *et al* [124] reported that Gd_5Sn_4, which has the Sm_5Ge_4 orthorhombic type structure, exhibits a GMCE ($\Delta S_M = -336\,\mathrm{mJ\,cm^{-3}\,K^{-1}}$) at $T_C = 82$ K. This ΔS_M value is significantly

smaller than the $Gd_5(Si_{1-x}Ge_x)$ values, but somewhat larger than those of the RCo_2 phases, see figure 3, point 45.

Campoy *et al* [125] have reported on the MCE in $Gd_5(Si_2Sn_2)$. Unfortunately these authors did not report any structural data. However, Wang *et al* [126] reported that a phase of this composition had the $Gd_5(Si_2Ge_2)$ monoclinic type structure and listed the lattice constants. Using these lattice constants we were able to calculate the ΔS_M value in volumetric units. The value for the $Gd_5(Si_2Sn_2)$ compound (density is $8.850\,g\,cm^{-3}$) is $-37\,mJ\,cm^{-3}\,K^{-1}$, which is somewhat smaller than the SOMT line of figure 3.

6. Mn-based compounds

A number of different metallic manganese compounds have interesting MCE behaviours. Several of them have quite large MCE values (e.g. some of the MnAs-based and $MnFeP_{0.45}As_{0.55}$ compounds); others exhibit fairly strong negative MCEs (e.g. Mn_3GaC alloys); and others have rather unique behaviours which are associated with decoupled structural and magnetic transitions which are tens of Kelvins apart (e.g. the Ni_2MnGa Heusler alloys). In addition, there are the oxide manganites which are discussed in section 8.

6.1. $Mn(As_{1-x}Sb_x)$ alloys

The base material MnAs (density is $6.799\,g\,cm^{-3}$) undergoes a coupled structural/magnetic FOMT at $318\,K$. The ferromagnetic hexagonal NiAs-type structure transforms to the paramagnetic orthorhombic MnP-type structure upon heating or demagnetizing. The MCE values are quite large and are considered to be in the GMCE class of magnetic refrigerants: $\Delta S_M = -218\,mJ\,cm^{-3}\,K^{-1}$ and $\Delta T_{ad} = 13\,K$ for a 0 to $50\,kOe$ field change [56] at T_C. The ΔS_M value lies above the $Gd_5(Si_{1-x}Ge_x)_4$ FOMT line (figure 3, point 36), while the ΔT_{ad} value is located near the value for $La(Fe_{11.1}Si_{1.56})H_{1.5}$ data for a 0 to $50\,kOe$ field change point (figure 4, point 32). The field dependence of ΔS_M is shown in figure 2(*a*) along with several other materials. It is seen that the ΔS_M response to magnetic fields is the best among the potential magnetic refrigerant materials (figure 2(*a*)). The corresponding field dependence of ΔT_{ad} is presented in figure 2(*b*), where it falls close to Gd metal, but is somewhat less than the field dependence of $Gd_5(Si_2Ge_2)$. There is, as expected for a substance undergoing a first-order structural transition, a significant hysteresis of $6.5\,K$ [127], also see section 11.3.1 and table 8. Fujieda *et al* [117] measured the thermal conductivity (κ) and thermal diffusivity (α) of several magnetocaloric regenerator materials, including MnAs, from 4 to $350\,K$. Both the α and κ values of MnAs are the lowest of the five materials studied. The thermal conductivity slowly increases with increasing temperature from $1.2\,W\,mK^{-1}$ at $25\,K$ to $2.0\,W\,mK^{-1}$ at T_C ($318\,K$), and then it rises more rapidly to $2.7\,W\,mK^{-1}$ at $350\,K$.

Wada *et al* [56, 127, 128] have studied the effect of substituting Sb for As in MnAs. They note that Sb stabilizes the NiAs-type structure when $x \geqslant 0.1$, and the FOMT changes to SOMT, which results in a reduction of ΔS_M and ΔT_{ad}. Sb also lowers the T_C (see figure 6(*a*)). The concentration dependence of ΔS_M is shown in figure 6(*b*). As is seen, T_C decreases in an almost linear manner until $x \cong 0.25$, and then it seems to be levelling-off, while ΔS_M drops slowly with the initial substitution of Sb for As, maintaining its high ΔS_M value until $x \cong 0.20$. The $MnAs_{1-x}Sb_x$ system behaves differently from most families of magnetic refrigerant materials in that ΔS_M decreases with decreasing T_C, see figure 3, and as a result the high value for ΔS_M of MnAs falls below those of the $Gd_5(Si_{1-x}Ge_x)_4$ family at $\sim 290\,K$ and the $MnFeP_{1-x}As_x$ family at $\sim 235\,K$ when Sb is substituted for As.
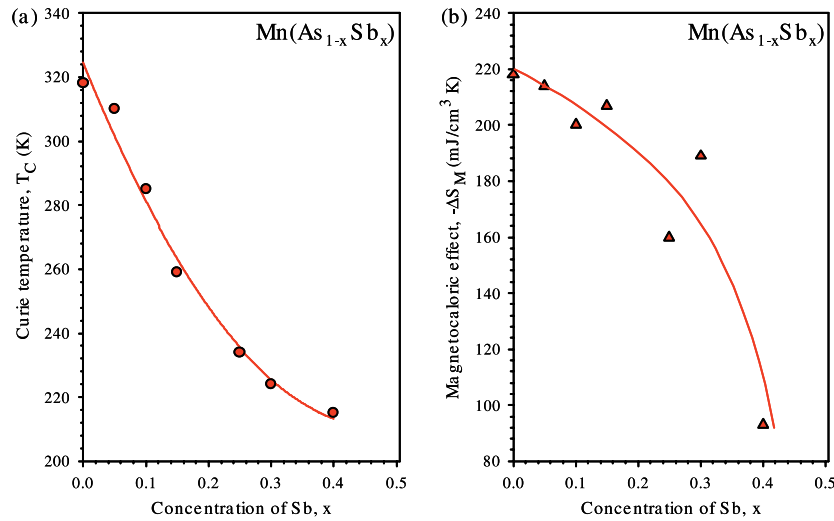
Figure 6. The Curie temperature versus composition for the $Mn(As_{1-x}Sb_x)$ alloys (*a*), and the isothermal entropy change for a 0–50 kOe field change versus composition for the $Mn(As_{1-x}Sb_x)$ alloys (*b*).

The effect of adding excess Mn to $Mn_{1+y}As_{0.75}Sb_{0.25}$ was to lower the transition from 234 K at $y = 0$ to 204 K for $y = 0.05$, but ΔS_M essentially remained the same (~ -150 mJ cm^{-3} K^{-1}) for a field change of 0 to 10 kOe [129]. For higher concentrations, i.e. $y = 0.08$ and 0.11, T_C continues to drop, but ΔS_M rapidly decreases by a factor of 10 to -14 mJ cm^{-3} K^{-1} for $y = 0.08$ and to nearly zero for $y = 0.11$.

The MCE properties of $MnAs_{1-x}Sb_x$ for $0.1 \leqslant x \leqslant 0.2$ are outstanding and these alloys are among the leading candidates as near room temperature magnetic refrigerant materials; however, the high vapour pressure of As (boiling point 876 K [603°C]) makes it difficult to prepare large quantities (tons) of MnAs in an economical way. $MnAs_{1-x}Sb_x$ is prepared by sealing the three components in a quartz tube and sintering at 873 to 1073 K for one week, then crushing the reaction products and resintering at 1073 K for another week [56, 127, 129]. A second problem is the fact that As is a governmentally regulated poison, which means special handling facilities would be required for preparing the $MnAs_{1-x}Sb_x$ material, and special environmental regulations will need to be met to place such cooling devices into commerce. Also see section 11.3.1.

6.2. $MnFe(P_{1-x}As_x)$ alloys

Recently, Tegus *et al* [130] pointed out that $MnFeP_{0.45}As_{0.55}$ (density is 7.256 g cm^{-3}) has some interesting MCE properties, $\Delta S_M = -132$ mJ cm^{-3} K^{-1} for a 0 to 50 kOe field change, and an ordering temperature of 307 K. The ΔS_M and T_C values place it close to the highest ordering $Gd_5(Si_{1-x}Ge_x)_4$ alloy [point 31 at the end of the $Gd_5(Si_{1-x}Ge_x)_4$ (FOMT) line] shown in figure 3, point 37, indicating that $MnFeP_{0.45}As_{0.55}$ is a competitive magnetic refrigerant for near room temperature applications. The effect of changing the P to As ratio on the MCE and T_C was reported by Tegus *et al* [88] in a second paper. As the As content (x) decreases, T_C is lowered (figure (7(*a*)) and ΔS_M generally increases as x decreases and seems to peak at $x = 0.35$ before falling off for smaller x (figure (7(*b*)). The increase in ΔS_M as T_C decreases is not nearly as large as that for the $Gd_5(Si_xGe_{1-x})_4$ alloys; at $T_C = 215$ K it is about two-thirds the value of that of the
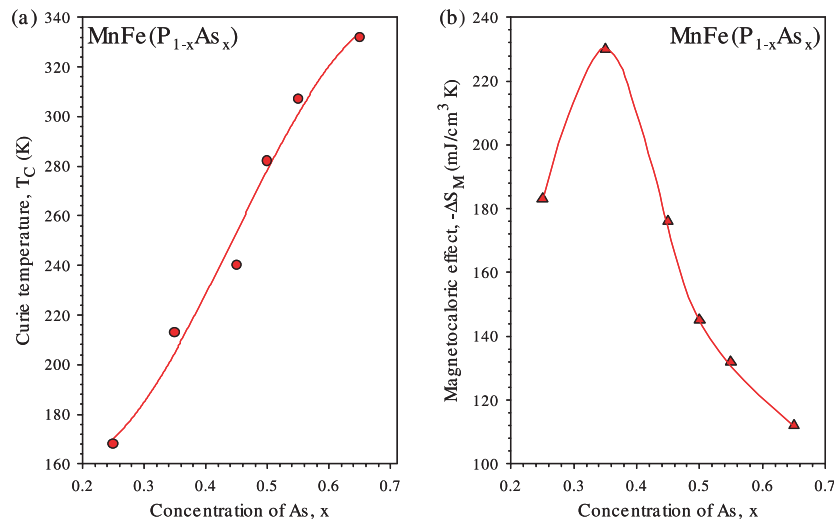
Figure 7. The Curie temperature versus composition for the MnFe($P_{1-x}As_x$) alloys (*a*), and the isothermal entropy change for a 0–50 kOe field change versus composition for MnFe($P_{1-x}As_x$) alloys (*b*).

corresponding $Gd_5(Si_xGe_{1-x})_4$ alloy (-230 versus -310 mJ cm^{-3} K^{-1}, see figure 3). All the alloys exhibit an FOMT, and there is a fairly uniform hysteresis of 4 K or 7 kOe for $0.25 \leqslant x \leqslant 0.65$ (also see section 11.3.1 and table 8). The effect of Mn substitution for Fe hardly changes T_C but increases ΔS_M, i.e. for $(Mn_{1+y}Fe_{1-y})P_{0.5}As_{0.5}$ (density is 7.267 g cm^{-3} for $y = 0.1$), T_C is lowered by 2 K at $y = 0.1$ but ΔS_M is increased by $\sim$40% from -145 to -203 mJ cm^{-3} K^{-1} [131] for a field change of 0 to 50 kOe. On the other hand, the substitution of Ge for As, i.e. MnFe($P_{0.5}As_{0.5-x}Ge_x$), has just the opposite effects—a large increase of T_C from 282 K for $x = 0$ to 570 K for $x = 0.5$, and a reduction of the MCE [132]. The only ΔS_M values reported were for $x = 0$ (density is 7.203 g cm^{-3}) and $x = 0.06$ (density is 6.575 g cm^{-3}). The MCE was reduced by more than 54% from -119 to -55 mJ cm^{-3} K^{-1} for a field change of 20 kOe.

Tegus *et al* [133] studied the effect of Cr and Co substitutions for Fe in MnFe($P_{1-x}As_x$). For the Mn($Fe_{1-x}Cr_x$)$P_{0.47}As_{0.53}$ alloy ($T_C = \sim 305$ K), Cr lowers both T_C and ΔS_M, and the FOMT changes to an SOMT: at $x = 0.02$, $T_C = \sim 275$ K and ΔS_M is lowered by $\sim$25% for $\Delta H = 20$ kOe, and at $x = 0.09$, $T_C = \sim 190$ K and ΔS_M is lowered by $\sim$65% for $\Delta H = 20$ kOe. For the alloy Mn($Fe_{1-x}Co_x$)$P_{0.5}As_{0.5}$, a 10% substitution of Co for Fe ($x = 0.1$) lowers T_C from 282 to 260 K and the ΔS_M value by $\sim$55% for $\Delta H = 20$ kOe.

The preparation of the MnFeP_{1-x}As alloys is similar to that of the MnAs$_{1-x}$Sb$_x$ alloys. For the former alloys, the components were sealed in Mo tubes and heated to 1273 K for 120 h followed by homogenization at 923 K for another 120 h, and then slow-cooled to 295 K. Although these alloys have good MCE properties, the high vapour pressure of As and its toxicity are obstacles in the utilization of MnFe$P_{1-x}As_x$ alloys in commercial devices, see the end of section 6.1 for additional comments. In addition, P presents some special problems including its high vapour pressure (boiling point 550 K [277°C] for white P and 704 K [431°C] for red P) and handling requirements. Also see section 11.3.1.

6.3. Ni–Mn–Ga Heusler alloys

The Heusler alloys have the ideal formula of Ni$_2$MnGa, but most alloys have variations of several atomic per cent from the ideal 2 : 1 : 1 composition for each component. This material

exhibits both a structural transformation (T_m) between $\sim$175 and $\sim$220 K and an FM to PM transition (T_C) between $\sim$315 and $\sim$380 K, depending upon the Ni : Mn : Ga ratios. It is interesting to note that there is an inverse relationship between T_m and T_C, i.e. the smaller T_m, the larger T_C and vice versa. The structural transformation is first order as the L1$_2$-type cubic structure changes to a tetragonal structure on cooling. Both phases are ferromagnetic, but the cubic modification is the magnetically softer phase. There has been considerable research on these alloys because of their unusual properties: large magnetostrictions, superelasticity and ferromagnetic shape memory effect. However, it was not until 2000 that the MCE properties were first reported by Hu *et al* [134], and since then several other papers have been published [88, 135–139]. All the studies indicate that there is a negative MCE associated with the first-order martensitic transition, which is quite large at low-magnetic fields and decreases as the magnetic change becomes larger. For example, Marcos *et al* [136] finds the maximum value of ΔS_M occurs at 13 kOe with $\Delta S_M = 90$ mJ cm^{-3} K^{-1} for single crystal Ni$_{49.5}$Mn$_{25.4}$Ga$_{25.1}$ ($T_m = 177$ K and density is 8.2 g cm^{-3}) with the magnetic field applied along the [100] direction. At the FM–PM transition the MCE is normal, i.e. ΔS_M has a negative value. The ΔS_M value is small at low fields and increases rapidly with increasing field. For example, Pasquale *et al* [137] report that ΔS_M increases from -15.6 to -30.0 to -144 mJ cm^{-3} K^{-1} for magnetic field changes of 0 to 10, 0 to 20 and 0 to 50 kOe, respectively, in single crystal Ni$_{51.0}$Mn$_{27.9}$Ga$_{21.1}$ (density is 8.0 g cm^{-3}) with H applied along the [100] direction. The only reported ΔT_{ad} value was given by Aliev *et al* [138] who found $\Delta T_{ad} = 1.2$ K for a field change of 0 to 26 kOe at the FM–PM transition temperature of 340 K for polycrystalline Ni$_{54.8}$Mn$_{20.2}$Ga$_{25.0}$.

More recently Albertini *et al* [139] reported an extremely large ΔS_M value (-121 mJ cm^{-3} K^{-1}) for Ni$_{54.8}$Mn$_{20.2}$Ga$_{25.0}$ (density is 7.8 g cm^{-3}) at its T_C (351 K) for a 0 to 18 kOe field change. This is the largest value reported to date for a Ni$_2$NiGa Heusler alloy for a $\Delta H < 50$ kOe. At about the same time Zhou *et al* [140] reported a large ΔS_M value for an alloy of nearly the same composition, i.e. Ni$_{55.2}$Mn$_{18.6}$Ga$_{26.2}$ (density is 8.247 g cm^{-3}). They obtained a value of -168 mJ cm^{-3} for $\Delta H = 50$ kOe at $T_C = 317$ K, and -78 mJ cm^{-3} K^{-1} for $\Delta H = 15$ kOe. The $\Delta H = 50$ kOe value (point 46 in figure 3) is slightly higher (more negative) than the ΔS_M values reported for the La(Fe$_{13-x}$Si$_x$)H$_y$ alloys. These data suggest that the Ni–Mn–Ga alloys near the Ni$_{55}$Mn$_{19}$Ga$_{26}$ composition might be good magnetic regenerator alloys for refrigerators/heat pumps operating between $\sim$300 and $\sim$350 K. The ΔS_M peak for Ni$_{55.2}$Mn$_{18.6}$Ga$_{26.2}$ for $\Delta H = 50$ kOe, however, is quite sharp, only 5 K wide at half of the peak height maximum [140], and this may limit the usefulness of the Ni–Mn–Ga Heusler alloys as a near room temperature magnetic refrigerant. For example, Gd$_5$(Si$_2$Ge$_2$) and La(Fe$_{11.44}$Si$_{1.56}$)H$_{1.5}$, which have ΔS_M peak height maxima comparable with Ni$_{55.2}$Mn$_{18.6}$Ga$_{26.2}$, have peak widths of 14 K [51] and 10 K [141] at half of the peak height maximum, respectively. The Ni$_{54.8}$Mn$_{20.2}$Ga$_{25.0}$ alloy exhibits a temperature hysteresis of 7 K, confirming this compound undergoes FOMT [139]. Also see section 11.3.1 and table 8.

The Ni–Mn–Ga Heusler alloys are fairly easy to prepare—the stoichiometric amounts of the desired alloy are just arc melted. However, to ensure that the samples are homogeneous they are heat treated in an inert atmosphere for eight to ten days at 850°C [140].

6.4. Miscellaneous compounds

6.4.1. Mn$_5$Si$_3$-based and Mn$_5$Ge$_3$-based alloys. The MCE of Mn$_5$Si$_3$ was studied by Tegus *et al* [88]. Mn$_5$Si$_3$ exhibits two FOMTs: one at 66 K between a non-collinear AFM and a collinear AFM state, and one at 99 K between the collinear AFM and PM. The ΔS_M values for Mn$_5$Si$_3$ at the lower FOMT are presented in table 5. There is no MCE peak at the upper FOMT

Table 5. The magnetocaloric properties of selected Mn-containing intermetallic compounds.

Compound	T_C (K)	$-\Delta S_M$ (mJ cm^{-3} K^{-1})		ΔT_{ad} (K)		Density (g cm^{-3})	Ref.
		0–20 kOe	0–50 kOe	0–20 kOe	0–50 kOe		
Mn$_{1.82}$V$_{0.18}$Sb	242	—	39	—	—	7.106	[144]
Mn$_{1.95}$Cr$_{0.05}$Sb	198	41	49	—	—	7.039	[88]
Mn$_3$GaC	160[a]	−103	−109	−5.5	−5.5	6.933	[145]
Mn$_{2.97}$Co$_{0.03}$GaC	130[a]	—	−96	—	—	6.937	[146]
Mn$_{2.95}$Co$_{0.05}$GaC	100[a]	—	−88	—	—	6.939	[146]
Mn$_5$Si$_3$	62.5[a]	−5.1	−24.5	—	—	5.987	[88]
DyMn$_2$Ge$_2$[b]	40	85	108	5.2	7.2	8.033	[148]
DyMn$_2$Ge$_2$[b]	35	58	−0.5	3.8	−2.4	8.033	[148]

[a] Néel temperature.
[b] Single crystal.

(99 K), but a small, normal MCE peak is observed at ∼68 K, i.e. $\Delta S_M = -8$ mJ cm^{-3} K^{-1} for a 0 to 50 kOe field change.

The ΔS_M values have been determined for a number of (Mn$_{5-x}$Fe$_x$)Si$_3$ alloys ($x = 0, 3, 4$ and 5) by Songlin et al [142]. The high Mn-containing alloys ($x = 0$ and 3) are antiferromagnetic and the Fe-rich phases ($x = 4$ and 5) are ferromagnetic. The substitution of Fe also raises the ordering temperatures: $T_{N_1} = 64$ K and $T_{N_2} = 100$ K for Mn$_5$Si$_3$ to $T_C = 375$ K for Fe$_5$Si$_3$. The MCE for Mn$_5$Si$_3$ exhibits a sharp peak slightly above T_{N_1} (70 K); a broad peak between T_{N_1} and T_{N_2} (centred at 175 K) for (Mn$_2$Fe$_3$)Si$_3$; and a caret-like peak at T_C for both (MnFe$_4$)Si$_3$ and Fe$_5$Si$_3$. In any event the $|\Delta S_M|$ values lie well below the dashed SOMT in figure 3, e.g. −25 mJ cm^{-3} K^{-1} for $\Delta H = 50$ kOe for Mn$_5$Si$_3$ (density is 5.987 g cm^{-3}).

Songlin et al [143] also measured the MCE in Mn$_5$Ge$_3$ (density is 7.241 g cm^{-3}) which orders at 298 K. The ΔS_M value for a 0 to 50 kOe field change is −67 mJ cm^{-3} K^{-1}, which is comparable with the SOMT values reported for a number of substances which order near 300 K (see figure 3). The authors also studied the substitution of Sb for Ge, Mn$_5$(Ge$_{1-x}$Sb$_x$)$_3$, and noted that T_C is increased to 312 K for $x = 0.1$ and ΔS_M is lowered to −40 mJ cm^{-3} K^{-1} for $x = 0.1$.

6.4.2. (Mn$_{1-x}$M$_x$)$_2$Sb alloys. The MCE of two (Mn$_{1-x}$M$_x$)$_2$Sb compounds (where M is a transition metal) have been studied. These compounds have the tetragonal Cu$_2$Sb-type structure. Tegus et al [88] found that (Mn$_{1.95}$Cr$_{0.05}$)Sb orders at 198 K with a modest MCE, see table 5, and essentially falls on the dashed SOMT line of figure 3.

Zhang and Zhang [144] reported on their investigation of (Mn$_{1.82}$V$_{0.18}$)Sb, which orders at 242 K. The MCE value for a 0–50 kOe field change is given in table 5, and it lies slightly below the dashed SOMT line shown in figure 3.

6.4.3. Mn$_3$GaC-based materials. Tohei et al [145] studied the MCE of Mn$_3$GaC which exhibits an FOMT from an AF to FM state with increasing temperature, which is the opposite of what occurs in most magnetic materials. As a result Mn$_3$GaC exhibits a fairly large negative MCE, see table 5. The ΔS_M value of this compound falls well above the dashed SOMT line of figure 3 and would lie on an extension of the RCo$_2$ FOMT solid line up to 160 K.

Tohei et al [146] also studied the influence of Co substitutions for Mn. They found that as the Co concentration increases both T_C and ΔS_M are lowered, see table 5.

6.4.4. Fe$_2$Mn(Si$_{1-x}$Ge$_x$). The magnetic properties of Fe$_2$MnSi$_{0.5}$Ge$_{0.5}$ (density is 7.624 g cm^{-3}), including the MCE, were measured by Zhang et al [147]. They found

$T_C = 260$ K and $\Delta S_M = -12.7$ mJ cm^{-3} K^{-1} for a field change of 50 kOe. This ΔS_M value falls far below the SOMT line established by many other intermetallic compounds shown in figure 3.

6.4.5. DyMn$_2$Ga$_2$. Wada *et al* [148] have studied the MCE in single crystalline DyMn$_2$Ge$_2$, which has two FOMTs at 36 and 40 K, and a metamagnetic transition above 40 K, and as a result the MCE behaviour is complex. A sharp, normal caret-like peak is observed at 35 K for $\Delta H = 20$ kOe, but for $\Delta H = 50$ kOe a negative MCE peak is observed, see table 5. However, above 40 K a broad table-like MCE peak is observed which is approximately constant between 40 and 47 K for $\Delta H = 20$ kOe, and between 40 and 55 K for $\Delta H = 50$ kOe, see table 5. The ΔS_M value at 40 K for $\Delta H = 50$ kOe is smaller than that of the dashed SOMT line in figure 3, but the ΔT_{ad} value is consistent with the values shown in figure 4 for $\Delta H = 50$ kOe and are significantly higher for $\Delta H = 20$ kOe.

7. La(Fe$_{13-x}$M$_x$)-based compounds

7.1. Unsubstituted La(Fe$_{13-x}$Si$_x$)

The existence of the La(Fe$_{13-x}$M$_x$) intermetallic compounds has been known since the late 1960s [149, 150], and their magnetic properties were initially characterized in the mid-1980s [151, 152]. The M element is usually Si or Al, but other metals such as Ga have been substituted for Fe. The LaFe$_{13}$ phase does not exist; as a matter of fact no intermetallic compounds form in the La-Fe binary system, and La and Fe form immiscible liquids at the Fe-rich side between $\sim$8 and 20 at% La above 1460°C [153]. Thus it is necessary to add other elements to the La–Fe alloys to form the intermetallic La(Fe$_{13-x}$M$_x$) phases. The La(Fe$_{13-x}$M$_x$) phases have the cubic NaZn$_{13}$ D2$_3$-type structure [149–152] with a lattice parameter of $\sim$11.5 Å, and tetragonal distortions have been reported for some compositions.

Palstra *et al* reported some unusual magnetic properties for the La(Fe$_{13-x}$Si$_x$) [151] and La(Fe$_{13-x}$Al$_x$) [152] phases. For the La(Fe$_{13-x}$Si$_x$) alloys T_C increases from 198 K at $x = 1.5$ to 262 K at $x = 2.5$, while the saturation magnetic moment decreases from 2.08 to 1.85 μ_B/Fe as x increases from 1.5 to 2.5. Furthermore, they noted a lattice softening near the Curie temperature which they thought was associated with the Invar effect [151]. For the La(Fe$_{13-x}$Al$_x$) system Palstra *et al* [152] found that for $x \geqslant 1.8$, a low temperature antiferromagnetic state which exhibited an extremely sharp metamagnetic transition in an applied magnetic field of a few kilooersteds, with a large hysteresis for field up versus field down. In 1999, Fujita *et al* [154] observed a large volume change ($\sim$1.5%) in La(Fe$_{11.44}$Si$_{1.56}$) just above the Curie temperature (195 K) during magnetization measurements in magnetic fields as low as 10 kOe. They claimed this behaviour was due to an IEM transition. This large volume change and the shape of the magnetization curves suggested that this alloy might have some interesting magnetocaloric properties. Indeed, a year later, Hu *et al* [155] and Zhang *et al* [156] reported that La(Fe$_{11.47}$Co$_{0.23}$Al$_{1.3}$) and La(Fe$_{10.6}$Si$_{2.4}$), respectively, exhibit a modest MCE. Subsequently a number of investigators have reported large MCE entropy changes in the La([Fe,T]$_{13-x}$Si$_x$) systems which are discussed below.

In 2001, Hu *et al* [157] were the first to find the GMCE in the La(Fe$_{1-x}$Si$_x$)$_{13}$ alloys. They reported that La(Fe$_{11.4}$Si$_{1.6}$) (density is 7.229 g cm^{-3}), which orders at 208 K, had an ΔS_M value of -140 mJ cm^{-3} K^{-1} for a magnetic field change of 0 to 50 kOe. They also found that when more of the Fe is replaced by Si the magnetic ordering temperature is raised and the MCE is substantially reduced: for La(Fe$_{10.4}$Si$_{2.6}$), $T_C = 243$ K and ΔS_M is about six times smaller than that of La(Fe$_{11.4}$Si$_{1.6}$) for a 0 to 20 kOe field change. In 2002 only
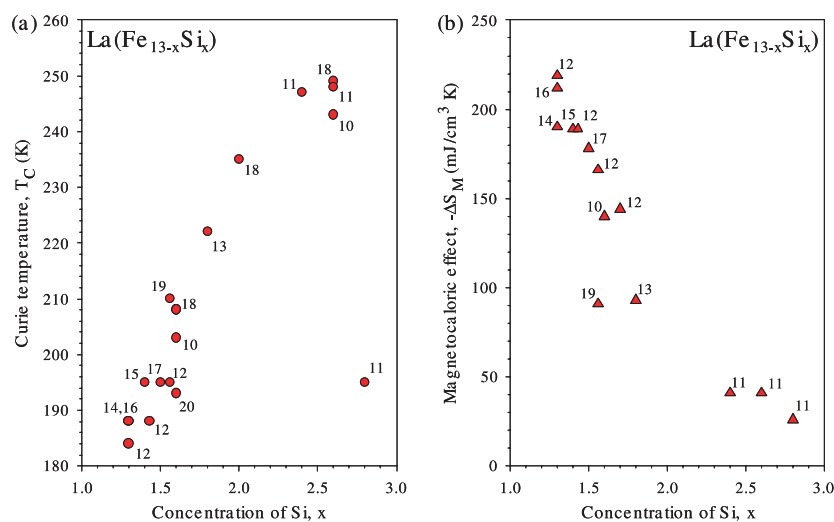
Figure 8. The Curie temperature versus Si content, x, for the La(Fe$_{13-x}$Si$_x$) alloy system (a), and ΔS_M for a 0 to 50 kOe field change versus Si content, x, for the La(Fe$_{13-x}$Si$_x$) alloy system (b).

Reference legend		
10—Hu *et al* [157]	14—Wang *et al* [160]	18—Liu *et al* [164]
11—Wen *et al* [158]	15—Chen *et al* [161]	19—Anh *et al* [165]
12—Fujita *et al* [141]	16—Hu *et al* [162]	20—Wang *et al* [166]
13—Hu *et al* [159]	17—Chen *et al* [163]	

three papers [52, 158, 159] were published on the MCE in the La(Fe$_{1-x}$Si$_x$) alloys, but all that changed in 2003 when eight additional papers [141, 159–166] were published in various journals. The T_C and ΔS_M values are plotted as a function of x in figure 8. It is seen that the Curie temperature increases monotonically from ~180 K at $x = 1.3$ to ~250 K at $x \cong 2.6$ (figure 8(a)). However, the T_C value reported for La(Fe$_{10.2}$Si$_{2.8}$) [158] is significantly out of line with the rest of the reported data. It should be noted that Wen *et al* [158] report T_C values for two other alloys ($x = 2.4$ and 2.6) which are consistent with the results reported by other investigators [52, 141, 159–166]. The T_C anomaly for $x = 2.8$ may be due to a change in the magnetic properties of the La(Fe$_{13-x}$Si$_x$) phases for $x > 2.6$ compared with those for $x < 2.6$. This is evident in the temperature dependences of the magnetization and the MCE of the $x = 2.8$ alloys compared with those for $x = 2.4$ and 2.6 [158].

The MCE as a function of x (figure 8(b)) shows that the ΔS_M drops rather rapidly with increasing x, i.e. from ~-215 mJ cm^{-3} K^{-1} at $x = 1.3$ to ~-100 mJ cm^{-3} K^{-1} at $x = 1.8$. For $x > 1.8$, ΔS_M is small and seems to level off at ~-40 mJ cm^{-3} K^{-1}. The value reported by Anh *et al* [165] for $x = 1.56$ seems to be anomalously low compared with the other reported values for the La(Fe$_{13-x}$Si$_x$) alloys. The ΔS_M versus T curves of the low x value alloys ($x \leqslant 1.7$) are sharp and have a skyscraper-like shape for low field changes (0 to 20 kOe), but broaden on the high temperature side of the MCE peak for large magnetic field changes (greater than 0 to 30 kOe). This behaviour is typical for an FOMT, e.g. see Fujieda *et al* [52]. However, for large x, i.e. >2.4, the ΔS_M versus T curves have the caret-like shape, which is typical for an SOMT, e.g. see Wen *et al* [158]. For $1.7 \leqslant x \leqslant 2.4$ the MCE peaks have a caret-like shape, but the heights are fairly large compared with those for $x \geqslant 2.4$.

The magnetization curves for an increasing field and for a decreasing field of the La(Fe$_{13-x}$Si$_x$) alloys for small x, i.e. ~1.3, have a hysteresis between 4 [141] and 6 kOe [162],

which is consistent with the magnetic transition being first order. The width of the hysteresis is ~ 2 times smaller than that typically observed in the $Gd_5(Si_xGe_{4-x})$ phases, which is about 10 kOe [167]. As expected, for those alloys which exhibit an SOMT there is no observable hysteresis, i.e. for alloys with $x \geqslant 2.4$ [158]. Hu *et al* [162] report a 3 K hysteresis in their direct measurement of ΔT_{ad} in a magnetic field of 14 kOe between an increasing field and decreasing field, which is about one-third of that observed in $Gd_5(Si_xGe_{4-x})$ alloys. Also see section 11.3.1 and table 8.

Heat capacity measurements of the $La(Fe_{13-x}Si_x)$ alloys for $x = 1.30$, 1.43 and 1.56 in magnetic fields of $H = 0$, 10, 20, 30 and 50 kOe by Fujita *et al* [141] show a sharp narrow peak at the ordering temperature, which shifts towards higher temperatures and becomes broader with increasing fields. Again, this confirms that the paramagnetic/ferromagnetic transition is first order.

X-ray powered diffraction measurement by Fujieda *et al* [168] of $La(Fe_{11.4}Si_{1.56})$ as a function of temperature from 270 to 300 K showed that the crystal structure did not change as the sample was swept through the Curie temperature (280 K) but that there was a significant shift of the x-ray diffraction peak, confirming the large volume change ($\sim 1\%$) observed in the thermal expansion measurements.

The first-order, purely magnetic transition and associated anomalous behaviours, giant magnetostrictions and the GMCE in $La(Fe_{13-x}Si_x)$ for $x < 1.7$, are due to an IEM transition, i.e. a field induced magnetic transition from the paramagnetic state to the ferromagnetic state above the respective Curie temperature [52, 141, 168, 169]. Yamada and Goto [169] showed that when spin fluctuations were included in the Ginzburg–Landau phenomenological theory, the GMCE would be expected in itinerant electron metamagnets when the coefficient of the M^4 term in the Landau energy expansion with respect to the magnetization is large and negative, which it is in the $La(Fe_{13-x}Si_x)$ phase with $x \leqslant 1.7$. Also see section 2.

Although the low x value $La(Fe_{13-x}Si_x)$ compounds exhibit large ΔS_M values, it does not follow that these materials will necessarily have large ΔT_{ad} values; in general many of the compounds reported here up to now to have large ΔS_M values do not have large ΔT_{ad} values [170]. The Japanese scientists [52, 141] have calculated ΔT_{ad} from heat capacity measurements and find them to be substantial, 8.6–12.1 K, for a magnetic field change of 0 to 50 kOe, and comparable with those of the $Gd_5(Si_xGe_{4-x})$ phases which have T_C's $\leqslant 200$ K. But for $T_C > 220$ K, the $Gd_5(Si_xGe_{4-x})$ phases have ΔT_{ad} values which are by 25–50% larger for the same field changes, see figure 10 of [171] (also unpublished data by the authors). Direct measurements of ΔT_{ad} have been reported for three $La(Fe_{13-x}Si_x)$-based alloys [141, 162, 172] and these are $\sim 25\%$ lower than the indirect values of ΔT_{ad} calculated from heat capacity measurements; this is discussed in more detail in section 7.7.

Fujita *et al* [141] noted that after repeated thermal cycles (the number was not specified) there was no observable change in the MCE values. This is consistent with the fact that there is no crystal structure change associated with IEM transitions, only a large volume change.

It should be pointed out that all the $La(Fe_{13-x}Si_x)$ samples prepared to date, including those in which La has been substituted for by Nd, and Fe by Co and Mn, and those alloys to which M and C have been added (see sections 7.3–7.6), are two phase alloys containing up to 5% α-Fe. This is not surprising considering that La and Fe form immiscible liquids (see above, section 7.1). Even long term anneals, up to 30 days, do not eliminate the second phase α-Fe. The annealing temperatures varied from 1000°C to 1050°C, and the shortest annealing period was 6 days.

Fujieda *et al* [117] measured the thermal conductivity (κ) and thermal diffusivity (α) of several magnetocaloric regenerator materials, including $La(Fe_{11.44}Si_{1.56})H_y$ for $y = 0$ and

1.0, from 4 to 350 K. The κ of the two alloys rises rapidly with increasing temperature from $\sim$1.5 W mK^{-1} at 25 K to 11.4 W mK^{-1} at 350 K. This behaviour is in contrast with the other magnetic refrigerant materials which generally do not change much with temperature. The values for the $y = 1.0$ sample are 10% to 20% higher than those for $y = 0$.

7.2. Mössbauer and neutron diffraction studies

Liu *et al* [164] carried out x-ray and Mössbauer spectroscopy studies on the La(Fe$_{13-x}$Si$_x$) alloys for $x = 1.6$, 2.0 and 2.6. They found that the La–Fe(2) distance decreased while the Fe(1)–Fe(2) distance increased, and the Fe(2)–Fe(2) distance remains unchanged as Si is substituted for Fe, i.e. as x is increased (the La atoms are located on the 8a sites, Fe(1) on the 8b sites and Fe(2) on the 96i sites of the NaZn$_{13}$-type structure). They stated that the different nature of the magnetic transitions (first order for $x = 1.6$ and 2.0 and second order for $x = 2.6$) with changing x originates from the spatial distribution of the Si atoms which only substitute for the Fe(2) atoms. They conclude that the replacement of the La–Fe pairs by La–Si pairs improves the structural stability because the average Fe–Fe distance increases with increasing x (although the lattice parameter decreases with increasing x). This larger Fe–Fe distance enhances the positive exchange interaction, which accounts for the increase of T_C with increasing x.

A Mössbauer study of La(Fe$_{10.53}$Si$_{2.47}$) by Hamdeh *et al* [173] confirmed the results reported by Liu *et al* [164] concerning the substitution of Si for the Fe(2) atoms. Furthermore, Hamdeh *et al* conclude from quadrupole splitting and isomer shift there is a redistribution of 3d electrons of Fe between the spin-up and spin-down subbands which reduces the Fe magnetic moment.

Neutron diffraction studies by Wang *et al* [166] are in disagreement with the Mössbauer results [164, 173] regarding the substitution of Si for Fe in the La(Fe$_{11.4}$Si$_{1.6}$) alloy. Wang *et al* find that the Si atoms, within experimental error of a Rietveld refinement, randomly occupy both the Fe(1) and Fe(2) sites. Furthermore, they find that all the spins are aligned ferromagnetically and the magnetic moment, p, on the Fe(1) atoms is smaller than that on the Fe(2) atoms: at 185 K ($T_C = 193$ K) $p_{Fe(1)} = 1.3\,\mu_B$ versus $p_{Fe(2)} = 1.7\,\mu_B$; and at 2 K $p_{Fe(1)} = 1.54\,\mu_B$ versus $p_{Fe(2)} = 2.16\,\mu_B$. Wang *et al* also found a large volume expansion ($\sim$1%) when the alloy orders magnetically, confirming the earlier observation of Fujita *et al* [154], and found that the paramagnetic and ferromagnetic phases coexist near T_C.

7.3. Substitution for La

Anh *et al* [165] found that Nd substitution for La in (La$_{1-z}$Nd$_z$)(Fe$_{11.44}$Si$_{1.56}$) (density is 7.233 g cm^{-3}) up to $z = 0.4$ lowered the lattice parameter linearly and slowly raised T_C from 210 to a maximum of 215 K at $z = 0.3$, which dropped to 205 K at $z = 0.4$ and lowered the MCE from $\Delta S_M = -91$ mJ cm^{-3} K at $z = 0$ to -68 mJ cm^{-3} K at $z = 0.3$ for a 0 to 50 kOe field change. These results indicate the substitution of Nd for La has an adverse effect on the MCE of the La(Fe$_{11.46}$Si$_{1.56}$) compound.

7.4. Substitution for Fe

Four studies have been carried out on the influence of Co substitutions for Fe in various La(Fe$_{13-x}$Si$_x$)-based alloys: Hu *et al* [174] studied the La(Fe$_{11.2}$Co$_{0.7}$Si$_{1.1}$) alloy (density is 7.390 g cm^{-3}), Liu and Altounian [175] the La(Fe$_{1-z}$Co$_z$)$_{11.4}$Si$_{1.6}$ series of alloys for $z = 0$ to $z = 0.10$; and Hu *et al* [159] the La(Fe$_{1-z}$Co$_z$)$_{11.2}$Si$_{1.8}$ series of alloys for $z = 0$ to $z = 0.08$. In

all cases, Co additions significantly and linearly increase T_C from ~ 210 to ~ 330 K at $z = 0.10$; but ΔS_M is lowered from -93 to -50 mJ cm^{-3} K^{-1} at $z = 0.08$ for La(Fe$_{1-z}$Co$_z$)$_{11.2}$Si$_{1.8}$ [159] and from ~ -150 to ~ -80 mJ cm^{-3} K^{-1} at $z = 0.07$ for La(Fe$_{1-z}$Co$_z$)$_{11.4}$Si$_{1.6}$ [175]. Liu *et al* [176] studied the magnetic transitions in the La(Fe$_{1-z}$Co$_z$)$_{11.4}$Si$_{1.6}$ alloys (where $0 \leqslant z \leqslant 0.08$) by dc magnetization measurements and Mössbauer spectroscopy and concluded that Co substitution for Fe ($z \geqslant 0.02$) drives the first-order ferromagnetic–paramagnetic transition towards second order, eliminating IEM transition.

Wang *et al* [160] found that the substitution of small amounts of Mn for Fe in La(Fe$_{1-z}$Mn$_z$)$_{11.7}$Si$_{1.3}$ (where $0 \leqslant z \leqslant 0.03$) has a large effect on T_C and the MCE. The Curie temperature is rapidly lowered in a nearly linear fashion from 188 K at $z = 0$ to 127 K at $z = 0.03$. The initial substitution of Mn ($z = 0.01$) barely changes the MCE, i.e. $|\Delta S_M|$ decreases from -190 to -187 mJ cm^{-3} K^{-1}. However, for larger amounts of Mn, the MCE drops off quite rapidly to -151 mJ cm^{-3} K^{-1} for $z = 0.02$ and -123 mJ cm^{-3} K^{-1} for $z = 0.03$. The influence of Mn on T_C is just the opposite of Co substitution, while the two alloying agents have a similar effect on the MCE: it is lowered, but the ΔS_M versus z plots are somewhat different.

7.5. Addition of interstitial elements—hydrogen

To date only H and C additions to La(Fe$_{13-x}$Si$_x$) have been studied, and the behaviours of these two interstitial elements are different. Both interstitials raise T_C, but C additions drastically lower ΔS_M, while for H additions, ΔS_M slightly decreases while ΔT_{ad} exhibits a large increase.

The hydrogen addition studies were carried out by Chen *et al* [177] on La(Fe$_{11.5}$Si$_{1.5}$)H$_y$ and by Fujita *et al* [141] and Fujieda *et al* [168] on various La(Fe$_{13-x}$Si$_x$)H$_y$ samples. The results reported by Chen *et al* [177] are based on magnetization measurements, while Fujita *et al* determined the MCE from heat capacity measurements as a function of temperature and magnetic field and from magnetization measurements [141] and by direct measurement of ΔT_{ad} [172]. The Curie temperature dependence on y is shown in figure 9(*a*), where it is seen that T_C increases in a linear fashion with increasing y, and is essentially independent of the Fe to Si ratio. The hydrogen concentration dependences of the MCE (both ΔS_M and ΔT_{ad}) are shown in figure 9(*b*), where ΔS_M slightly decreases with increasing y (ignoring the low values reported by Chen *et al* for $y = 0.3$ to $y = 1.5$), but ΔT_{ad} increases by about 50% when $y = 1.5$ compared with $y = 0$. According to Fujita *et al* [141], this non-parallelism between ΔS_M and ΔT_{ad} is due to the fact that the lattice heat capacity, C_L, remains essentially constant as y increases but that T_C increases with y, and thus C_L / T_C decreases, and since $\Delta T_{ad} \propto T/C$ (see equation (4) of [141]), ΔT_{ad} rises rapidly with increasing H content. However, when one examines the ΔT_{ad} values for a 0 kOe to 20 kOe magnetic field change, ΔT_{ad} remains essentially constant, i.e. $= 6.5$ K, 6.0 K, 6.2 K and 6.8 K for $y = 0$, 0.5, 1.0 and 1.5, respectively. This behaviour is more or less consistent with the nearly constant ΔS_M value for both the 0 to 20 kOe and 0 to 50 kOe field changes. Thus the explanation for the non-parallelism may be more complicated than what was proposed by the authors of [141].

The results reported for ΔS_M versus y by Chen *et al* [177] (see squares in figure 9(*b*)) are a little difficult to understand in view of the results of Fujita *et al* [141] (noted above and the circles in figure 9(*b*)), especially since the $y = 0$ and $y = 1.8$ values for ΔS_M reported by Chen *et al* are in good agreement with the data of Fujita *et al*. No explanation was given by Chen *et al* for this discrepancy. As seen in figure 9(*a*) all the results reported by the two groups for the variation of T_C versus y are in excellent agreement, and thus we conclude that the alloys, which have anomalously low ΔS_M values, have the correct hydrogen content. Thus the anomaly is not due to an incorrect hydrogen concentration. A possible explanation is that the starting
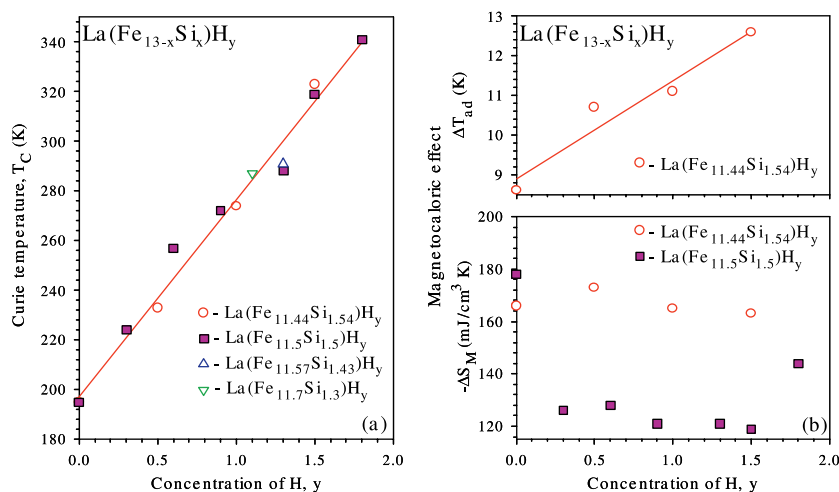
Figure 9. The Curie temperature versus the hydrogen concentration, y (*a*) and the adiabatic temperature rise (top) and the magnetic entropy change (bottom) versus the hydrogen concentration, y (*b*) for the La(Fe$_{13-x}$Si$_x$)H$_y$ alloy system.

Table 6. The Curie temperature, magnetic entropy change and adiabatic temperature rise for some La(Fe$_{13-x}$Si$_x$)H$_y$ alloys for a magnetic field change of 0–50 kOe.

Compound	T_C (K)	$-\Delta S_M$ (mJ cm^{-3} K^{-1})	Density (g cm^{-3})	ΔT_{ad} (K)
La(Fe$_{11.7}$Si$_{1.3}$)H$_{1.1}$	287	222	7.156	15.4
La(Fe$_{11.57}$Si$_{1.43}$)H$_{1.3}$	291	200	7.139	12.8
La(Fe$_{11.44}$Si$_{1.56}$)H$_{1.0}$	274	165	7.164	11.1

La(Fe$_{13-x}$Si$_x$) master alloys for making the hydrogen containing alloys are of two slightly different Fe to Si ratios. That is, the master alloy for $y = 0$ and 1.8 had a composition close to La(Fe$_{11.44}$Si$_{1.56}$) and that for the five alloys with $y = 0.3$ to 1.5 has a composition close to La(Fe$_{11.3}$Si$_{1.7}$). As discussed below, and shown in table 6, the Fe to Si ratio is more critical than the hydrogen content in determining ΔS_M.

As seen in figure 9(*a*), there is an excellent correlation between T_C and the hydrogen content, y, regardless of the Fe : Si ratio; and for a fixed Fe : Si ratio, ΔT_{ad} and ΔS_M show a dependence on y (figure 9(*b*)). A closer examination of the available data indicates that both ΔT_{ad} and ΔS_M have a strong dependence on the Fe : Si ratio at a fixed y value. This is quite evident as shown in table 6 for the three La(Fe$_{13-x}$Si$_x$)H$_y$, where $y \cong 1.1$, the higher the Fe content the larger ΔS_M and ΔT_{ad}. This is also consistent with the data obtained for these alloys where $y = 0$, see figure 8(*b*).

The thermal conductivity and thermal diffusivity of La(Fe$_{11.44}$Si$_{1.56}$)H$_{1.0}$ has been measured by Fujieda *et al* [117], see the end of section 7.1 for more details and a comparison with the alloy of the same La : Fe : Si ratios but without any hydrogen.

7.6. Addition of interstitial elements—carbon

Chen *et al* studied the effect of C additions to La(Fe$_{11.6}$Si$_{1.4}$)C$_y$ [161] and to La(Fe$_{11.5}$Si$_{1.5}$)C$_y$ [163]. In both cases, carbon increased T_C by about the same amount for the same y value,

from 195 K for $y = 0$ to 250 K for $y = 0.6$, but ΔS_M was lowered—somewhat for low values of y ($\leqslant 0.2$) and then much more rapidly for $y \geqslant 0.4$—e.g. for the LaFe$_{11.5}$Si$_{1.5}$C$_y$ alloys it dropped from ~ -178 mJ cm^{-3} K^{-1} for $y = 0$ to -165 mJ cm^{-3} K^{-1} at $y = 0.2$ and to -91 mJ cm^{-3} K^{-1} at $y = 0.5$. This rapid drop in ΔS_M for $y \geqslant 0.4$ occurs because the first-order IEM transition changes to a second-order transition.

7.7. Direct measurement of MCE

The adiabatic temperature rise has been measured directly for three alloys of the La(Fe$_{13-x}$Si$_x$)H$_y$ series. Hu *et al* [162] reported a ΔT_{ad} value of 4 K for a 0 to 14 kOe field increase at 183 K for La(Fe$_{11.7}$Si$_{1.3}$). Assuming a linear magnetic field dependence we estimate a ΔT_{ad} value of 5.7 K for a 0 to 20 kOe field change, which is probably a little high by 0.2–0.5 K. But since they did not make calorimetric measurements, this value cannot be compared with an indirect value obtained on the same sample. However, Fujita *et al* [141] reported an indirect $\Delta T_{ad} = 8.1$ K for a 0 to 20 kOe field change for an alloy of the same composition and $T_C = 184$ K—a difference of 30%. But since the measurements were made on two different samples, some variation might be expected, but not 30%. Fujieda *et al* [172] also made both indirect and direct ΔT_{ad} measurements on the same sample, La(Fe$_{11.44}$Si$_{1.56}$). The directly measured ΔT_{ad} value was 6 K at $T_C = 188$ K for a 0–20 kOe field change, which compared with a calculated value of 7.6 K as determined from heat capacity measurement as a function of temperature and magnetic field—a discrepancy of $\sim 20\%$. Fujieda *et al* [172] also measured ΔT_{ad} for La(Fe$_{11.44}$Si$_{1.56}$)H$_{1.6}$ and reported a measured value of 4 K for a 0–20 kOe field change at $T_C = 319$ K which is probably lower than the indirect value by 2 to 3 K, based on his indirect values for samples with a similar Fe : Si ratio and similar hydrogen doping levels—a discrepancy of 50–75%. This topic is further addressed in section 10.1.

7.8. La(Fe$_{13-x}$Al$_x$)-based alloys

Not nearly as much work has been done on the Al-substituted alloys as for the Si-substituted ones, primarily because the MCE is rather modest. Hu *et al* [178] reported that La(Fe$_{11.375}$Al$_{1.625}$) exhibited two magnetic transitions, $T_N = 181$ K (a second-order paramagnetic to antiferromagnetic transition) and $T_C = 140$ K (a first-order antiferromagnetic to ferromagnetic transition). The MCE exhibits two peaks, a sharp one at 140 K and a broad one at 180 K. The upper peak is quite small at low-magnetic fields, but becomes more pronounced as the magnetic field increases, especially for $H > 20$ kOe, and it exceeds the first-order peak by 20% at 50 kOe (ΔS_M for a 0–50 kOe field change is -44 mJ cm^{-3} K^{-1} at 140 K and -54 mJ cm^{-3} K^{-1} at 181 K). In a second paper, Hu *et al* [53] reported that this alloy has the cubic NaZn$_{13}$-type structure from room temperature down to ~ 10 K, but there is a large lattice parameter discontinuity at ~ 140 K which is consistent with the first-order nature of the transition at this temperature. The authors [178] reported there is a 5 K hysteresis associated with this transition. Since the two ordering peaks are only 40 K apart, the MCE has a table-like characteristic making it a candidate magnetic refrigerant for the Ericsson cycle [53]. The authors also note that even in a small field there is a large change in ΔS_M, i.e. $\Delta S_M = -22$ mJ cm^{-3} K^{-1} for $\Delta H = 5$ kOe.

Hu *et al* [155] also studied the MCE behaviour of La(Fe$_{11.47}$Co$_{0.23}$Al$_{1.3}$) and noted that this small amount of Co is sufficient to change La(Fe$_{11.7}$Al$_{1.3}$) from an antiferromagnet to a ferromagnet with $T_C = 198$ K. The ΔS_M value for $\Delta H = 50$ kOe is -10.6 J kg^{-1} K^{-1} (i.e. ~ -74 mJ cm^{-3} K^{-1}—the exact volumetric value cannot be determined because neither the lattice parameter nor the density were given), which is quite a bit smaller than the GMCE values

reported for the $La(Fe_{13-x}Si_x)$ and $Gd_5(Si_{4-x}Ge_x)$ alloys (~-160 to $\sim-200\,mJ\,cm^{-3}\,K^{-1}$) which have comparable T_C values.

Liu *et al* [179] reported the variation of the lattice parameters, magnetization, Curie temperature and MCE (ΔS_M) for the $LaFe_{11}(Si_{2-z}Al_z)$ pseudo-binary system. As might be expected from the values of the two end members, T_C and ΔS_M both decrease as Si is replaced by Al, while the lattice parameter increases.

8. Manganites

The rare-earth manganites have been known for over 50 years [180], but their interesting magnetocaloric properties were not reported until 1996 [7]. Since then, their MCEs have been heavily studied, but to date the highest reported values are reasonable, but not outstanding like those reported for several families of compounds discussed in the previous sections (4.1.1, 5, 6.1, 6.2, 6.3 and 7). As a matter of fact several of the manganites have ΔS_M values comparable with Gd, but most are smaller.

Another major problem is that the MCE values reported by different groups generally vary quite widely (factors of 2 are not uncommon, and factors as much as 7 can be found among the data reported in the literature). Part of this difficulty is that the phase diagrams are very complex [180], and slight changes in the chemical compositions including oxygen deficiencies could easily account for differences in behaviour and in the reported values. Also heating and processing variables can contribute to this problem. This is evident when one examines figure 10, where ΔS_M is plotted against T_C for a magnetic field change of 0–10 kOe. As one can see, there is no correlation, not like what is observed for other families of compounds, see figure 3.

The preparation of the manganites is generally quite involved, regardless of the method used: mixing of the solid components, a sol–gel process or an aqueous process. After the initial mixing of the starting ingredients by one of these three methods, the mixture is heated to between 800°C and 1200°C for 10–24 h, cooled, reground, reheated, cooled, ground once more and then sintered into pellets.

8.1. $(La_{1-x}M_x)MnO_3$ where M = Na and Ag

Chen *et al* [181] measured the change in the MCE of rhombohedral $(La_{0.8}Na_{0.2})MnO_{3-\delta}$ as a function of the oxygen deficiency, δ, up to $\delta = 0.07$. They found that the maximum ΔS_M value ($\Delta S_M = -23.2\,mJ\,cm^{-3}\,K^{-1}$ for $\Delta H = 10\,kOe$ at 364 K) occurs for $\delta = 0.06$, which is one of the highest ΔS_M values reported for a manganite phase, see figure 10, point 2. But when compared with other materials, see figure 3, the ΔS_M value is quite small. This phase also has one of the highest Curie temperatures for manganite materials.

The MCE of some rhombohedral $(La_{1-x}Ag_x)MnO_3$ phases was reported by Tang *et al* [182] for $x = 0.05, 0.20, 0.25$ and 0.30 and by Wang *et al* [183] for $x = 0.22$. The compounds for $x = 0.05, 0.25$ and 0.30 exhibit an SOMT and the ΔS_M value is quite small ($\sim$one half) compared with that for $x = 0.20$ ($\Delta S_M = -22.8\,mJ\,cm^{-3}K^{-1}$), which undergoes an FOMT at 278 K [182]. This value is somewhat larger than that reported for $(La_{0.78}Ag_{0.22})MnO_3$ at $T_C = 301\,K(-18.2\,mJ\,cm^{-3}K^{-1})$. Both values are for $\Delta H = 10\,kOe$ and are shown in figure 10, points 3 and 4, respectively.

8.2. $(La_{1-x}Ca_x)MnO_3$

8.2.1. La deficiency. The MCE of the $(La_{1-x}Ca_x)MnO_3$ phases has been extensively studied, probably the most thoroughly investigated manganite family. Chen *et al* [184] have studied the
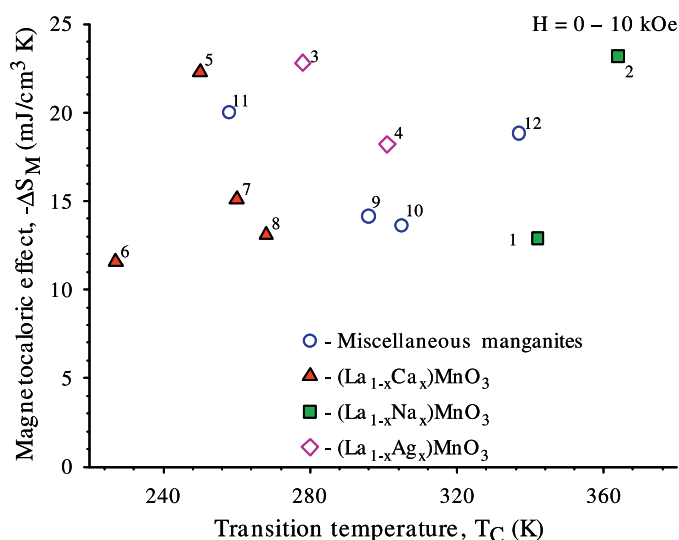
Figure 10. The magnetocaloric entropy change for $\Delta H = 10\,\mathrm{kOe}$ of the lanthanide manganites versus the Curie temperature. A magnetic field change of 0–10 kOe was used, since a major fraction of the manganites were studied at low-magnetic fields, <30 kOe. The most common field change was for 0–10 kOe, while ΔS_M values measured in 50 kOe were rare. The value for $(La_{0.835}Na_{0.165})MnO_3$, point 1, was taken from [7], the remaining values are taken from the references cited in section 8.

<div align="center">Compound legend</div>

1—$(La_{0.835}Na_{0.165})MnO_3$ [6.142]	7—$(La_{0.60}Ca_{0.40})MnO_3$ [5.705]
2—$(La_{0.8}Na_{0.2})MnO_{2.94}$ [6.009]	8—$(La_{0.60}Ca_{0.40})MnO_3$ [5.683]
3—$(La_{0.8}Ag_{0.2})MnO_3$ [6.699]	9—$(La_{0.66}Ca_{0.11}Pb_{0.23})MnO_3$ [6.704]
4—$(La_{0.78}Ag_{0.22})MnO_3$ [6.682]	10—$(La_{0.65}Sr_{0.35})MnO_3$ [6.4]
5—$(La_{0.77}Ca_{0.20})MnO_3$ [5.938]	11—$(Nd_{0.67}Sr_{0.33})MnO_3$ [6.3]
6—$(La_{0.70}Ca_{0.30})MnO_3$ [5.957]	12—$(La_{0.67}Ba_{0.33})MnO_3$ [6.797]

effect of La deficiencies on T_C and the MCE of $(La_{0.8-y}Ca_{0.2})MnO_3$ (density is $5.938\,\mathrm{g\,cm^{-3}}$). The Curie temperature rises from 182 K for no La deficiency to 260 K for $y = 0.05$, and then T_C tends to remain nearly constant or decrease slightly up to $y = 0.10$. As y increases, the nature of the magnetic transformation changes from SOMT (for $y = 0$ and 0.01) to FOMT (for $y = 0.03$ to 0.10), and the maximum value of the MCE increases from $\Delta S_M = -7.7$ at $y = 0$ to $\Delta S_M = -22.3\,\mathrm{mJ\,cm^{-3}K^{-1}}$ at $y = 0.03$ for $\Delta H = 10\,\mathrm{kOe}$ (point 5 in figure 10). For $0.05 \leqslant y \leqslant 0.10$, ΔS_M remains approximately constant at $-16.0\,\mathrm{mJ\,cm^{-3}\,K^{-1}}$. Phan *et al* [185] also studied the influence of La deficiencies in single crystalline $(La_{0.8-y}Ca_{0.2})MnO_3$ for $y = 0.05$ and 0.20. The results reported by the latter authors differ considerably from Chen *et al*'s results noted above. The T_Cs for $y = 0.05$ differ by nearly 100 K (170 K for Phan *et al*'s sample versus 260 K for Chen *et al*'s sample) and ΔS_M is considerably smaller when considering the difference in the magnetic field change of $-18.5\,\mathrm{mJ\,cm^{-3}\,K^{-1}}$ (assuming a density of $5.94\,\mathrm{g\,cm^{-3}}$) for a $\Delta H = 50\,\mathrm{kOe}$ [185] versus $-16.0\,\mathrm{mJ\,cm^{-3}\,K^{-1}}$ for $\Delta H = 10\,\mathrm{kOe}$ [184]. Phan *et al* reported that they observed spin glass behaviour in their sample ($y = 0.05$) with $T_{SG} = 100\,\mathrm{K}$, which may account for some of the differences in the properties of the two $(La_{0.75}Ca_{0.2})MnO_3$ samples.

8.2.2. Unsubstituted La or Ca. Another study [55] of a single crystal, specifically $(La_{0.7}Ca_{0.3})MnO_3$ (density is $5.947\,\mathrm{g\,cm^{-3}}$), is consistent with the results noted in the previous

paragraph. Sun *et al* [186] report $T_C = 227$ K and $\Delta S_M = -11.6$ mJ cm^{-3} K^{-1} for $\Delta H = 10$ kOe (point 6 in figure 10) and -38.3 mJ cm^{-3} K^{-1} for $\Delta H = 50$ kOe. The more recent results reported by Phan *et al* [187] for both a single crystal and a polycrystalline sample of this composition are essentially identical to those reported by Sun *et al* .

Both Sun *et al* [186] and Xu *et al* [188] measured the MCE (ΔS_M) for $(La_{0.67}Ca_{0.33})MnO_3$ (density is 5.947 g cm^{-3}). The former gives $\Delta S_M = -38.1$ mJ cm^{-3} K^{-1} at $T_C = 267$ K for a 0–30 kOe magnetic field change, while the latter reports -20 mJ cm^{-3} K^{-1} at $T_C = 275$ K for $\Delta H = 20$ kOe. These results are in reasonable agreement with each other considering the difference in the magnetic field change. The MCE properties of orthorhombic $(La_{0.6}Ca_{0.4})MnO_3$ were studied by Bohigas *et al* [189] and Dinesen *et al* [190] for several field changes between $\Delta H = 5$ kOe and $\Delta H = 30$ kOe (by both groups). The lattice parameters were given by both groups; in general those reported by Dinesen *et al* were larger by about 0.01 A and thus the density was slightly smaller, 5.705 g cm^{-3} [189] versus 5.683 g cm^{-3} [190]. Also, T_C was larger (268 K versus 260 K), but the MCE values for the corresponding field changes were ~15% smaller for the material of Dinesen *et al*. The $\Delta H = 10$ kOe values are shown in figure 10, points 7 [189] and 8 [190]. The preparation techniques might account for these differences: Bohigas *et al* [189] used a solid state technique, while Dinesen *et al* [190] used an aqueous approach.

8.2.3. Substitution for La. The substitution of other lanthanides for La has been reported by Wang *et al* [191] for Nd substitutions and by Chen *et al* [192] for Ce, Gd, Tb and Dy substitutions. Wang *et al* studied $(La_{0.7-y}Nd_yCa_{0.3})MnO_3$ (density is 5.957 g cm^{-3} for $y = 0$) at doping levels of $y = 0$, 0.03, 0.10, 0.15 and 0.20. They found that ΔS_M increased and T_C decreased with increasing x. ΔS_M for $\Delta H = 10$ kOe rose from -8.2 mJ cm^{-3} K^{-1} ($T_C = 256$ K) at $y = 0$ to -13.9 mJ cm^{-3} K^{-1} ($T_C = 213$ K) at $y = 0.20$.

In contrast to the continuous increase in ΔS_M noted in the previous paragraph for $(La_{0.7-y}Nd_yCa_{0.3})MnO_3$, Chen *et al* [192] found the ΔS_M value peaked at $x = 0.1$ for $([La_{1-y}R_y]_{0.67}Ca_{0.33})MnO_3$, where R = Ce, Gd, Tb and Dy. In most cases, doping concentration of $y = 0, 0.1$ and 0.3 were studied, except for Gd, where only $y = 0.1$ was investigated. The base parameters (i.e. $y = 0$ (density is 5.947 g cm^{-3})) were: $\Delta S_M = -22.9$ mJ cm^{-3} K^{-1} at $T_C = 246$ K for a $\Delta H = 15$ kOe. The maximum ΔS_M values ($y = 0.1$) for the same field change are: -27.0 mJ cm^{-3} K^{-1} for Ce; -34.8 mJ cm^{-3} K^{-1} for Gd; -28.7 mJ cm^{-3} K^{-1} for Tb; and -36.8 mJ cm^{-3} K^{-1} for Dy. ΔS_M appears to increase with increasing atomic number, except for Tb. The depression of T_C is greatest in Tb, followed by Dy, Gd and Ce in decreasing effectiveness.

8.2.4. Substitution for Ca. Sr and Pb substitutions for Ca in $(La_{1-x}Ca_x)MnO_3$ have been reported by Zhang *et al* [193] and Sun *et al* [194], respectively. Zhang *et al* studied orthorhombic $(La_{0.75}[Ca_{1-y}Sr_y]_{0.25})MnO_3$ (density is 6.21 g/cm^{-1} for $y = 0.075$) for $y = 0.075$ and 0.10. For $y = 0.075$ the MCE values for a 0–14 kOe field change are $\Delta T_{ad} = 0.78$ and $\Delta S_M = -16.7$ mJ cm^{-3} K^{-1} at $T_C = 295$ K. With additional Sr ($y = 0.10$), the peak at T_C changes from a sharp peak to a broad flat maximum between 285 and 315 K, with $\Delta T_{ad} = 0.49$ K; no ΔS_M value was reported for this composition.

Sun *et al* [194] studied an orthorhombic $(La_{0.66}Ca_{0.11}Pb_{0.23})MnO_3$ single crystal which had been grown from a PbF$_2$/PbO flux. The MCE was determined for four field changes, $\Delta H = 10$, 20, 40 and 70 kOe. The ΔS_M value for $\Delta H = 10$ kOe is -14.1 mJ cm^{-3} K^{-1}, point 9 in figure 10. They concluded that the manganites do not seem to be promising candidates for magnetic refrigeration.

8.3. $(R_{1-x}Sr_x)MnO_3$

8.3.1. $(La_{1-x}Sr_x)MnO_3$. Demin and Koroleva [195] investigated ΔT_{ad} for a series of single crystal $(La_{1-x}Sr_x)MnO_3$ compounds, where $0.1 \leqslant x \leqslant 0.3$, and found that both ΔT_{ad} and T_C increased with an increased Sr level. The ΔT_{ad} values for $\Delta H = 8.2\,kOe$ and T_C values are: 0.2 K at 175 K for $x = 0.1$; 0.37 K at 180 K for $x = 0.125$; 0.7 K at 260 K for $x = 0.175$; and 0.78 K at 346 K for $x = 0.3$. Szewczyk *et al* [196] measured the MCE properties of $(La_{0.845}Sr_{0.155})MnO_3$ (the density is $\sim 6.3\,g\,cm^{-3}$) for a field change of 70 kOe. They report $\Delta T_{ad} = 3.3\,K$ as measured directly, and 3.5 as calculated from the heat capacity at $T_C = 234\,K$; and $\Delta S_M = -42\,mJ\,cm^{-3}\,K^{-1}$.

Xu *et al* [188] reported that $\Delta S_M = -1.7\,mJ\,cm^{-3}\,K^{-1}$ at $T_C = 368\,K$ for $\Delta H = 0.5\,kOe$ for $(La_{0.67}Sr_{0.33})MnO_3$ (density is $6.230\,g\,cm^{-3}$). The MCE of $(La_{0.65}Sr_{0.35})MnO_3$ (density is $\sim 6.4\,g\,cm^3$) was investigated by Phan *et al* [197]. They report $\Delta S_M = -13.6\,mJ\,cm^{-3}\,K^{-1}$ for a field change of 10 kOe (point 10 in figure 10) and $T_C = 305\,K$.

8.3.2. Substitution for Sr or Mn. Phan *et al* [197] studied the effect of substituting Ca and Ba for Sr. For $(La_{0.6}Sr_{0.2}Ca_{0.2})MnO_3$ (density is $\sim 6.3\,g\,cm^{-3}$) they reported $T_C = 337\,K$ and $\Delta S_M = -12.3\,mJ\,cm^{-3}\,K^{-1}$ for $\Delta H = 10\,kOe$, and for $(La_{0.6}Sr_{0.2}Ba_{0.2})MnO_3$ with a density of $\sim 6.5\,g\,cm^{-3}$ they give $T_C = 354\,K$ and $\Delta S_M = -14.7\,mJ\,cm^{-3}\,K^{-1}$ for the same field change. It is difficult to state whether the Ca or Ba substitutions are beneficial or not since the unsubstituted compound had a different La to Sr ratio, i.e. $(La_{0.65}Sr_{0.35})MnO_3$ (see previous paragraph). Considering that the ΔS_M values are for $\Delta H = 10\,kOe$ and the high T_C values, these two compounds are potential candidate active magnetic regenerator materials above room temperature, especially $(La_{0.6}Sr_{0.2}Ba_{0.2})MnO_3$.

Chau *et al* [198], on the other hand, substituted Cu for Mn in the compound $(La_{0.7}Sr_{0.3})(Mn_{1-z}Cu_z)O_3$, where $z = 0.05$ and 0.10 (the densities are 6.311 and 6.298 $g\,cm^3$, respectively). The T_C value was the same for both values of z, 350 K, while $\Delta S_M = -12.4\,mJ\,cm^{-3}\,K^{-1}$ for $z = 0.05$ and $-13.0\,mJ\,cm^{-3}\,K^{-1}$ for $= 0.10$ for a field change of 12.5 kOe. Again no information was given for the unsubstituted compound and so comparisons and/or trends cannot be made or established.

8.3.3. $(Nd_{0.67}Sr_{0.33})MnO_3$. Si *et al* [199] measured the MCE in $(Nd_{0.67}Sr_{0.33})MnO_3$ (density is $\sim 6.3\,g\,cm^{-3}$) for field changes of 10, 15, 20, 30 and 50 kOe. For $\Delta H = 10\,kOe$, $\Delta S_M = -20\,mJ\,cm^{-3}\,K^{-1}$ at $T_C = 257.5\,K$, point 11 in figure 10. The $\Delta H = 50\,kOe$ value of ΔS_M is $-47\,mJ\,cm^{-3}\,K^{-1}$, which falls close to the SOMT line in figure 3.

8.4. Charge Order

In some of the $(R_{1-x}Sr_x)MnO_3$ compounds when the FM-metallic state transforms to a low temperature AFM-insulator state a spatial ordering of the Mn^{3+} and Mn^{4+} ions occurs. This first-order transition is known as a charge order transition, with a characteristic temperature T_{CO}. At T_{CO}, there is a sudden large change in the lattice parameters (usually a and b increase and c decreases), but the unit cell volume hardly changes [200]. Magnetic fields have a large influence on T_{CO}, i.e. a 50 kOe field change lowers T_{CO} by $\sim 40\,K$ and induces a large negative MCE (i.e. a positive ΔS_M). There is also a large hysteresis associated with the influence of the magnetic field on the charge ordering, i.e. $\sim 10\,kOe$ and $\sim 10\,K$ near T_{CO}.

8.4.1. $(Pr_{1-x}Sr_x)MnO_3$. Chen *et al* [201] studied the $(Pr_{1-x}Sr_x)MnO_3$ system at three different compositions, $x = 0.3$, 0.4 and 0.5. As x increases, T_C was lowered from 260 K

($x = 0.3$) to 243 K ($x = 0.4$) to 205 K ($x = 0.5$), and the ΔS_M for $\Delta H = 10$ kOe increased from -11.6 to -13.1 to -17.5 mJ cm^{-3} K^{-1} for the respective x values. Of these three compositions, only the $(Pr_{0.5}Sr_{0.5})MnO_3$ phase (density is 6.650 g cm^{-3}) exhibited charge ordering at $T_{CO} = 161$ K and $\Delta S_M = +47.2$ mJ cm^{-3} K^{-1} for $\Delta H = 10$ kOe. Chen and Du [202] found that when Nd is substituted for Pr in $([Pr_{1-y}Nd_y]_{0.5}Sr_{0.5})MnO_3$ ($y = 0$, 0.3, 0.5, 0.7 and 1.0), T_C and T_{CO} are increased from 205 to 267 K for T_C and from 161 to 183 K for T_{CO}, but ΔS_M seems to be approximately constant ($\sim 47.5 \pm 5.0$ mJ cm^{-3} K^{-1}) for a change of 10 kOe for the five samples, varying from $+43.2$ mJ cm^{-3} K^{-1} for $y = 0.7$ to $+52.5$ mJ cm^{-3} K^{-1} for $y = 0.5$, with the other three values falling between these two limits. Also see section 8.4.2.

Reis *et al* [203, 204] found that charge ordering co-exists with an AFM insulator state for $0.30 \leqslant x \leqslant 0.85$ in the $(Pr_{1-x}Ca_x)MnO_3$ system (density is ~ 5.1 g cm^{-3} for $x = 0.32$). In the composition region $0.30 \leqslant x \leqslant 0.40$ the CO/AFM-insulator phase transforms at ~ 50 K to the CO/FM-insulator phase. At ~ 25 K, the charge ordered state is completely melted if the applied magnetic field is large enough and an insulator to metal transition is induced, leading to a large ΔS_M value. For $x = 0.32$ and $\Delta H = 40$ kOe, $\Delta S_M = -106$ mJ cm^{-3} K^{-1}. This ΔS_M value falls well below the SOMT dashed line shown in figure 3. Gomes *et al* [205] report that Gd, when substituted for Pr (i.e. $(Pr_{0.43}Gd_{0.25}Sr_{0.32})MnO_3$), drastically lowers the ΔS_M value of the undoped $(Pr_{0.68}Sr_{0.32})MnO_3$ material.

8.4.2. $(Nd_{1-x}Sr_x)MnO_3$.

The MCE in the charge order compound $(Nd_{0.5}Sr_{0.5})MnO_3$ (the density is 6.405 g cm^3) has been studied by three groups of investigators, Chen and Du [202] (also see section 8.4.1), Sande *et al* [206] and Chau *et al* [207]. The reported values for T_C, T_{CO} and ΔS_M vary widely. Chen and Du give the following values: $T_C = 268$ K, $T_{CO} = 183$ K and $\Delta S_M = +48.5$ mJ cm^{-3} K^{-1} at T_{CO} for $\Delta H = 10$ kOe. Sande *et al* found $T_C = 240$ K, $T_{CO} = 155$ K and $\Delta S_M = +17.9$ mJ cm^{-3} K^{-1} at T_{CO} for $\Delta H = 10$ kOe. The latter also give $\Delta S_M = -5.8$ mJ cm^{-3} K^{-1} at T_C for $\Delta H = 10$ kOe. Chau *et al* report $T_C = 265$ K, $T_{CO} = 175$ and $\Delta S_M = +8.6$ mJ cm^{-3} K^{-1} at T_{CO} for $\Delta H = 10$ kOe. Similarly, when the results reported by Chau *et al* [207] are compared with those of Chen and Du [202] for $(Nd_{0.25}Pr_{0.25}Sr_{0.5})MnO_3$, there are again some significant differences. For this alloy, Chen and Du give $T_C = 225$ K, $T_{CO} = 168$ K and $\Delta S_M = +52.5$ mJ cm^{-3} K^{-1} at T_{CO} for $\Delta H = 10$ kOe, while Chau *et al* report $T_C = 265$ K, $T_{CO} = 170$ K and $\Delta S_M = +7.3$ mJ cm^{-3} K^{-1} at T_{CO} for $\Delta H = 10$ kOe. There are no obvious reasons for these large discrepancies, but as noted in the introductory paragraphs of this section (8), the manganite phase diagrams are quite complex, and slight variations from the assumed, nominal compositions might account for the variations in the reported results.

Chau *et al* [207] examined the effect of substituting Cu for Mn on the charge ordering behaviour in $(Nd_{0.5}Sr_{0.5})(Mn_{1-y}Cu_y)O_3$. When $y = 0.02$, T_C is lowered from 265 K (for $y = 0$) to 230 K and T_{CO} is lowered from 175 to 170 K; and when $y = 0.10$, charge ordering is destroyed and T_C rises back up from 230 K at $y = 0.02$ to 260 K. Presumably the ΔS_M value at T_{CO} is lowered for $y = 0.02$, since charge ordering is destroyed when additional Cu ($y > 0.02$) is substituted for Mn.

8.5. $(La_{1-x}Ba_x)MnO_3$

The MCE properties of $(La_{0.67}Ba_{0.33})MnO_3$ have been reported by Xu *et al* [188] and Zhong *et al* [208]. The former found $T_C = 345$ K and $\Delta S_M = -0.8$ mJ cm^{-3} K^{-1} for a field change of 0.5 kOe, while the latter stated that at $T_C = 337$ K, $\Delta S_M = -18.8$ mJ cm^{-3} K^{-1} for $\Delta H = 10$ kOe (point 12 in figure 10). As one can see, the T_Cs are in fair agreement and

the ΔS_M values are probably in agreement, considering the differences in the magnetic field changes.

Zhong *et al* [208] also studied the effect of oxygen deficiencies in $(La_{0.67}Ba_{0.33})MnO_{3-z}$. Five compositions were studied: $z = 0, 0.02, 0.05, 0.08$ and 0.10. Both T_C and ΔS_M decrease nearly linearly with increasing z: T_C is lowered from 337 K for $z = 0$ to 268 K for $z = 0.10$, and ΔS_M for $\Delta H = 10$ kOe is lowered from -18.8 to -12.0 mJ cm^{-3} K^{-1} for the same z values.

The compound $(La_{0.70}Ba_{0.24}Ca_{0.06})MnO_3$ (density is 6.46 g cm^3) was investigated by Phan *et al* [197], who found $T_C = 320$ K and $\Delta S_M = -11$ mJ cm^{-3} K^{-1} for $\Delta H = 10$ kOe. Since no baseline composition was studied, the influence of Ca substitution for Ba is not known.

8.6. $(La_{1-x}M_x)_3Mn_2O_7$

The $(La_{1-x}M_x)_3Mn_2O_7$ phases crystallize in the $Sr_3Ti_2O_7$-type structure. Zhu *et al* [209] studied the MCE properties of $(La_{1.4}Ca_{1.6})Mn_2O_7$ at 20 and 50 kOe. They report that ΔS_M at $T_C = 270$ K for $\Delta H = 20$ kOe is -62.6 mJ $^{-3}$ K^{-1}, and for $\Delta H = 50$ kOe it is -93.0 mJ cm^{-3} K^{-1}. This latter value lies above the SOMT line in figure 3 (point 44), close to the Gd point (17), and thus might make a reasonably good AMR refrigerant.

Zhong *et al* [210] measured the MCE properties of a series of $(La_{2.5-x}K_{0.5+x})Mn_2O_7$, where $x = 0.05, 0.15, 0.25, 0.35$ and 0.45. They found that with increasing x, T_C increased in a nearly linear fashion from 200 K ($x = 0.05$) to 254 K ($x = 0.45$), while the ΔS_M value for $\Delta H = 10$ kOe increased from -4.1 mJ cm^{-3} K^{-1} at $x = 0.05$ to a maximum of -8.3 mJ cm^{-3} K^{-1} at $x = 0.35$ and then the ΔS_M value decreased to -6.2 mJ cm^{-3} K^{-1} at $x = 0.45$.

9. Nanocomposites

As a bulk magneto-thermal property, the MCE of nanocomposites, in general, is expected to be quite low because magnetocaloric nanoparticles must be dispersed in a matrix so as to prevent their agglomeration associated with the minimization of surface energy. The matrix usually shows little if any magnetocaloric activity in the same temperature range as the active magnetocaloric nanoparticles do. Furthermore, in a typical nanocomposite material, the concentration of nanoparticles usually remains below 50% by volume. Thus, the extensive measure of the MCE is reduced by a factor proportional to the ratio of the volumes (or the masses) of the inactive matrix and the active particulate, while the resultant intensive MCE is suppressed because the matrix acts as a high-capacity heat sink. Matrix effects aside, nanoparticles, which usually show superparamagnetic behaviour, have been known to exhibit enhancement of the MCE when compared with conventional paramagnets. It is, therefore, feasible that basic research on the MCE of nanocomposites will lead to a better understanding of the relationships between the structure, magnetism and thermodynamics of solids. These materials may also find future applications in low-temperature (below 20 K) magnetic refrigeration devices, especially because high surface areas intrinsic to nanoparticles could result in improvements of the heat transfer. However, use of nanocomposites in practical near room temperature magnetic refrigerators remains problematic for the foreseeable future.

In recent years, only a few reports about the MCE of nanocomposites have been published. Thus, Yamamoto *et al* [211] and [212] investigated Fe_2O_3–Ag nanocomposites containing 9 at% and 40 at% of iron oxide particulate ranging in size from 10 to 35 nm. In the low iron content material, iron oxide was in the form of γ-Fe_2O_3, while in the high iron content material, the formation of α-Fe_2O_3 has been detected. The isothermal magnetic entropy

change around 250 K in the 9% Fe and 40% Fe samples reached $\sim 2.1 \times 10^{-3}$ J mol^{-1} (Fe) and $\sim 1.5 \times 10^{-3}$ J mol^{-1} (Fe), respectively, in magnetic fields varying from 0 to 7 T (because of the lack of information about the densities, the values were not converted into mJ cm^{-3} K^{-1} units). Despite the very small absolute ΔS_M values, they exceed those of normal paramagnetic Fe^{3+} in the same temperature and magnetic field range by about two orders of magnitude. This enhancement has been attributed to the superparamagnetic behaviour of iron oxide nanoparticles. The same authors [212] examined the MCE of iron nitride nanoparticles, also embedded into a silver matrix. Two different iron nitrides (γ'-Fe$_4$N and ε-Fe$_3$N) were observed in a 6 at% Fe–Ag nanocomposite. Iron nitride nanoparticles exhibited a factor of 2–3 enhancement of the MCE when compared with the 9% Fe–Ag nanocomposite. This improvement has been associated with the two-component effect: one was due to preferred orientation of the effective magnetic moments of nanograins and the other was due to the temperature dependence of the ferromagnetic coupling strength between electrons in the ε-Fe$_3$N phase.

It is well established [213] that nanostructuring may lead to a nanoparticle exhibiting an effective magnetic moment which is greater than the magnetic moments of the constituent atoms. Thus, Yamamoto *et al* [214] examined how the magnitude of the effective magnetic moment influences the resulting MCE of 12 at% Fe to 33 at% Fe iron oxide nanoparticles ranging in size from 10 to 30 nm which were embedded in a silver matrix. They concluded that for a maximum enhancement of the MCE, it is desirable to have as uniform distribution as possible of particle sizes because the latter controls their effective magnetic moments. This hypothesis was later confirmed experimentally by Kinoshita *et al* [215], who examined magnetite—Au nanocomposites with a narrow size distribution of Fe$_3$O$_4$ particles ranging from 4.6 to 7.4 nm in diameter. The measured ΔS_M value was several times greater when compared with iron oxide–Ag composites with 10–30 nm size variance.

In addition to iron-based nanocomposites, a few materials containing rare-earth elements have been examined with respect to their magnetocaloric properties. Thus, Provenzano *et al* [216] report that heat treatment has a considerable effect on the MCE of R$_3$Ga$_{5-x}$Fe$_x$O$_{12}$ materials with R = Gd, Dy and Ho and x ranging from 0 to 5. These garnets are nanocomposites, in which clusters of iron atoms naturally form during the material's synthesis. It was established that ΔS_M decreases from R = Gd to Ho and Dy despite the fact that the total angular momentum decreases in the series Ho–Dy–Gd. This counterintuitive observation was explained by a reduction of the interaction strength between the rare-earth elements and the Fe as the Gd is replaced by Dy and Ho and the fact that Dy reduces this interaction strength faster than does Ho. The largest MCE ($\Delta S_M \cong -1.7$ J kg^{-1} K^{-1}, which corresponds to ~ 12 mJ cm^{-3} K^{-1} assuming that the density of this iron-substituted garnet is ~ 7 g cm^{-3}) was observed around 10 K in Gd$_3$Ga$_{2.5}$Fe$_{2.5}$O$_{12}$ for a magnetic field change of 10 kOe. Provenzano *et al* [217] also studied Gd$_{60}$Al$_{28}$Fe$_{12}$ and Gd$_{45}$Al$_{33}$Fe$_{22}$ alloys, where the addition of Gd to Fe–Al alloys 'was expected to form magnetic clusters with much larger moment of the Gd atom'. The alloy chemistries were based on the binary Gd$_3$Al$_2$ intermetallic compound, earlier studied by Pecharsky *et al* [218], and the non-existent 'Gd$_4$Al$_5$' compound, respectively. Addition of Fe to the Gd$_3$Al$_2$ lowers the two MCE maxima from 49 and 282 K to ~ 10 and ~ 50 K, respectively; the ΔS_M value of the lower temperature peak is increased by about a factor of 3, but the MCE of the high-temperature peak is lowered by approximately the same factor when compared with Gd$_3$Al$_2$. Nelson *et al* [219] attempted to prepare nanoparticles of Gd in solution, yet they had considerable difficulties in preventing particle oxidation. The majority of particles were 10–15 nm in diameter and their MCE is essentially zero at all temperatures above ~ 100 K (bulk Gd is one of the best known MCE materials, with the MCE exhibiting a peak around 294 K, see figure 3, point 17). The MCE of these 'Gd ' nanoparticles increases as

temperature decreases, as one would expect for a normal Curie-type paramagnet. It is worth noting that theoretical predictions by Shir *et al* [220] indicate that Gd nanoclusters may have a substantial MCE at the same temperature as bulk Gd metal does. Unfortunately, this theoretical result clearly disagrees with the earlier experiments [219], yet Shir *et al* [220] give no details on how to bring the Curie temperature of Gd nanoclusters all the way to room temperature.

10. Correlations

10.1. Adiabatic temperature rise: direct versus indirect measurements

As noted by Gschneidner and Pecharsky [7], an FOMT presents some special problems when determining ΔT_{ad} by either direct or indirect methods. These authors noted that the kinetics of the first-order transformation may be slow and the rapid magnetic field change required to fulfil adiabatic conditions may not be slow enough to allow the transformation to go to completion. And if the thermal isolation of the sample is not good enough, the directly measured ΔT_{ad} value can be underestimated.

The authors [7] also pointed out that the ΔT_{ad} value obtained from indirect measurements can also be in error, although the kinetics may not be a limiting condition since the experimental data are taken under quasi-equilibrium conditions. The major problem may occur when applying the Maxwell equations (3) and (4) at the FOMT, especially if it is a sharp first-order transition. In practice, for the majority of materials the transitions are not ideal (i.e. not truly discontinuous) and thus one can calculate the derivative $\partial M(T, B)/\partial T$ and it is possible to use the Maxwell equations. For more details the reader is referred to [19, 221].

As mentioned earlier in this review, there are some discrepancies between the direct ΔT_{ad} measurements and the ΔT_{ad} values determined from heat capacity measurements for both $Gd_5(Si_2Ge_2)$, see section 5.2, and $La(Fe_{13-2}Si_x)$, see section 7.7. The direct measurement of ΔT_{ad} for a material which exhibits an FOMT needs to be carried out under nearly equilibrium conditions, i.e. the field change needs to be sufficiently slow to enable the completion of the phase transition, much slower than is used normally [109]. For $Gd_5(Si_2Ge_2)$ the normal procedure leads to a too small a value by ~50% for ΔT_{ad} (i.e. 8.5 K) [108] compared with the indirect value obtained from heat capacity measurements (16.5 K) [109], while the ΔT_{ad} value determined by slowly ramping the field up or down agrees with the indirect value within $\pm5\%$ [109]. For $La(Fe_{13-x}Si_x)$ base materials, the direct and indirect ΔT_{ad} values are available for two different alloy compositions. The direct ΔT_{ad} value of 5.7 K for $La(Fe_{11.7}Si_{1.3})$ (see section 7.7) is ~30% smaller than the indirect value of 8.1 K [141], and for $La(Fe_{11.44}Si_{1.56})$ ΔT_{ad} (direct) $= 6$ K is ~20% smaller than ΔT_{ad} (indirect) $= 7.6$ K [172]. These results suggest that there may be a time dependence of the ΔT_{ad} measurement for an FOMT, which probably varies from one material to another.

For SOMT materials, the direct and indirect ΔT_{ad} values are generally in good to excellent agreement, even when pulse field techniques are used to measure ΔT_{ad} [54, 222]. For the same Gd sample the pulse field ΔT_{ad} value was in agreement with the calorimetric value within ~2%, and for different Gd samples the two ΔT_{ad}s agree within $\pm5\%$ [54, 222]. However, for one sample which had a high C content, the dynamic pulse field values were ~50% smaller than the calorimetric ΔT_{ad} value [54].

The difference between the SOMT and FOMT is that it is only the spin system responding to the magnetic field change during SOMT, but for FOMT materials, both the magnetic and crystal sublattices couple to the external magnetic field and, as a result, atoms are displaced during the transformation. In the former case, the response time is in nanoseconds, while for the latter it can be many orders of magnitude longer.

It should be noted that these values are based on static (heat capacity) and semi-static (magnetization and direct), i.e. equilibrium or near-equilibrium, measurements. But in most magnetic refrigerators the magnetization and demagnetization steps are dynamic, and in some cases may become non-equilibrium processes, i.e. the devices run at from 0.1 to 4 Hz and thus the direct measurements of ΔT_{ad} may closer approximate the actual conditions experienced in a magnetic refrigerator than the static values of ΔT_{ad} determined from heat capacity measurements.

10.2. The lattice entropy

A recent study of a magnetic field induced structural transformation (FIST) in Gd_5Ge_4 has led to a better understanding of the GMCE [223]. This transformation, which occurs below 30 K, was studied by powder x-ray diffraction in magnetic fields of up to 35 kOe in addition to magnetization and heat capacity measurements. The results demonstrated that GMCE arises from the amplification of the conventional magnetic entropy change by the entropy difference between the two structures: the low-temperature (high-magnetic field) ferromagnetic Gd_5Si_4-type structure and the high-temperature (low-magnetic field) antiferromagnetic Sm_5Ge_4-type structure. For a FIST the total measured entropy, ΔS_{T}, can be partitioned into two components, ΔS_{M} and ΔS_{st}, where ΔS_{M} is given by equation (3) and ΔS_{st} is the entropy difference between the two crystallographic modifications. Unfortunately, when the magnetic and structural transitions are coupled, one can only measure the total entropy change, ΔS_{T}, and this is why ΔS_{st} has been called a 'hidden parameter' [223]. However, the authors estimated that at low-magnetic fields (<20 kOe) ΔS_{st} could account for about half of ΔS_{T}. In a more recent paper [224] these authors were able to quantify ΔS_{st} by considering the ΔS_{T} for $Gd_5(Si_2Ge_2)$, which orders at 270 K, undergoing a coupled magnetic/structural transformation exhibiting the GMCE, and the ΔS_{M} for $Gd_5(Si_{2.5}Ge_{1.5})$, which orders at 312 K, undergoing a pure magnetic transformation (i.e. a SOMT). Since the former transforms structurally from a monoclinic $Gd_5Si_2Ge_2$ modification to the orthorhombic Gd_5Si_4 structure, and the latter maintains the orthorhombic Gd_5Si_4 structure in both the paramagnetic and ferromagnetic states, the differences between $\Delta S_{\mathrm{T}}[Gd_5(Si_2Ge_2)]$ and $\Delta S_{\mathrm{M}} = \Delta S_{\mathrm{T}}[Gd_5(Si_{2.5}Ge_{1.5})]$ give ΔS_{st} for the monoclinic $\leftrightarrow$ orthorhombic structures. From the difference in the MCE peak values of the respective ΔS_{T} versus T plots, they obtained a value of $74 \pm 3\,\mathrm{mJ\,cm^{-3}\,K^{-1}}$ ($1.08 \pm 0.04\,\mathrm{J\,g\,at^{-1}\,K^{-1}}$) for ΔS_{st}. The authors point out that ΔS_{st} is of the same order of magnitude as the entropies of transformation of the pure metals.

In the case of $Tb_5(Si_2Ge_2)$, Morellon et al [225] showed that the magnetic and structural transformations are decoupled at atmospheric pressure: the former takes place at $T_{\mathrm{C}} = 111$ K and the latter occurs at $T_{\mathrm{st}} = 93$ K. When hydrostatic pressure is applied, both T_{C} and T_{st} increase, but the structural transformation temperature rises more rapidly, such that they merge ($T_{\mathrm{C}} = T_{\mathrm{st}} \cong 115$ K) at 8.6 kbar. From the pressure dependence of the MCE, Morelon et al estimate a ΔS_{st} of not less than $70\,\mathrm{mJ\,cm^{-3}\,K}$ ($1.0\,\mathrm{J\,g\,at^{-1}\,K^{-1}}$), which is in excellent agreement with that of $Gd_5(Si_2Ge_2)$, especially considering the difference in the ordering temperatures of the two materials. The nearly ideal match of the ΔS_{st} of $Tb_5(Si_2Ge_2)$ with that of $Gd_5(Si_2Ge_2)$, determined using two different approaches, reflects the fact that both the low-field (monoclinic paramagnetic state) and high-field (orthorhombic ferromagnetic state) crystal structures of the two compounds are the same.

For those materials which exhibit an FOMT due to IEM, there is also a hidden entropy change associated with the large volume (or lattice parameter) change that occurs when the material undergoes the magnetic transition, i.e. ΔS_{IEM}. Since most of these materials [$La(Fe_{13-x}Si_x)$ and $MnFe(P_{1-x}As_x)$] will change from an FOMT to an SOMT upon alloying,

it is possible that one can estimate ΔS_{IEM} in a manner similar to the way ΔS_{st} was determined for the $Gd_5(Si_{1-x}Ge_x)_4$ alloys. As far as we are aware this has not been done.

10.3. The magnetic field dependence of the MCE

The isothermal entropy change as a function of the applied magnetic field for a select number of key magnetocaloric materials is shown in figure 2(*a*). It is noted that the materials that exhibit an FOMT [MnAs, $La(Fe_{11.44}Si_{1.56})$, $DyCo_2$ and $Gd_5(Si_2Ge_2)$] show a rapid rise at low-magnetic fields as compared with the materials which have an SOMT [Gd, $La(Fe_{11.375}Al_{1.625})$ and $(La_{0.7}Ca_{0.3})MnO_3$]. This enhancement is due to the ΔS_{st} or ΔS_{IEM} contributions (see section 10.2) which are field independent as long as the magnetic field is sufficiently high to induce and complete an FOMT. This is also consistent with the almost uniform slopes of ΔS_M versus H above $H = 20$ kOe. These data suggest that $|\Delta S_{st}(MnAs)| > |\Delta S_{st}(Gd_5Si_2Ge_2)|$, while the ΔS_{IEM} values of $La(Fe_{11.44}Si_{1.56})$ and $DyCo_2$ are comparable and, perhaps, somewhat greater than the $|\Delta S_{st}(Gd_5Si_2Ge_2)|$.

The comparable plot of the adiabatic temperature rise versus H for $\Delta H \leqslant 20$ kOe (figure 2(*b*)) shows that all of the materials have about the same initial slope regardless of the order of the magnetic transition. For $H > 20$ kOe the two materials which exhibit FOMT due to IEM [$La(Fe_{11.44}Si_{1.56})$ and $DyCo_2$] have considerably smaller slopes than either Gd or the two materials which exhibit a coupled structural/magnetic FOMT [MnAs and $Gd_5(Si_2Ge_2)$].

Furthermore, these two plots, figures 2(*a*) and (*b*), show that just because a material exhibits a large ΔS_M value, ΔT_{ad} will not also be large. This is especially true for the two materials which exhibit an FOMT due to IEM, $La(Fe_{11.44}Si_{1.56})$ and $DyCo_2$, which exhibit the opposite behaviour—a large ΔS_M value (figure 2(*a*) and a relatively small ΔT_{ad} value (figure 2(*b*)).

10.4. The temperature dependence of the MCE

10.4.1. The magnetic entropy change, ΔS_M. Several years ago it was pointed out that the lattice heat capacity, C_L, could account for the variation in ΔS_M values for the RAl_2 phases and for the difference in ΔS_M for GdPd and $(Dy_{0.5}Er_{0.5})Al_2$, both of which order at ∼40 K [226]. The authors noted that the larger C_L, the smaller ΔS_M. This is due to the fact that a high C_L value increases the thermal load and more energy is required to heat the sample itself, i.e. there is an entropy loss. The reduction of ΔS_M is expected to be the largest at high temperatures, above 50–100 K, since C_L is inversely proportional to the Debye temperature, Θ_D, see figure 11. With this in mind we now examine the temperature dependence of the magnetic entropy change for a 0 to 50 kOe field change for many of the ferromagnetic materials, which is shown in figure 3. Except for the $Mn(As_{1-x}Sb_x)$ family of alloys, ΔS_M tends to rise as T decreases, regardless of the order of the transformation. At high temperatures, over 150 K, ΔS_M is nearly independent of temperature for the SOMT materials (figure 3), which is consistent with the nearly saturated C_L for $T \geqslant 150$ K (figure 11). For the FOMT RCo_2, $Gd_5(Si_{1-x}Ge_x)_4$ and $MnFe(P_{1-x}As_x)$ families of alloys, ΔS_M also decreases with increasing temperature.

It is seen that the $Mn(As_{1-x}Sb_x)$ family of compounds shows a different trend: even if we exclude the ΔS_M values below ∼240 K, the ΔS_M values slightly increase with increasing temperature. This behaviour, however, is consistent with the trend noted above (when C_L is large ΔS_M is small) because Sb has a lower Θ_D than does As [227], and thus Sb has a higher C_L than does As at $T < 300$ K (see figure 11), and when Sb is substituted for As, both ΔS_M and T_C become smaller, see figure 6.
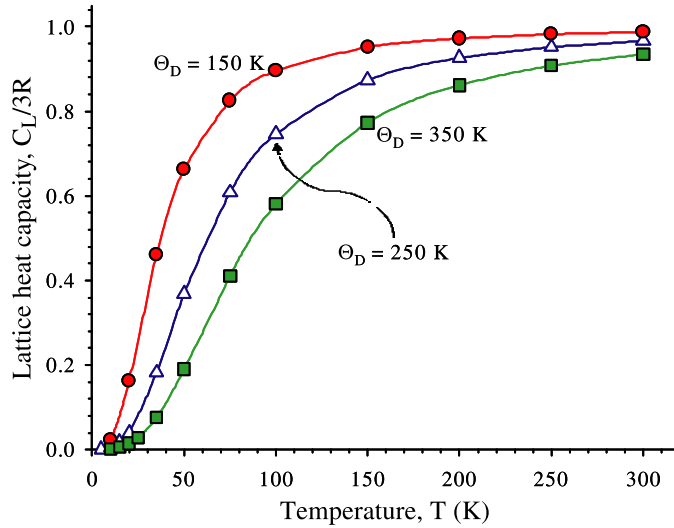
Figure 11. The dimensionless lattice heat capacity of three solids with different Debye temperatures, Θ_D, versus temperature. Most of the materials discussed in this review have Θ_D values between 150 and 350 K.

The rapid drop in ΔS_M for the $\mathrm{Mn(As_{1-x}Sb_x)}$ and $\mathrm{MnFe(P_{1-x}As_x)}$ families near the low-temperature terminus of the ΔS_M versus T curves for these two families is unusual. For the former family, the FOMT changes to SOMT for $T \cong 250$ K, and $\Delta S_{st} = 0$ for the high Sb alloys ($x > 0.3$). However, for the $\mathrm{MnFe(P_{1-x}As_x)}$ family, all the alloys are FOMT materials, and thus the drop-off cannot be due to a change in the order of the transformation, but it might be due to a decrease of IEM energetics which leads to a reduction in ΔS_M but not a change in the order of the transformation. Another possible explanation for this drop-off at large P concentrations ($x < 0.35$) may be due to the stronger antiferromagnetic exchange and subsequent reduction in the Mn magnetic moments.

10.4.2. The adiabatic temperature rise, ΔT_{ad}. More recently it was shown in a thermodynamic analysis of the MCE that ΔT_{ad} is proportional to T/C and that for the same ΔS_M, ΔT_{ad} is expected to be large as the T increases and/or C decreases [170]. Since C goes more rapidly to zero than T, T/C becomes quite large and ΔT_{ad} is expected to be large as T approaches 0 K (we note that at $T = 0$ K, both the magnetic entropy change and adiabatic temperature change are also zero). At high T, i.e. >200 K, C approaches the DuLong–Petit limit and ΔT_{ad} will increase with increasing temperature for the same ΔS_M. Since $C \cong C_L$, except for $T < 10$ K, C will have a temperature dependence similar to that shown in figure 11, and T/C will have a minimum between ~50 and ~100 K, and thus ΔT_{ad} will also have a minimum in the same temperature range. Of course the temperature of the T/C minimum depends on Θ_D of the solid (see figure 11).

We now examine figure 4 which is a plot of ΔT_{ad} versus T for $\Delta H = 20$ kOe and for $\Delta H = 50$ kOe. One can see that there is a trend of the data to be large for $T < 25$ K, reach a minimum between 50 and 80 K and then rise as T goes to 350 K. There is a great deal of scatter, especially for $T > 150$ K, but this is to be expected since the dependence of ΔT_{ad} on T/C was based on the assumption that ΔS_M values are equal, and from the data presented in figure 3 this is far from being correct, and secondly the C/T dependence will also depend

on Θ_D. The major problem is that the materials which have large ΔT_{ad} values above 200 K are FOMT compounds and the ΔS_M values are much greater than those for the SOMT alloy (figure 3). So if one ignores the FOMT data points and concentrates on the SOMT data points 1–4 and 25–30 for $T > 230$ K there is a slight increase in ΔT_{ad} with increasing temperature as predicted. At a low temperature, below 230 K, there is a paucity of SOMT data points and one cannot come to any valid conclusions, but the high ΔT_{ad} value for $ErAl_2$ (point 31) is consistent with the thermodynamic model.

10.5. The relationship between the magnetoresistance and the MCE

Recently Rawat and Das [72] noted the striking similarity between the temperature dependence of the magnetoresistance, MR, and the MCE. In a study of the MR and MCE of TmCu and TmAg the authors showed that in spite of the fact that TmCu undergoes an FOMT and TmAg an SOMT, the $\Delta\rho(H)$ versus T (where ρ is the resistivity) and ΔS_M versus T curves for $\Delta H = 80$ kOe for both compounds are nearly identical and, if properly scaled, lie on top of one another for the respective compound. A low temperature minimum at $\sim$7 K in TmCu and $\sim$5 K in TmAg, and a high temperature maximum at $\sim$9 K in TmCu and $\sim$10 K in TmAg are observed in both plots. Also, they point out that ΔS_M has a H^2 dependence in the paramagnetic state due to the suppression of spin fluctuations which is similar to that observed in $\Delta\rho(H)$. This is an interesting observation, and more thought needs to be given to this relationship, both theoretically and experimentally.

11. Magnetic refrigeration

Magnetic refrigeration came of age on February 20, 1997 in Madison, Wisconsin when the Ames Laboratory/Astronautics Corporation of America (AL/ACA) unveiled their near room temperature reciprocating magnetic refrigerator (MR) which had a cooling power of 600 W in a 50 kOe magnetic field over a 10 K temperature span (the temperature difference between the hot and cold heat exchangers), a coefficient of performance (COP) of 10 and a Carnot efficiency approaching 75% [9]. The refrigerator used 3.0 kg of commercial grade Gd spheres. This COP greatly exceeded that of the common vapour cycle refrigerator in use today (i.e. COP = 2 to 4). Since then, eight more near room temperature MRs have been constructed and tested, see below.

The developments that occurred prior to 1997 which led to this breakthrough can be found in several recent reviews [5–7] and will not be summarized here. In addition to a brief summary of the known existing near room temperature (298 K) MRs, the current status of thermodynamic refrigeration cycles, magnetic refrigerant regenerator materials and magnetic arrays is reviewed in the following subsections. The reader is also referred to several other reviews concerning some of the pre-2000 research and development work on these topics [6, 12, 13, 20, 228].

11.1. Magnetic refrigerators

Most of the work in the past seven years has been devoted to the 298 K MRs, but some research is also being carried out on MRs which operate at liquid H_2 (20 K) and liquid He (4 K) temperatures. The former is of interest for the utilization of MRs in the hydrogen economy, while the latter is of interest in space applications.

11.1.1. Near room temperature magnetic refrigerators. A brief summary of the operational 298 K MRs is presented in table 7. The first machine listed is the proof-of-principle MR which

Table 7. Room temperature magnetic refrigerators.

Name	Location	Announcement date	Type	Max. cooling power (W)	Max. ΔT (K)	Max. magnetic field[a] (kOe)	Regenerator material	Ref.
Ames Laboratory/ Astronautics	Madison, Wisconsin, USA	20 February 1997	Reciprocating	600	10	50 (S)	Gd spheres	[9]
Mater. Science Institute Barcelona	Barcelona, Spain	May 2000	Rotary	?	5	9.5 (P)	Gd foil	[229]
Chubu Electric/Toshiba	Yokohama, Japan	Summer 2000[b]	Reciprocating	100	21	40 (S)	Gd spheres	[230]
University of Victoria	Victoria, British Columbia Canada	July 2001	Reciprocating	2	14	20 (S)	Gd & $Gd_{1-x}Tb_x$L.B.[c]	[231, 232]
Astronautics	Madison, Wisconsin, USA	18 September 2001	Rotary	95	20	15 (P)	Gd spheres	[233]
Sichuan Inst. Tech./ Nanjing University	Nanjing, China	23 April 2002[d]	Reciprocating	?	23	14 (P)	Gd spheres; $Gd_5(Si, Ge)_4$pwdr.[e]	[234]
Chubu Electric/Toshiba	Yokohama, Japan	5 October 2002[f]	Reciprocating	40	27	6 (P)	$Gd_{1-x}Dy_x$L.B.[c]	[235]
Chubu Electric/Toshiba	Yokohama, Japan	4 March 2003	Rotary	60	10	7.6 (P)	$Gd_{1-x}Dy_x$L.B.[c]	[235]
Lab. d'Electrontechnique Grenoble	Grenoble, France	April 2003	Reciprocating	8.8	4	8 (P)	Gd foil	[236]

[a] Magnetic field source: S, superconducting magnet; P, permanent magnet. [b] Local announcement only. [c] L.B. = layered bed.
[d] Privately to KA Gschneidner, Jr.; publicly March 4, 2003. [e] Actual composition $Gd_5(Si_{1.985}Ge_{1.985}Ga_{0.03})$. [f] *Electric Industry News*, October 5, 2002.

demonstrated that magnetic refrigeration is a viable cooling technology which is competitive with conventional gas compression refrigeration. It ran 8 h a day, 5 days a week, logging in over 1500 operational hours over an 18 month period without any major maintenance or repairs, indicating that it was a robust apparatus. The third machine on the list (Chubu Electric/Toshiba [CE/T]) was a modified version of the AL/ACA refrigerator, and the former had similar performance parameters considering the Japanese used a smaller amount of Gd and a lower magnetic field. This was an important development since it showed that the AL/ACA refrigerator was not a fluke.

The University of Victoria refrigerator showed that the operational frequency could be increased by nearly ten-fold from 0.167 Hz (for the AL/ACA and CE/T apparati) to 1 Hz [231]. They also confirmed that the refrigeration power could be improved by using a layered regenerator bed with two materials with different T_Cs [232].

The Astronautics Corporation of America's second refrigerator (called a laboratory prototype MR) was a much smaller device than their first machine. It is a rotary device using a C-shaped permanent magnet to generate the field (see figure 12(a)). It achieved a no load cooling power of 95 W running at a frequency of 4 Hz. It was put on public display on May 1, 2002 at the Global Eight (G8) Energy Ministers meeting in Detroit, Michigan. This MR runs on a 6 V motorcycle battery, and it can run continuously for 6 h before the battery needs recharging.

The Sichuan/Nanjing cooling apparatus was the first refrigerator to use a GMCE material, the $Gd_5(Si_{1.985}Ge_{1.985}Ga_{0.03})$ alloy, as an AMR magnetic refrigerant in an MR. The temperature span could be increased over that of Gd by 1 K.

The CE/T team built two more MRs. The first was a reciprocating device using a permanent magnet to generate the magnetic field, while the second MR had four stationary regenerator beds on the circumference of a circle with a rotating bar magnet inside the circle to generate the magnetic fields as it passed by the beds (see figure 12(b)).

The two European MRs (Materials Science Institute Barcelona [MSIB] and Laboratoire de Electrontechnique de Grenoble) both used Gd foil as the magnetic refrigerant, while all the other seven MRs used various powders. Both teams used permanent magnets: the Barcelona group used two bar magnets parallel to one another to generate the field between them, while the Grenoble group used a Halbach magnetic cylinder. Furthermore, the MSIB's MR used olive oil as the heat transfer fluid.

11.1.2. Low-temperature magnetic refrigerators. Yayama *et al* [237] proposed a new hybrid cryogenic refrigerator which combined a Brayton magnetic cooling cycle with a common Gifford–McMahon (GM) gas cooling cycle. They evaluated the cooling power of the MR with an ErNi magnetic regenerator using a numerical simulation technique with the hot and cold reservoirs at 30 K and 4 K, respectively. They concluded that this hybrid MR has a significantly higher refrigeration power compared with a conventional GM cryocooler.

The design of a 0.1 ton/day hydrogen liquefier MR was described by Zhang *et al* [238]. Their analysis showed that the efficiency of a two stage MR operating between 77 and 20 K was comparable with that of large (5–20 tons/day) gas cycle liquefaction plants. The small hydrogen liquefaction MRs are expected to play an important role in the hydrogen economy.

11.2. Thermodynamic cycles

There are a number of thermodynamic cycles which have been utilized in magnetic cooling: AMR, Ericsson and Stirling. The AMR cycle has received the most attention, especially for near room temperature applications.
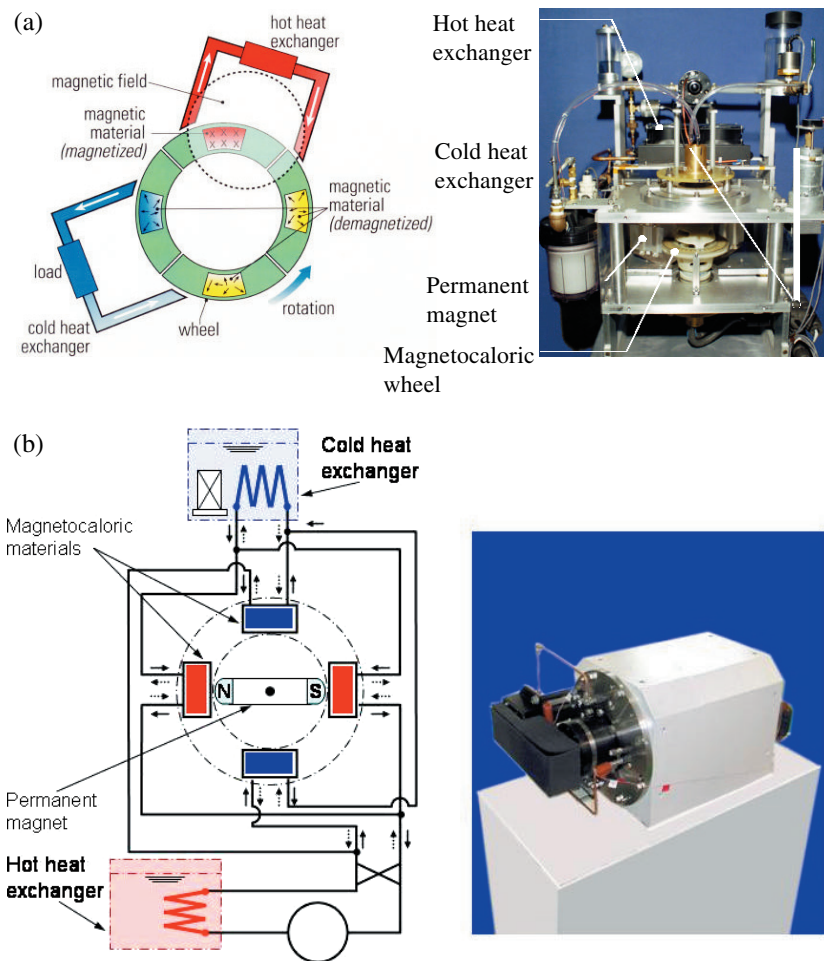
Figure 12. (*a*) The Astronautics Corporation of America rotary magnetic refrigeration (right) and a schematic representation of the device (left). A 14 kOe magnetic field around the magnetocaloric wheel filled with Gd spheres is produced by a permanent magnet. The refrigerator operates near room temperature with a maximum temperature span of ∼20°C with a maximum cooling power of 95 W and operates at a frequency between 1 and 4 Hz. The photograph is courtesy of Astronautics Corporation of America, Inc., Milwaukee, Wisconsin. (*b*) The Chubu/Toshiba rotary magnetic refrigerator (right) and a schematic representation of the device (left). The 7.6 kOe permanent magnet rotates inside of the four magnetocaloric beds, stopping momentarily to allow the appropriate fluid flows to occur before it moves to the next pair of beds. The beds contain Gd–Dy spheres of different Gd : Dy ratios. Using an alcohol water solution as the heat transfer fluid a cooling power of 40 W was obtained at a frequency of 0.28 Hz. The photograph and schematic is courtesy of Chubu Electric Power Co., Inc., Nagoya, Japan.

11.2.1. Active magnetic regenerator cycle. The early (1978) evaluation of the Stirling cycle for magnetic refrigerators and heat engines by Steyert [239] played an important role in the development of the AMR concept. The seminal paper [240] (and patent [241]) on the AMR cycle for MR was presented by Barclay at a NASA conference in 1983 [240]. He showed that one can get much larger temperature lifts than just the ΔT_{ad} of the magnetic refrigerant by using the magnetic material simultaneously as a regenerator and the active magnetic component. Chen *et al* [242] evaluated a number of thermodynamic cycles (Carnot,

Ericsson, Stirling and AMR) for 298 K MRs and concluded that the AMR cycle is the most efficient one.

For many years the conventional wisdom held that the ideal temperature profile of the magnetic refrigerant, ΔT_{ad} versus T, should be a linear function of the absolute temperature [243], but several years ago Hall *et al* [244] showed that this approximation was incorrect. They also showed that there is no unique ΔT_{ad} versus T profile for an idealized AMR MR. Furthermore, acceptable profiles must satisfy boundary conditions on ΔT_{ad} at the hot and cold ends of the regenerator as well as an integral constraint on the total magnetic work input. They showed that a convex temperature–distance profile results in minimized entropy generation in the AMR. These ideas were subsequently tested in an AMR test apparatus a few years later [231, 244]. In the most recent paper Rowe and Barclay [245] conclude that an ideal reverse Brayton-type magnetic cycle cannot be achieved using magnetic materials which undergo a SOMT, i.e. using such a cycle results in entropy generation.

In addition to Barclay's early work [240, 241] on using the AMR cycle for subliquid N_2 temperature refrigeration, several papers dealing with the AMR cycle for hydrogen [243, 246] and helium [243, 247] liquefaction have been published. The basic refrigeration design and modelling for cooling to 4 K from 80 K, and experimental verification, was reported by DeGregoria *et al* [243]. More details on the modelling of a hydrogen liquefier were given by DeGregoria [246], while those of a helium liquefier were presented by Johnson and Zimm [247].

11.2.2. Ericsson and other cycles.

The temperature–entropy relationship in the ideal Ericsson cycle for magnetic cooling requires that ΔT_{ad} be a constant over the temperature span between the hot and cold ends of the magnetic regenerator. The effect of heat transfer on the performance of an Ericsson MR was studied theoretically by He *et al* [248]. These authors developed the optimum relationships between the cooling rate and the COP, and between the power input and the COP of an ideal Ericsson magnetic refrigerant using the basic heat transfer laws and the Curie law. In another theoretical study, von Ranke *et al* [66] calculated the MCE of a number of RNi$_2$ (R = Nd, Gd, Tb, Dy, Ho and Er) intermetallic compounds. They suggested that a composite sample consisting of approximately equal amounts of TbNi$_2$ + DyNi$_2$ + ErNi$_2$ would make a suitable Ericsson cycle AMR refrigerant for the 7–22 K temperature range.

Annaorazov *et al* [249] proposed a scheme for a heat pump using FeRh ($T_C \cong 300$ K) as the active magnetic material. FeRh undergoes a first-order antiferromagnetic to ferromagnetic transition upon heating, which results in a negative MCE, i.e. $\Delta T_{ad} = -12.9$ K for $\Delta H = 19$ kOe. The calculated heat transfer for 5 and 10 K temperature spans and a magnetic field change of 25 kOe suggest that FeRh would be an effective magnetic refrigerant near room temperature [249]. Unfortunately the cost of Rh ($\$20\,000$ per kilogram) puts this material outside the realm of a commercial device, but nevertheless it is a scientifically interesting material.

11.3. Regenerator materials

Gadolinium metal is considered the prototype magnetic refrigerant material for the 298 K MRs. It is a good refrigerant, but to make magnetic refrigeration even more efficient, it is necessary to find new materials with better MCE properties than Gd. Of course, there are other ways to improve the efficiency, but in this review we are only concerned with the magnetic refrigerant. Since the discovery of the GMCE in Gd$_5$(Si$_{1-x}$Ge$_x$)$_4$, see section 5, a number of materials have been proposed as substitutes for Gd. These include the manganites (section 8), Mn(As$_{1-x}$Sb$_x$) alloys (section 6.1), MnFe(P$_{1-x}$As) alloys (section 6.2), the Ni$_{\sim2}$Mn$_{\sim1}$Ge$_{\sim1}$ Heusler alloys

(section 6.3) and La(Fe$_{13-x}$M$_x$)-based materials (section 7). In the following subsections we have evaluated these materials as magnetic refrigerants and discussed large scale production and some special effects.

11.3.1. Evaluation of magnetic refrigerant materials. The most common method used by scientists and engineers to compare MCE materials is to use ΔS_M values, which are usually reported in mass units (J kg^{-1} K^{-1}), of material 'X' with Gd. However, these are the wrong units for making such a comparison since the engineer designing the MR wants the largest entropy change in the smallest possible volume, i.e. the largest cooling power per cubic centimetre. For this reason we have converted all the ΔS_M values in this review to mJ cm^{-3} K^{-1} units. A comparison of the ΔS_M values for many of the magnetic refrigerant candidate materials is found in figure 3.

A second problem with comparing ΔS_M values is that the ΔT_{ad} value is not taken into account. A better parameter for comparing magnetic materials is the refrigerant capacity, which is defined as

$$q = \int_{T_1}^{T_2} \Delta S_M(T)\, dT,\tag{6}$$

where T_1 and T_2 are the temperatures of the hot and cold sinks, respectively, and $\Delta S_M(T)$ is the refrigerant's magnetic entropy change as a function of temperature. The refrigerant capacity, therefore, is a measure of how much heat can be transferred between the cold and hot sinks in one ideal refrigeration cycle.

In figure 13 we plot q versus T_C for many of the materials discussed in this review. Generally the temperature dependence of ΔS_M is not known and so the reported values of q are limited, especially when compared with ΔS_M. As noted, most of the materials with $T_C \cong 298$ K have q values which are slightly higher than that of Gd. As might be expected, q increases with decreasing temperature for the same reason that ΔS_M shows the same temperature dependence, see section 10.4.1.

Another common mistake is that many times the T_Cs of the two materials being compared are more than 25 K apart, and such a comparison is not valid since ΔS_M has a strong temperature dependence as discussed in section 10.4.1. The same is true for q.

The cost of the raw materials is generally stated to be an advantage of material 'X', because Gd is thought to be rather expensive. This is probably correct in many instances. But what is neglected in most cases is the other costs involved in preparing large quantities (>1 kg) of the refrigerant materials on a production basis and in fabricating this material into a useful form to be used in the AMR regenerator beds—spheres, wires, screens, foils, etc—and thus the competitive advantage may be quickly lost. For most of the candidate magnetic refrigerants, namely the manganites, La(Fe$_{13-x}$Si$_x$), Mn(As$_{1-x}$Sb$_x$), MnFe(P$_{1-x}$As$_x$) and Ni$_{\sim2}$Mn$_{\sim1}$Ge$_{\sim1}$ Heusler alloys (see sections 8, 7.1, 6.1, 6.2 and 6.3, respectively, for more details on sample preparation), these materials have only been made on a small scale, 5–25 g, and generally there are long-term anneals ($\geqslant$24 h), sometimes more than one annealing step, necessary to homogenize the sample. When MRs are mass produced, tons of magnetic refrigerant per day will be required; and the factory space and amount of high temperature vacuum equipment to carry out such annealing processes will be vast and require an extremely large capital investment, much more than what is needed for preparing Gd metal and Gd$_5$(Si$_{1-x}$Ge)$_4$ (see section 11.3.2). Since most of the magnetic refrigerant materials are inorganic compounds or brittle intermetallic compounds, these materials will be difficult to fabricate in high-efficiency forms—wires, screens or foils. On the other hand, Gd is a ductile metal and can be, in comparison, easily fabricated into these forms.
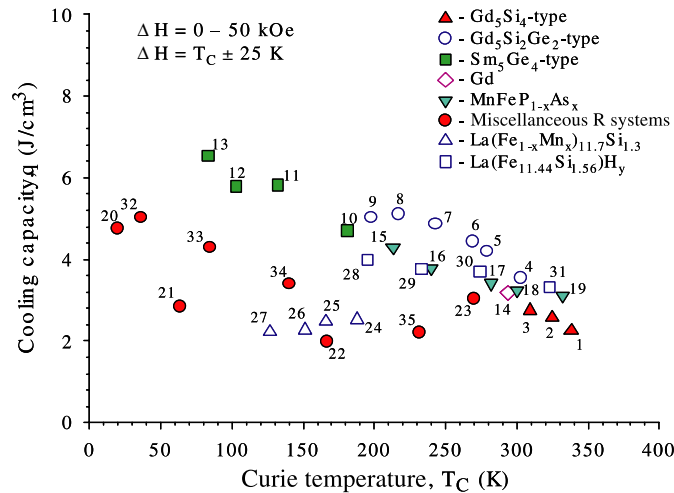
Figure 13. The refrigeration capacity, q, as a function of the Curie temperature for a field change of 50 kOe, with $T_1 = T_C - 25$ K and $T_2 = T_C + 25$ K (see equation (6)) for the RCo_2, RAl_2, $R_5(Si_{1-x}Ge_x)_4$, $MnFe(P_{1-x}As_x)$ and $La(Fe_{13-x}Si_x)$ families and Gd metal (the prototype AMR material), plus a few other intermetallic compounds and alloys. Some of the q values [RCo_2 phases and some of the $Gd_5(Si_{1-x}Ge_x)_4$ compounds] are unpublished values of the authors.

Compound legend

1—$Gd_{5.00}Si_{4.00}$
2—$Gd_5Si_{3.00}Ge_{1.00}$
3—$Gd_5Si_{2.30}Ge_{1.70}$
4—$Gd_5Si_{2.10}Ge_{1.90}$
5—$Gd_5Si_{2.02}Ge_{1.98}$
6—$Gd_5Si_{1.98}Ge_{2.02}$
7—$Gd_5Si_{1.80}Ge_{2.20}$
8—$Gd_5Si_{1.60}Ge_{2.40}$
9—$Gd_5Si_{1.50}Ge_{2.50}$
10—$Gd_5Si_{1.30}Ge_{2.70}$
11—$Gd_5Si_{1.01}Ge_{2.99}$
12—$Gd_5Si_{0.64}Ge_{3.36}$

13—$Gd_5Si_{0.50}Ge_{2.50}$
14—Gd
15—$MnFeP_{0.65}As_{0.35}$
16—$MnFeP_{0.55}As_{0.45}$
17—$MnFeP_{0.50}As_{0.50}$
18—$MnFeP_{0.45}As_{0.55}$
19—$MnFeP_{0.65}As_{0.35}$
20—$DyNi_2$
21—$DyAl_2$
22—$GdAl_2$
23—$Gd_{0.85}Er_{0.15}$
24—$LaFe_{11.7}Si_{1.3}$

25—$La(Fe_{0.99}Mn_{0.01})_{11.7}Si_{1.3}$
26—$La(Fe_{0.98}Mn_{0.02})_{11.7}Si_{1.3}$
27—$La(Fe_{0.97}Mn_{0.03})_{11.7}Si_{1.3}$
28—$La(Fe_{11.44}Si_{1.56})$
29—$La(Fe_{11.44}Si_{1.56})H_{0.5}$
30—$La(Fe_{11.44}Si_{1.56})H_{1.0}$
31—$La(Fe_{11.44}Si_{1.56})H_{1.5}$
32—$ErCo_2$
33—$HoCo_2$
34—$DyCo_2$
35—$TbCo_2$

Another problem with the intermetallic Mn refrigerants containing As and/or P is the fact that both have high vapour pressures (the boiling point of As is 876 K and that of P is 550 K). This makes the handling of these elements in the production of the appropriate compound an additional challenge and will add additional costs in manufacturing the magnetic refrigerant alloy. Most developed countries have strict environmental regulations, and thus enormous investments will be required to ensure triple or even quadruple redundancy in safety, thus eliminating potentially devastating accidents releasing As and/or P into the environment.

Environmental concerns associated with As, P and Sb, all of which are poisons, complicates matters because alloys containing these elements will require special handling facilities, assuming that the various governmental health and environment agencies around the world allow these elements to be utilized in magnetic refrigerant regenerators. We estimate that household cooling appliances will require on the average hundreds of grams of the magnetic refrigerant.

Recently Provenzano *et al* [250] reiterated the well-known notion that hysteresis might be a problem for magnetic refrigerant materials which exhibit the GMCE because of the first-order

Table 8. The hysteresis associated with the first-order GMCE mangetic transition in the materials.

Compound	ΔT (K)	Ref.	ΔH (kOe)	Ref.	Type of transformation
$DyCo_2$	—	—	2	[36, 38]	IEM
$HoCo_2$	—	—	3	[36, 38]	IEM
$ErCo_2^a$	—	—	5	[38]	IEM
$ErCo_2^b$	—	—	11	[40]	IEM
$Gd_5(Si_2Ge_2)$	2–14	[167]	10	[167]	Magnetostructural
MnAs	6.5	[127]	—	—	Magnetostructural
$MnFe(P_{1-x}As_x)$ $0.25 \leqslant x \leqslant 0.65$	4	[88]	7	[88]	Magnetostructural
$Ni_{54.8}Mn_{20.2}Ga_{25.0}$	7	[139]	—	—	Magnetostructural
$La(Fe_{11.44}Si_{1.56})$	3	[162]	5 ± 1	[141, 162]	IEM

[a] Polycrystalline sample.
[b] Single crystal, [111] parallel to H.

magnetic/structural transition. Even though in general this may be correct, it still remains to be demonstrated that one cannot utilize a particular GMCE material in an MR. Indeed, as noted in section 11.1.1, the Chinese [234] have successfully utilized a $Gd_5Si_{1.975}Ge_{1.975}Ga_{0.03}$ GMCE material in an MR, and its performance was slightly better than that obtained using SOMT Gd under the same conditions and in the same MR. The amount of hysteresis for some of the candidate magnetic refrigerant regenerator materials is summarized in table 8. It is noted that as a whole the hystereses are larger for the four compounds which undergo a magnetic/structural FOMT as compared with those which exhibit an FOMT due to IEM. Thus, if hysteresis is a problem, it would be the worst for the $Gd_5(Si_{1-x}Ge_x)_4$ compounds, slightly less for the three Mn-based alloys and the least for $La(Fe_{11.44}Si_{1.56})$ and the RCo_2 phases.

Of even greater concern is not the hysteresis of the FOMTs, but the time dependence of ΔT_{ad}, see section 10.1. In the case of $Gd_5(Si_2Ge_2)$ and $La(Fe_{11.44}Si_{1.56})$ the directly measured ΔT_{ad}s are significantly smaller than those obtained indirectly from heat capacity measurements because of the kinetics of the transformation—the more rapidly ΔT_{ad} is measured the smaller the value of ΔT_{ad}, by 30–50%. This could be a real problem because MRs will operate between 1 and 10 Hz and much of the MCE will be lost (i.e. not utilized) during the magnetic field increase and the field decrease. How much of the MCE is not utilized in one cycle remains to be determined. Nothing is known about the time dependence of ΔT_{ad} for the manganites, which exhibit an FOMT, and the $Mn(As_{1-x}Sb_x)$, $MnFe(P_{1-x}As_x)$ and Heusler alloy families, but it is reasonable to expect they will exhibit similar behaviours. As noted in section 10.1, there is no time dependence for Gd metal.

Corrosion may be a problem since a water-based solution is used as the heat transfer fluid in most MRs built to date. Gd spheres have been successfully used in several MRs and no corrosion has been reported in any of the reports on the operational results of these devices. As a matter of fact, the Gd spheres used in the AL/ACA proof-of-principle apparatus are still as shiny after 1500 h of operation as when they were loaded into the MR. The $Gd_5(Si_{1-x}Ge_x)_4$ alloys are much more stable to oxidation (no measurable weight gain in air at 123°C over a five month period) and corrosion (no evidence of a reaction of the powders with tap water) than Gd metal [251]. The $La(Fe_{13-x}Si_x)$ alloys may suffer some corrosion problems, since all the samples prepared to date contain α-Fe (see section 7). No information is available concerning the compatibility of the manganites and the three Mn-based intermetallic compounds with water, but they all seem to be stable in ambient (humid) air, which suggests aqueous corrosion may not be a problem.

Table 9. Advantages and disadvantages of various magnetic refrigerants.

Factor	Gd	Gd_5T_4	$RMnO_3$	LaFeSi	MnAs	FeMnPAs	Ni_2MnGa
Raw material costs	0	−	++	++	++	++	+
Preparation	0	−	−−	−−	−−	−−	−−
Vapour pressure	0	0	0	0	−−	−−−	0
Fabrication (sheet)	0	−	−	−	−	−	−
MCE, $|\Delta S_M|$	0	++	−	+	+	+	+
MCE, ΔT_{ad}	0	+	−	−	−	−	?
Refrigeration capacity	0	+	?	+	?	+	?
Hysteresis	0	−−	0^a	−	−	−	−
Time dependence of ΔT_{ad}	0	−	?	−	?	?	?
Environmental concerns	0	0	0	0	—	—	0
Corrosion	0	++	?	−	?	?	?

^{a} For SOMT manganites; for the few FOMT maganites the zero becomes a minus.

The advantages and disadvantages of the candidate magnetic regenerator materials are summarized in table 9. The comparison is made with Gd metal, the prototype magnetic refrigerant. A zero indicates that the factor is essentially the same as for Gd; a plus means that the behaviour is somewhat better than Gd, and two pluses mean it is much better. A minus sign indicates that the property is inferior to that of Gd, and two or three minus signs indicate the behaviour is much worse, or much more worse than for Gd. Most of the properties have been discussed in the above paragraphs of this subsection, while the ΔS_M, ΔT_{ad} and q values are found in figures 3, 4 and 13, respectively. It is seen that there is no clear favourite GMCE material as a replacement for Gd and Gd-based solid solution alloys, Gd–R. As a matter of fact Gd and its solid solution alloys do well in holding their own as the near room temperature magnetic refrigerant of choice as of today.

11.3.2. Large scale production. There has only been one investigation of developing a method for the large scale production of magnetic refrigerant regenerator materials. Gschneidner *et al* [103, 252] described a kilogram scale process for manufacturing the $Gd_5(Si_{1-x}Ge_x)_4$ alloys from commercial grade Gd metal. The major obstacles overcome in making a high-quality product were the finding of a suitable crucible material (Ta) for reacting the components and melting the refractory $Gd_5(Si_{1-x}Ge_x)_4$ alloy (the melting point exceeds 1750°C), and the developing of a heat treating protocol for reducing the carbon impurity from the Gd starting material and minimizing the eutectoid transformation of the monoclinic form to the orthorhombic modification between 400°C and 700°C. Over 10 kg of the $Gd_5(Si_2Ge_2)$ material with good GMCE values, two-thirds of that prepared by arc-melting using high-purity Gd, was produced.

As far as we are aware no other study has been made to prepare large scale quantities of other AMR regenerator materials.

11.3.3. Special effects. Luo *et al* [253] developed a method for fabricating porous monolithic regenerator forms starting with fine powders of the magnetic refrigerant material. The regenerator bed was prepared by bonding the ~230 μm powders using a low-temperature epoxy. Several single layers and multilayer beds with porosities of ~0.39 were prepared and tested with good results. The authors claim their technique is a cost effective way of fabricating efficient magnetic regenerators.

Lewis *et al* describe a simple way of improving the MCE in ferromagnetic materials by coating slices of the GMCE $Gd_5(Si_{1.5}Ge_{2.5})$ with pure Fe [115] or Al [116]. The coating layers

were 0.1 and 0.2 μm thick for Fe and 0.1 μm for Al. The 0.1 μm Fe coating increased the GMCE by $\sim$11%, while the 0.2 μm coating had no appreciable difference in the effect. The Al coating improved the GMCE by 20%. The enhancement was thought to be due to a strain that the coatings imparted on the $Gd_5Si_{1.5}Ge_{2.5}$ particles.

11.4. Permanent magnet arrays

An important aspect of magnetic refrigeration is the magnetic field source, since the efficiency scales directly with magnetic field. For large scale applications, e.g. building climate control, supermarket chillers, refrigeration plants, etc, superconducting magnets will be utilized without losing the efficiency associated with the need to use liquid helium or a cryocooler to maintain a superconducting magnet close to 4 K. But for household and automotive applications, superconducting magnets are out of the question and we will have to rely on permanent magnets at least in the foreseeable future. Thus the design of high-field, low-cost permanent magnet arrays for magnetic refrigeration is an important aspect of the commercialization of MRs in the consumer market. Several recent papers have addressed this problem. Lee and Jiles [254] describe geometrical enhancements to permanent magnet flux sources. Their design generated a magnetic field of 30 kOe in a 1.52 cm gap. Tang *et al* [255] presented a description of a permanent magnet circuit with an air gap. Their optimum magnet array had a flux of 8.2 kOe in a gap of 1.5 cm. Xu *et al* [256] described the design of a 16 piece hollow cylindrical permanent magnet array. They also calculated the effect of cutting a slot (10 cm) in this array to allow the magnetic refrigerant to enter and exit the magnetic field. However, no field strengths were given for their design.

12. Conclusions and summary

Over the past seven years there has been an upsurge in our knowledge of the MCE and many materials have been investigated for their MCE properties. A number of new materials with GMCE properties have been discovered and proposed as viable magnetic refrigerants. The MCE properties of the best magnetic materials have been compared. However, there is no clear winner as a replacement for Gd metal, the prototype 298 K magnetic refrigerant material. As of today, Gd and Gd-based solid solution alloys are still the materials of choice.

Acknowledgments

References

[1] Warburg E 1881 *Ann. Phys. (Leipzig)* **13** 141
[2] Debye P 1926 *Ann. Phys.* **81** 1154
[3] Giauque W F 1927 *J. Am. Chem. Soc.* **49** 1864
[4] Giauque W F and MacDougall D P 1933 *Phys. Rev.* **43** 768

[5] Gschneidner K A Jr and Pecharsky V K 1997 *Rare Earths: Science, Technology and Applications III* ed R G Bautista *et al* (Warrendale, PA: The Minerals, Metals and Materials Society) p 209

[6] Pecharsky V K and Gschneidner K A Jr 1999 *J. Magn. Magn. Mater.* **200** 44

[7] Gschneidner K A Jr and Pecharsky V K 2000 *Annu. Rev. Mater. Sci.* **30** 387

[8] Gschneidner K A Jr and Pecharsky V K 2002 *Fundamentals of Advanced Materials for Energy Conversion* ed D Chandra and R G Bautista (Warrendale, PA: The Minerals, Metals and Materials Society) p 9

[9] Zimm C, Jastrab A, Sternberg A, Pecharsky V K, Gschneidner K Jr, Osborne M and Anderson I 1998 *Adv. Cryog. Eng.* **43** 1759

[10] Pecharsky V K and Gschneidner K A Jr 1997 *Phys. Rev. Lett.* **78** 4494

[11] Gschneidner K A Jr and Pecharsky V K 2000 *Mater. Sci. Eng.* A **287** 301

[12] Gschneidner K A Jr and Pecharsky V K 2002 *Intermetallic Compounds* vol 3 *Principles and Practice* ed J H Westabook and R L Fleischer (New York: Wiley) p 519

[13] Tishin A M and Spichkin Y I 2003 *The Magnetocaloric Effect and its Applications* (Bristol: Institute of Physics Publishing)

[14] Pecharsky V K, Gschneidner K A Jr, Pecharsky A O and Tishin A M 2001 *Phys. Rev.* B **64** 144406

[15] Gopal B R, Chahine R, Foeldeaki M and Bose T K 1995 *Rev. Sci. Instrum.* **66** 232

[16] Gopal B R, Chahine R and Bose T K 1997 *Rev. Sci. Instrum.* **68** 1818

[17] Dan'kov S Yu, Tishin A M, Pecharsky V K and Gschneidner K A Jr 1997 *Rev. Sci. Instrum.* **68** 2432

[18] Foldeaki M, Chahine R and Bose T K 1995 *J. Appl. Phys.* **77** 3528

[19] Pecharsky V K and Gschneidner K A Jr 1999 *J. Appl. Phys.* **86** 565

[20] Tishin A M 1999 *Handbook of Magnetic Materials* vol 12, ed K H J Buschow (Amsterdam: Elsevier) p 395

[21] Gschneidner K A Jr, Pecharsky V K and Pecharsky A O 2000 *The Science of Alloys for the 21st Century: A Hume-Rosery celebration* ed E A Turchi *et al* (Warrendale, PA: The Minerals, Metals and Materials Society) p 201

[22] Yamada H and Goto T 2003 *Phys. Rev.* B **68** 184417

[23] Yamada H and Goto T 2003 *Physica* B **346–347** 104

[24] Amaral V S and Amaral J S 2004 *J. Magn. Magn. Mater.* **272–276** 2104

[25] von Ranke P J, de Oliveira N A and Gama S 2004 *J. Magn. Magn. Mater.* **277** 78

[26] Lima A L, Gschneidner K A Jr and Pecharsky V K 2004 *J. Appl. Phys.* **96** 2164

[27] Zhitomirsky M E 2003 *Phys. Rev.* B **67** 104421

[28] de Oliveira I G, von Ranke P J and Nóbrega E P 2003 *J. Magn. Magn. Mater.* **261** 112

[29] Korte B J, Pecharsky V K and Gschneidner K A Jr 1998 *J. Appl. Phys.* **84** 5677

[30] Chernyshov A S, Tishin A M, Gschneidner K A Jr, Pecharsky A O, Pecharsky V K and Lograsso T A 2002 *Adv. Cryog. Eng.* **48** 19

[31] Dai W, Shen B G, Li D X and Gao Z X 2000 *J. Alloys Compounds* **311** 22

[32] Zhang X, Yang L, Zhou S, Qi L and Liu Z 2001 *Mater. Trans.* **42** 2622

[33] Wang D, Huang S, Han Z, Su Z, Wang Y and Du Y 2004 *Solid State Commun.* **131** 97

[34] Wu Y L, Pecharsky A O, Pecharsky V K and Gschneidner K A Jr 2002 *Adv. Cryog. Eng.* **48** 3

[35] Wang D, Liu H, Tang S, Yang S, Huang S and Du Y 2002 *Phys. Lett.* A **297** 247

[36] Duc N H, Anh D T K and Brommer P E 2002 *Physica* B **319** 1

[37] Gomes A M, Reis M S, Oliveira I S, Guimarães A P and Takeuchi A Y 2002 *J. Magn. Magn. Mater.* **242–245** 870

[38] Duc N H and Anh D T K 2002 *J. Magn. Magn. Mater.* **242–245** 873

[39] de Oliveira N A and von Ranke P J 2003 *J. Magn. Magn. Mater.* **264** 55

[40] Wada H, Tanabe Y, Shiga M, Sugawara H and Sato H 2001 *J. Alloys Compounds* **316** 245

[41] Wang D H, Liu H D, Tang S L, Tang T, Wen J F and Du Y W 2002 *Solid State Commun.* **121** 199

[42] Liu H, Wang D, Tang S, Cao Q, Tang T, Gu B and Du Y 2002 *J. Alloys Compounds* **346** 314

[43] Wang Y, Yang S and Song X 2003 *J. Alloys Compounds* **354** 81

[44] Wang D, Tang S, Liu H, Zhong W and Du Y 2003 *Mater. Lett.* **57** 3884

[45] Singh N K, Suresh K G and Nigam A K 2003 *Solid State Commun.* **127** 373

[46] Troper A, von Rande P J and de Oliveira N A 2004 *J. Magn. Magn. Mater.* **272–276** 583

[47] Singh N K, Tripathy S K, Banerjee D, Tomy C V, Suresh K G and Nigam A K 2004 *J. Appl. Phys.* **95** 6678

[48] Wang D H, Tang S L, Liu H D, Gao W L and Du Y W 2002 *Intermetallics* **10** 819

[49] Pecharsky A O, Gschneidner K A Jr and Pecharsky V K, MCE of RCo_2 (R = Tb, Dy, Ho and Er) unpublished

[50] Foldeaki M, Giguere A, Chahine R and Bose T K 1998 *Adv. Cryog. Eng.* **43** 1533

[51] Pecharsky A O, Gschneidner K A Jr and Pecharsky V K 2003 *J. Appl. Phys.* **93** 4722

[52] Fujieda S, Fujita A and Fukamichi K 2002 *Appl. Phys. Lett.* **81** 1276

[53] Hu F X, Qian X L, Wang G J, Wang J, Sun J R, Zhang X X, Cheng Z H and Shen B G 2003 *J. Phys.: Condens. Matter* **15** 3299

[54] Dan'kov S Yu, Tishin A M, Pecharsky V K and Gschneidner K A Jr 1998 *Phys. Rev.* B **57** 3478

[55] Tian S B, Phan M H, Yu S C and Hur N H 2003 *Physica* B **327** 221

[56] Wada H and Tanabe Y 2001 *Appl. Phys. Lett.* **79** 3302

[57] de Oliveira N A, von Ranke P J, Costa M V T and Troper A 2002 *J. Appl. Phys.* **91** 8879

[58] de Oliveira N A, von Ranke P J and Troper A 2004 *Phys. Rev.* B **69** 064421

[59] Dan'kov S Yu, Ivtchenko V V, Tishin A M, Gschneidner K A Jr and Pecharsky V K 2000 *Adv. Cryog. Eng.* **46** 397

[60] Wang F W, Zhang X X and Hu F X 2000 *Appl. Phys. Lett.* **77** 1360

[61] Bohigas X, Tejada J, Torres F, Arnaudas J I, Joven E and del Moral A 2002 *Appl. Phys. Lett.* **81** 2427

[62] von Ranke P J, de Oliveira N A, Costa M V T, Nobrega E P, Caldas A, de Oliveira I G 2001 *J. Magn. Magn. Mater.* **226–230** 970

[63] von Ranke P J, de Oliveira I G, Guimarães A P and da Silva X A 2000 *Phys. Rev.* B **61** 447

[64] Lima A L, Oliveira I S, Gomes A M and von Ranke P J 2002 *Phys. Rev.* B **65** 172411

[65] von Ranke P J, Nóbrega E P, de Oliveira I G, Gomes A M and Sarthour R S 2001 *Phys. Rev.* B **63** 184406

[66] von Ranke P J, Grangeia D F, Caldas A and de Oliveira N A 2003 *J. Appl. Phys.* **93** 4055

[67] Nakagawa T, Sako K, Arakawa T and Yamamoto T Y 2004 *J. Alloys Compounds* **364** 53

[68] Yamamoto T A, Nakagawa T, Sako K, Arakawa T and Nitani H 2004 *J. Alloys Compounds* **376** 17

[69] Long Y, Chen Y and Wan F 2003 *J. Rare Earths* **21** 477

[70] Plaza E J R, Alves C S, Coelho A A, Gama S and von Ranke P J 2004 *J. Magn. Magn. Mater.* **272–276** 2373

[71] Tristan N V, Nikitin S A, Palewski T, Nenkov K and Skokov K 2003 *J. Magn. Magn. Mater.* **258–259** 583

[72] Rawat R and Das I 2001 *J. Phys.: Condens. Matter* **13** L379

[73] Aoki Y, Urakawa J, Sugawara H, Sato H, Markin P E, Bostrem I G and Baranov N V 2000 *Phys. Rev.* B **62** 8935

[74] von Ranke P J, Lima A L, Nobrega E P, da Silva X A, Guimarães A P and Oliveira I S 2001 *Phys. Rev.* B **63** 024422

[75] Canepa F, Napoletano M and Cirafici S 2002 *Intermetallics* **10** 731

[76] Ilyn M I, Tishin A M, Gschneidner K A Jr, Pecharsky V K and Pecharsky A O 2001 *Cryocoolers 11* ed R G Ross Jr (New York: Kluwer/Plenum) p 457

[77] Niu X J, Gschneidner K A Jr, Pecharsky A O and Pecharsky V K 2001 *J. Magn. Magn. Mater.* **234** 193

[78] Niu X J 1999 *MS Thesis* Iowa State University, Ames Iowa, USA

[79] Vollmer R, Goll G, Pfleiderer C, Löhneysen H V, Maple M V and Canfield P C 2002 *Physica* B **312–313** 855

[80] Si L, Ding J, Wang L, Li Y, Tan H and Yao B 2001 *J Alloys Compounds* **316** 260

[81] Zhang X X, Wang F W and Wen G H 2001 *J. Phys.: Condens. Matter* **13** L747

[82] Canepa F, Manfrinetti P, Palenzona A, Cirafici S, Merlo F and Cimberle M R 2000 *Intermetallics* **8** 267

[83] Napolentano M, Canepa F, Manfrinetti P and Merlo F 2000 *J. Mater. Chem.* **10** 1663

[84] Rawat R and Das I 2001 *J. Phys.: Condens. Matter* **13** L57

[85] Das I and Rawat R 2000 *Solid State Commun.* **115** 207

[86] Sampathkumaran E V, Das I, Rawat R and Majumdar S 2000 *Appl. Phys. Lett.* **77** 418

[87] Majumdar S, Sampathkumaran E V, Paulose P L, Bitterlich H, Löser W and Behr G 2000 *Phys. Rev.* B **62** 14207

[88] Tegus O, Brück E, Zhang L, Dagula, Buschow K H J and de Boer F R 2002 *Physica* B **319** 174

[89] Rawat R and Das I 2001 *Phys. Rev.* B **64** 052407

[90] Tegus O, Duong N P, Dagula W, Zhang L, Brück E, Buschow K H J and de Boer F R 2002 *J. Appl. Phys.* **91** 8528

[91] Vasylyev D, Syshchenko O, Sechovský V, Šebek J, Stadnyk Yu, Mudryk Ya and Romaka L 2002 *Czech. J. Phys.* **52** (Suppl. A) A205

[92] El Massalami M, Takeya H and Chaves C M 2004 *Phys. Rev.* B **70** 014429

[93] Pecharsky V K and Gschneidner K A Jr 2001 *Adv. Mater.* **13** 683

[94] Pecharsky V K and Gschneidner K A Jr 1997 *J. Alloys Compounds* **260** 98

[95] Choe W, Pecharsky V K, Pecharsky A O, Gschneidner K A Jr, Young V G Jr and Miller G J 2000 *Phys. Rev. Lett.* **84** 4617

[96] Morellon L, Blasco J, Algarabel P A and Ibarra M R 2000 *Phys. Rev* B **62** 1022

[97] Pecharsky V K and Gschneidner K A Jr 1997 *Appl. Phys. Lett.* **70** 3299

[98] Pecharsky A O, Gschneidner K A Jr, Pecharsky V K and Schindler C E 2002 *J. Alloys Compounds* **338** 126

[99] Pecharsky V K, Pecharsky A O and Gschneidner K A Jr 2002 *J. Alloys Compounds* **344** 362

[100] Pecharsky A O, Gschneidner K A Jr and Pecharsky V K 2003 *J. Magn. Magn. Mater.* **267** 60

[101] Pecharsky V K and Gschneidner K A Jr 1997 *J. Magn. Magn. Mater.* **167** L179
[102] Gschneidner K A Jr and Pecharsky V K 1999 *J. Appl. Phys.* **85** 5365
[103] Gschneidner K A Jr, Pecharsky A O, Pecharsky V K, Lograsso T A and Schlagel D L 2000 *Rare Earths and Actinides: Science, Technology and Applications IV* ed R G Bautista and B Mishra (Warrendale, PA: The Minerals, Metals and Materials Society) p 63
[104] Gschneidner K A Jr 1993 *J. Alloys Compounds* **193** 1
[105] Thuy N P, Tai L T, Hien N T, Nong N V, Vinh T Q, Thang P D, Nguyen T P and Molinié P 2001 *Proc. 8th Asia-Pacific Physics Conf. (Taipei, Taiwan)* (Singapore: World Scientific) p 354
[106] Thuy N P 2002 *Solid State Sci. Technol. (Malaysia)* **10** 1
[107] Zhuo Yi, Chahine R and Bose T K 2003 *IEEE Trans. Magn.* **39** 3358
[108] Giguère A, Foldeaki M, Gopal B R, Chahine R, Bose T K, Frydman A and Barclay J A 1999 *Phys. Rev. Lett.* **83** 2262
[109] Gschneidner K A Jr, Pecharsky V K, Brück E, Duijn H G M and Levin E M 2000 *Phys. Rev. Lett.* **85** 4190
[110] Spichkin Y I, Pecharsky V K and Gschneidner K A Jr 2001 *J. Appl. Phys.* **89** 1738
[111] Xie K, Sun Z, Zhu Y, Yang S and Song X 2004 *J. Alloys Compounds* **372** 49
[112] von Ranke P J, de Oliveira N A and Gama S 2004 *J. Magn. Magn. Mater.* **277** 78
[113] Casanova F, Batlle X, Labarta A, Marcos J, Mañosa L and Planes A 2002 *Phys. Rev.* B **66** 212402
[114] Casanova F, Batlle X, Labarta A, Marcos J, Mañosa L and Planes A 2003 *J. Appl. Phys.* **93** 8313
[115] Lewis L H, Yu M H and Gambino R J 2003 *Appl. Phys. Lett.* **94** 515
[116] Lewis L H, Yu M H, Welch D O and Gambino R J 2004 *J. Appl. Phys.* **95** 6912
[117] Fujieda S, Hasegawa Y, Fujita A and Fukamichi K 2004 *J. Appl. Phys.* **95** 2429
[118] Morellon L, Magen C, Algarabel P A, Ibarra M R and Ritter C 2001 *Appl. Phys. Lett.* **79** 1318
[119] Huang H, Pecharsky A O, Pecharsky V K and Gschneidner K A Jr 2002 *Adv. Cryog. Eng.* **48** 11
[120] Thuy N P, Nong N V, Hien N T, Tai L T, Vinh T Q, Thang P D and Brück E 2002 *J. Magn. Magn. Mater.* **242–245** 841
[121] Tegus O, Dagula O, Brück E, Zhang L, de Boer F R and Buschow K H J 2002 *J. Appl. Phys.* **91** 8534
[122] Ivtchenko V V, Pecharsky V K and Gschneidner K A Jr 2000 *Adv. Cryog. Eng.* **46** 405
[123] Thuy N P, Chen Y Y, Yao Y D, Wang C R, Lin S H, Ho J C, Nguyen T P, Thang P D, Klaasse J C P, Hien N T and Tai L T 2003 *J. Magn. Magn. Mater.* **262** 432
[124] Ryan D H, Elounge-Jamróz M, van Lierop J, Altounian Z and Wang H B 2003 *Phys. Rev. Lett.* **90** 117202
[125] Campoy J C P, Plaza E J R, Magnus A, Carvalho G, Coelho A A, Gama S and von Ranke P J 2004 *J. Magn. Magn. Mater.* **272–276** 2375
[126] Wang H B, Altounian Z and Ryan D H 2002 *Phys. Rev.* B **66** 214413
[127] Wada H, Taniguchi K and Tanabe Y 2002 *Mater. Trans.* **43** 73
[128] Wada H, Morikawa T, Taniguchi K, Shibata T, Yamada Y and Akishige Y 2003 *Physica* B **328** 114
[129] Morikawa T and Wada H 2004 *J. Magn. Magn. Mater.* **272–276** e583
[130] Tegus O, Brück E, Buschow K H J and de Boer F R 2002 *Nature* **415** 150
[131] Brück E, Tegus O, Li X W, de Boer F R and Buschow K H J 2003 *Physica* B **327** 431
[132] Li X W, Tegus O, Zhang L, Dagula W, Brück E, Buschow K H J and de Boer F R 2003 *IEEE Trans. Magn.* **39** 3148
[133] Tegus O, Brück E, Li W X, Zhang L, Dagula W, de Boer F R and Buschow K H J 2004 *J. Magn. Magn. Mater.* **272–276** 2389
[134] Hu F-X, Shen B-G and Sun J-R 2000 *Appl. Phys. Lett.* **76** 3460
[135] Hu F-X, Sun J-R, Wu G-H and Shen B-G 2001 *J. Appl. Phys.* **90** 5216
[136] Marcos J, Planes A, Mañosa L, Casanova F, Batlle X, Labarta A and Martínez B 2002 *Phys. Rev.* B **66** 224413
[137] Pasquale M, Sasso C P and Lewis L H 2004 *J. Appl. Phys.* **95** 6918
[138] Aliev A, Batdalov A, Bosko S, Buchelnikov V, Dikshtein I, Khovailo V, Koledov V, Levitin R, Shavrov V and Takagi T 2004 *J. Magn. Magn. Mater.* **272–276** 2040
[139] Albertini F, Canepa F, Cirafici S, Franceschi E A, Napoletano M, Paoluzi A, Pareti L and Solzi M 2004 *J. Magn. Magn. Mater.* **272–276** 2111
[140] Zhou X, Li W, Kunkel H P and Williams G 2004 *J. Phys.: Condens. Matter* **16** L39
[141] Fujita A, Fujieda S, Hasegawa Y and Fukamichi K 2003 *Phys. Rev.* B **67** 104416
[142] Songlin, Dagula, Tegus O, Brück E, Klaasse J C P, de Boer F R and Buschow K H J 2002 *J. Alloys Compounds* **334** 249
[143] Songlin, Dagula, Tegus O, Brück E, de Boer F R and Buschow K H J 2002 *J. Alloys Compounds* **337** 269
[144] Zhang Y Q and Zhang Z D 2004 *J. Alloys Compounds* **365** 35
[145] Tohei T, Wada H and Kanomata T 2003 *J. Appl. Phys.* **94** 1800
[146] Tohei T, Wada H and Kanomata T 2004 *J. Magn. Magn. Mater.* **272–276** e585

[147] Zhang L, Brück E, Tegus O, Buschow K H J and de Boer F R 2003 *Physica* B **328** 295
[148] Wada H, Tanabe Y, Hagiwara K and Shiga M 2000 *J. Magn. Magn. Mater.* **218** 203
[149] Kripyakevich P I, Zarechnyuk O S, Gladyshevskii E I and Bodak O I 1968 *Z. Anorg. Chem.* **358** 90
[150] Bodak O I and Gladyshevskii E I 1969 *Dopov. Akad. Nauk Ukr. RSR. Ser.* A **12** 1125
[151] Palstra T T M, Mydosh J A, Nieuwenhuys G J, van der Kraan A M and Buschow K H J 1983 *J. Magn. Magn. Mater.* **36** 290
[152] Palstra T T M, Werij H G C, Neiuwenhuys G J, Mydosh J A, de Boer F R and Buschow K H J 1984 *J. Phys. F: Met. Phys.* **14** 1961
[153] Massalski T B 1990 *Binary Alloy Phase Diagrams* vol 2, 2nd edn (Materials Park Ohio, USA: ASM International) p 1718
[154] Fujita A, Akamatsu K and Fukamichi K 1999 *J. Appl. Phys.* **85** 4756
[155] Hu F-X, Shen B-G, Sun J-R, Cheng Z-H and Zhang X-X 2000 *J. Phys.: Condens. Matter* **12** L691
[156] Zhang X X, Wen G H, Wang F W, Wang W H, Yu C H and Wu G H 2000 *Appl. Phys. Lett.* **77** 3072
[157] Hu F-X, Shen B-G, Sun J-R, Cheng Z-H, Rao G-H and Zhang X-X 2001 *Appl. Phys. Lett.* **78** 3675
[158] Wen G H, Zheng R K, Zhang X X, Wang W H, Chen J L and Wu G H 2002 *J. Appl. Phys.* **91** 8537
[159] Hu F X, Qian X L, Sun J R, Wang G J, Zhang X X, Cheng Z H and Shen B G 2002 *J. Appl. Phys.* **92** 3620
[160] Wang F, Chen Y-F, Wang G-J and Shen B-G 2003 *J. Phys. D: Appl. Phys.* **36** 1
[161] Chen Y-F, Wang F, Shen B-G, Wang G-J and Sun J-R 2003 *J. Appl. Phys.* **93** 1323
[162] Hu F-X, Ilyn M, Tishin A M, Sun J R, Wang G J, Chen Y F, Wang F, Cheng Z H and Shen B G 2003 *J. Appl. Phys.* **93** 5503
[163] Chen Y-F, Wang F, Shen B-G, Sun J-R, Wang G-J, Hu F-X, Cheng Z-H and Zhu T 2003 *J. Appl. Phys.* **93** 6981
[164] Liu X B, Altounian Z and Ryan D H 2003 *J. Phys.: Condens. Matter* **15** 7385
[165] Anh D T K, Thuy N P, Duc N H, Nhien T T and Nong N V 2003 *J. Magn. Magn. Mater.* **262** 427
[166] Wang F, Wang G-J, Hu F-X, Kurbakov A, Shen B-G and Cheng Z-H 2003 *J. Phys.: Condens. Matter* **15** 5269
[167] Levin E M, Pecharsky V K and Gschneidner K A Jr 1999 *Phys. Rev.* B **60** 7993
[168] Fujieda S, Fujita A, Fukamichi K, Yamazaki Y and Iijima Y 2001 *Appl. Phys. Lett.* **79** 653
[169] Yamada H and Goto T 2003 *Phys. Rev.* B **68** 184417
[170] Pecharsky V K and Gschneidner K A Jr 2001 *J. Appl. Phys.* **90** 4614
[171] Pecharsky V K and Gschneidner K A Jr 1998 *Adv. Cryog. Eng.* **43** 1729
[172] Fujieda S, Hasegawa Y, Fujita A and Fukamichi K 2004 *J. Magn. Magn. Mater.* **272–276** 2365
[173] Hamdeh H H, Al-Ghanem H, Hikal W M, Taher S M, Ho J C, Anh D T K, Thuy N P, Duc N H and Thang P D 2004 *J. Magn. Magn. Mater.* **269** 404
[174] Hu F-X, Shen B-G, Sun J-R, Wang G-J and Cheng Z-H 2002 *Appl. Phys. Lett.* **80** 826
[175] Liu X B and Altounian Z 2003 *J. Magn. Magn. Mater.* **264** 209
[176] Liu X B, Ryan D H and Altounian Z 2004 *J. Magn. Magn. Mater.* **270** 305
[177] Chen Y-F, Wang F, Shen B-G, Hu F-X, Sun J-R, Wang G-J and Cheng Z-H 2003 *J. Phys.: Condens. Matter* **15** L161
[178] Hu F-X, Wang G-J, Wang J, Sun Z-G, Dong C, Chen H, Zhang X-X, Sun J-R, Cheng Z-H and Shen B-G 2002 *J. Appl. Phys.* **91** 7836
[179] Liu X B, Altounian Z and Beath A D 2004 *J. Appl. Phys.* **95** 6924
[180] Goodenough J B 2003 *Handbook on the Physics and Chemistry of Rare Earths* vol 33, ed K A Gschneidner Jr *et al* (Amsterdam: Elsevier) p 249
[181] Chen W, Zhong W, Hou D L, Gao R W, Feng W C, Zhu M G and Du Y W 2002 *J. Phys.: Condens. Matter* **14** 11889
[182] Tang T, Gu K M, Gao Q Q, Wang D H, Zhang S Y and Du Y W 2000 *J. Magn. Magn. Mater.* **222** 110
[183] Wang Z M, Tang T, Wang Y P, Zhang S Y and Du Y W 2002 *J. Magn. Magn. Mater.* **246** 254
[184] Chen W, Zhong W, Pan C F, Chang H and Du Y W 2001 *Acta Phys. Sin.* **50** 319
[185] Phan M H, Yu S C and Hur N H 2003 *J. Magn. Magn. Mater.* **262** 407
[186] Sun Y, Xu X and Zhang Y 2000 *J. Magn. Magn. Mater.* **219** 183
[187] Phan M-H, Yu S-C, Hur N H and Jeong Y-H 2004 *J. Appl. Phys.* **96** 1154
[188] Xu Y, Memmert U and Hartmann U 2002 *J. Magn. Magn. Mater.* **242–245** 698
[189] Bohigas X, Tejada J, Marinez-Sarrión M L, Tripp S and Black R 2000 *J. Magn. Magn. Mater.* **208** 85
[190] Dinesen A R, Linderoth S and Mørup S 2002 *J. Magn. Magn. Mater.* **253** 28
[191] Wang Z M, Ni G, Xu Q Y, Sang H and Du Y W 2001 *J. Appl. Phys.* **90** 5689
[192] Chen H, Lin C and Dai D 2003 *J. Magn. Magn. Mater.* **257** 254
[193] Zhang Y X, Liu Z G, Zhang H H and Xu X N 2000 *Mater. Lett.* **45** 91
[194] Sun Y, Salamon M B and Chun S H 2002 *J. Appl. Phys.* **92** 3235
[195] Demin R V and Koroleva L I 2004 *Phys. Solid State* **46** 1081

[196] Szewczyk A, Gutowska M, Piotrowski K and Dabrowski B 2003 *J. Appl. Phys.* **94** 1873

[197] Phan M H, Tian S B, Hoang D Q, Yu S C, Nguyen C and Ulyanov A N 2003 *J. Magn. Magn. Mater.* **258–259** 309

[198] Chau N, Niem P Q, Nhat H N, Luong N H and Tho N D 2003 *Physica* B **327** 214

[199] Si L, Chang Y L, Ding J, Ong C K and Yao B 2003 *Appl. Phys.* A **77** 641

[200] Kuwahara H, Tomioka Y, Asamitsu A, Moritomo Y and Tokura Y 1995 *Science* **270** 961

[201] Chen P, Du Y W and Ni G 2000 *Europhys. Lett.* **52** 589

[202] Chen P and Du Y W 2001 *J. Phys. D: Appl. Phys.* **34** 1868

[203] Reis M S, Gomes A M, Araújo J P, Tavares P B, Amaral J S, Oliveira I S and Amaral V S 2004 *Mater. Sci. Forum* **455–456** 148

[204] Reis M S, Gomes A M, Araújo J P, Tavares P B, Oliveira I S and Amaral V S 2004 *J. Magn. Magn. Mater.* **272–276** 2393

[205] Gomes A M, Reis M S, Guimarães A P, Tavares P B, Araújo J P and Amaral V S 2004 *J. Magn. Magn. Mater.* **272–276** 2385

[206] Sande P, Hueso L E, Miguéns D R, Rivas J, Rivadulla F and López-Quintela M A 2001 *Appl. Phys. Lett.* **79** 2040

[207] Chau N, Cuong D H, Tho N D, Nhat H N, Luong N H and Cong B T 2004 *J. Magn. Magn. Mater.* **272–276** 1292

[208] Zhong W, Chen W, Au C T and Du Y W 2003 *J. Magn. Magn. Mater.* **261** 238

[209] Zhu H, Song H and Zhang Y H 2002 *Appl. Phys. Lett.* **81** 3416

[210] Zhong W, Chen W, Jiang H Y, Liu X S, Au C T and Du Y W 2002 *Eur. Phys. J.* B **30** 331

[211] Yamamoto T A, Tanaka M, Nakayama T, Nishimaki K, Nakagawa T, Katsura M and Niihara K 2000 *Japan. J. Appl. Phys.* **39** 4761

[212] Yamamoto T A, Tanaka M, Shiomi K, Nakayama T, Nishimaki K, Nakagawa T, Numazawa T, Katsura M and Niihara K 2000 *Mater. Res. Soc. Symp. Proc.* **581** 297

[213] McMichael R D, Ritter J J and Shull R D 1993 *J. Appl. Phys.* **73** 6946

[214] Yamamoto T A, Tanaka M, Misaka Y, Nakagawa T, Nakayama T, Niihara K and Numazawa T 2002 *Scr. Mater.* **46** 89

[215] Kinoshita T, Seino S, Maruyama H, Otome Y, Okitsu K, Nakayama T, Niihara K, Nakagawa T and Yamamoto T A 2004 *J. Alloys Compounds* **365** 281

[216] Provenzano V, Li J, King T, Canavan E, Shirron P, DiPirro M and Shull R D 2003 *J. Magn. Magn. Mater.* **266** 185

[217] Provenzano V, Shapiro A J, Shull R D, King T, Canavan E, Shirron P and DiPirro M 2004 *J. Appl. Phys.* **95** 6909

[218] Pecharsky V K, Gschneidner K A Jr, Dan'kov S Yu and Tishin A M 1999 *Cryocoolers 10* ed R G Ross (Amsterdam: Kluwer/Plenum) p 639

[219] Nelson J A, Bennett L H and Wagner M J 2002 *J. Am. Chem. Soc.* **124** 2979

[220] Shir F, Yanik L, Bennet L H, Torre E D and Shull R D 2003 *J. Appl. Phys.* **93** 8295

[221] Pecharsky V K and Gschneidner K A Jr 1999 *J. Appl. Phys.* **86** 6315

[222] Dan'kov S Yu, Tishin A M, Pecharsky V K and Gschneidner K A Jr 1997 *Rev. Sci. Instrum.* **68** 2432

[223] Pecharsky V K, Holm A P, Gschneidner K A Jr and Rink R 2003 *Phys. Rev. Lett.* **91** 197204

[224] Pecharsky V K and Gschneidner K A Jr 2005 *Magnetism and Structure in Functional Materials (Springer Series on Materials Science)* vol 79 ed A Planes *et al* (Springer) to be published

[225] Morellon L, Arnold Z, Magen C, Ritter C, Prokhnenko O, Skorokhod Y, Algarabel P A, Ibarra M R and Kamarad J 2004 *Phys. Rev. Lett.* **93** 137201

[226] Gschneidner K A Jr, Pecharsky V K, Gailloux M J and Takeya H 1996 *Adv. Cryog. Eng.* **42** 465

[227] Gschneidner K A Jr 1964 *Solid State Phys.* **16** 275

[228] Yu B F, Gao Q, Zhang B, Meng X Z and Chen Z 2003 *Int. J. Refrig.* **26** 622

[229] Bohigas X, Molins E, Roig A, Tejada J and Zhang X X 2000 *IEEE Trans. Magn.* **36** 538

[230] Hirano N, Nagaya S, Takahashi M, Kuriyama T, Ito K and Nomura S 2002 *Adv. Cryog. Eng.* **47** 1027

[231] Rowe A M and Barclay J A 2002 *Adv. Cryog. Eng.* **47** 995
Rowe A M and Barclay J A 2002 *Adv. Cryog. Eng.* **47** 1003

[232] Richard M A, Rowe A M and Chahine R 2004 *J. Appl. Phys.* **95** 2146

[233] Zimm C 2003 Paper No K7.003 *Am. Phys. Soc. Meeting*, March 4, Austin, TX, http://www.aps.org/meet/MAR03/baps/tocK.html

[234] Wu W 2003 Paper No K7.004 *Am. Phys. Soc. Meeting*, March 4, Austin, TX, http://www.aps.org/meet/MAR03/baps/tocK.html

[235] Hirano N 2003 Paper No K7.002 *Am. Phys. Soc. Meeting* March 4, Austin, TX, http://www.aps.org/meet/MAR03/baps/tocK.html

[236] Clot P, Viallet D, Allab F, Kedous-LeBouc A, Fournier J M and Yonnet J P 2003 *IEEE Trans. Magn.* **30** 3349

[237] Yayama H, Hatta Y, Makimoto Y and Tomokiyo A 2000 *Japan. J. Appl. Phys.* **39** 4220

[238] Zhang L, Sherif S A, DeGregoria A J, Zimm C B and Veziroglu T N 2000 *Cryogenics* **40** 269

[239] Steyert W A 1978 *J. Appl. Phys.* **49** 1216

[240] Barclay J A 1983 *Proc. 2nd Biennial Conf. on Refrigeration for Cryocooler Sensors and Electronic Systems*, NASA-CP-2287, Goddard Space Flight Center, Greenbelt, MD

Barclay J A 1983 *Los Alamos National Laboratory Report* LA-UR-82-1792

[241] Barclay J A and Steyert W A 1982 *US Patent* 4,332,135

[242] Chen F C, Murphy R W, Mei V C and Chen G L 1992 *J. Eng. Gas Turbine Power* **114** 715

[243] DeGregoria A J, Feuling L J, Laatsch J F, Rowe J R, Trueblood J R and Wang A A 1992 *Adv. Cryog. Eng.* **37** 875

[244] Hall J L, Reid C E, Spearing I G and Barclay J A 1996 *Adv. Cryog. Eng.* **41** 1653

[245] Rowe A M and Barclay J A 2003 *J. Appl. Phys.* **93** 1672

[246] DeGregoria A J 1992 *Adv. Cryog. Eng.* **37** 867

[247] Johnson J W and Zimm C B 1996 *J. Appl. Phys.* **79** 2171

[248] He J, Chen J and Wu C 2002 *J. Non-Equilib. Thermodyn.* **27** 57

[249] Annaorazov M P, Ünal M, Nikitin S A, Tyurin A L and Asatryan K A 2002 *J. Magn. Magn. Mater.* **251** 61

[250] Provenzano V, Shapiro A J and Shull R D 2004 *Nature* **429** 853

Provenzano V, Shapiro A J and Shull R D 2004 *Nature* **430** 810

[251] Gschneidner K A Jr, Pecharsky V K, Pecharsky A O and Zimm C B 1999 *Mater. Sci. Forum* **315–317** 69

[252] Gschneidner K A Jr, Pecharsky A O and Pecharsky V K 2003 *US Patent* 6,589,366

[253] Luo E, Barclay J A, Reedeker P G and Wysokinski T W 2002 *Adv. Cryog. Eng.* **47** 1011

[254] Lee S J and Jiles D C 2000 *IEEE Trans. Magn.* **36** 3105

[255] Tang Y B, Chen Y G, Teng B H, Fu H, Li H X and Tu M J 2004 *IEEE Trans. Magn.* **40** 1597

[256] Xu X N, Lu D W, Yuan G Q, Han Y S and Jin X 2004 *J. Appl. Phys.* **95** 6302